23-340

TFBP-TR-228

for U.S. Nuclear Regulatory Commission

W/RIL #25

FRAP-S3: A COMPUTER CODE FOR STEADY-STATE ANALYSIS OF OXIDE FUEL RODS VOLUME 2 - MODEL VERIFICATION REPORT

October 1977

EG&G Idaho, Inc.

IDAHO NATIONAL ENGINEERING LABORATORY

ENERGY RESEARCH AND DEVELOPMENT ADMINISTRATION

IDAHO OPERATIONS OFFICE UNDER CONTRACT EY-76-C-07-1570

1569 119

7912140 418

23-341

TFBP-TR-228
August 1977

FRAP-S3 - A COMPUTER CODE FOR STEADY-STATE ANALYSIS OF OXIDE FUEL RODS

VOLUME 2

MODEL VERIFICATION REPORT

BY

D. R. COLEMAN

E. T. LAATS

N. R. SCOFIELD

Reviewed by:

FARAD Branch Manager ______________________
J. A. Dearien

Original signed by
J. G. CROCKER

TFB Program Manager ______________________
J. G. Crocker

THERMAL FUELS BEHAVIOR PROGRAM

EG&G IDAHO, INC.

1569 120

ACKNOWLEDGMENT

Acknowledgment is given to J. D. Kerrigan for conducting Standard Design Analyses, to G. A. Berna for providing timely model development support, and to N. L. Hampton for assistance in data processing and report preparation.

1569 121

23-342

TABLE OF CONTENTS

Page

I. SUMMARY AND CONCLUSIONS 1

II. INTRODUCTION 7

1. Model 7

2. General Verification Approach 8

2.1 Types of Analyses. 8

2.2 Scope of Analyses. 9

III. VERIFICATION RESULTS 13

1. Input 13

2. Standard Design Study 19

2.1 Model Comparison 19

2.2 Output Characterization. 40

2.2.1 Applications. 40

2.2.2 Procedures. 41

2.2.2.1 Input Parameters 41

2.2.2.1.1 Design. 41

2.2.2.1.2 Model Uncertainty . . . 44

2.2.2.1.3 Operating History . . . 44

1569 122

2.2.2.2 Statistical Methods. 46

2.2.3 Output. 52

3. Data Comparison Study 58

3.1 Thermal Model 59

3.1.1 Fuel Centerline Temperature 59

3.1.1.1 Duplicate Comparison Study 59

3.1.1.2 Summary Fuel Temperature Results . 69

3.1.2 Gap Conductance 78

3.2 Fission Gas Model 84

3.2.1 Gas Release Fraction 84

3.2.1.1 Current Model Results 85

3.2.1.2 Data Analysis 88

3.2.2 Rod Internal Pressure 95

3.3 Rod Deformation Model 102

3.3.1 Gap Closure Conditions 102

3.3.2 Fuel Deformation 106

3.3.2.1 Fuel Thermal Expansion 106

3.3.2.2 Fuel Stack Permanent Deformation . 110

3.3.3 Cladding Deformation 115

3.4 Cladding Surface and Impurity Effects 121

3.4.1 Corrosion 121

3.4.2 Hydrogen Pickup 126

IV. REFERENCES 131

23-343

LIST OF FIGURES

Figure		Page
1	FRAP-S2 and FRAP-S3 center temperature histories for a core average 7 x 7 rod	21
2	FRAP-S2 and FRAP-S3 center temperature histories for a core average 15 x 15 rod	22
3	FRAP-S2 and FRAP-S3 stored energy histories for a core average 7 x 7 rod.	23
4	FRAP-S2 and FRAP-S3 internal pressure histories for a core average 7 x 7 rod	24
5	FRAP-S2 and S3 stored energy versus local heat rating for a 7 x 7 rod at beginning of life	26
6	FRAP-S2 and FRAP-S3 stored energy histories for a core average 15 x 15 rod.	27
7	FRAP-S2 and FRAP-S3 internal pressure histories for a core average 15 x 15 rod	28
8	FRAP-S2 and FRAP-S3 gap histories for a core average 7 x 7 rod.	29
9	FRAP-S2 and FRAP-S3 gap histories for a core average 15 x 15 rod.	31
10	FRAP-S2 and FRAP-S3 cladding hoop strain histories for a core average 15 x 15 rod	32
11	FRAP-S2 and FRAP-S3 cladding hoop strain histories for a core average 7 x 7 rod	33
12	FRAP-S2 and FRAP-S3 cladding hoop strain vs. local heat rating for a core average 15 x 15 rod @ EOL . . .	34
13	FRAP-S2 and FRAP-S3 cladding surface corrosion histories for a core average 7 x 7 rod	36
14	FRAP-S2 and FRAP-S3 cladding surface corrosion histories for a core average 15 x 15 rod	37
15	FRAP-S2 and FRAP-S3 cladding hydrogen concentration histories for a core average 7 x 7 rod	38
16	FRAP-S2 and FRAP-S3 cladding hydrogen concentration histories for a core average 15 x 15 rod	39
17	First core loading arrangement for FRAP-S3 standard design study	45

1569 124

18 Range in region wise core power distributions for FRAP-S3 standard design study. 47

19 Treatment of variable power history effects for FRAP-S3 standard design study. 50

20 FRAP-S3 calculated distribution of rod internal pressure for standard design PWR cores at beginning, middle, and end of life. 53

21 FRAP-S3 calculated distribution of stored energy for standard design PWR cores at beginning, middle, and end of life. 54

22 FRAP-S3 calculated distribution of gap porosity for standard design PWR cores at beginning, middle, and end of life. 55

23 Comparison between predicted - measured fuel center temperatures using FRAP-S3 with and without relocation/k effective models. 62

24 Comparison between center temperature error frequencies using FRAP-S3 with and without relocation/k effective models - Summary Data. 64

25 Comparison between center temperature error frequencies using FRAP-S3 with and without relocation/k effective models - Low Burnup Pressurized Rod Data 64

26 Comparison between center temperature error frequencies using FRAP-S3 with and without relocation/k effective models - Moderate to high Burnup data. 64

27 Comparison between predicted - measured pellet temperature drops using FRAP-S3 with and without relocation/k effective models. 66

28 Comparison between measured and predicted pellet temperature distribution using FRAP-S3 with and without relocation/k effective models - Small gap rod. 67

29 Comparison between measured and predicted pellet temperature distribution using FRAP-S3 with and without relocation/k effective models - Large gap rod. 67

30 Comparison between measured and predicted pellet temperature distribution using FRAP-S3 with and without relocation/k effective models - Helium backfill. . . . 68

31 Comparison between measured and predicted pellet temperature distribution using FRAP-S3 with and without relocation/k effective models - Argon backfill 68

1569 125

23-344

32	FRAP-S3 predicted versus measured center temperatures for unpressurized rods	71
33	FRAP-S3 predicted versus measured center temperatures for pressurized rods	72
34	Effect of gap size on FRAP-S3 center temperature error.	73
35	Effect of local heat rating on FRAP-S3 center temperature error.	74
36	Effect of fuel density on FRAP-S3 center temperature error.	75
37	Effect of local burnup on FRAP-S3 center temperature error.	76
38	FRAP-S3 predicted versus experimentally inferred gap conductance - pressurized rods	80
39	FRAP-S3 predicted versus experimentally inferred gap conductance - unpressurized rods	81
40	Effect of gap size on FRAP-S3 gap conductance error. .	82
41	Effect of local heat rating on FRAP-S3 gap conductance error.	83
42	FRAP-S3 predicted versus measured fission gas release fraction	86
43	Effect of maximum fuel temperature on FRAP-S3 fission gas release error.	87
44	Measured fission gas release fraction versus burnup for different maximum fuel temperature ranges.	89
45	Measured fission gas release fraction versus maximum fuel temperature for different burnup ranges	90
46	Measured fission gas release fraction versus average fuel temperature for different burnup ranges	91
47	Measured fission gas release fraction versus diffusion dependent parameter t_{max}/t_o.	92
48	FRAP-S3 predicted versus measured rod internal pressure	97
49	Effect of burnup on FRAP-S3 rod internal pressure error.	98

1569 126

50 Effect of plenum volume fraction on FRAP-S3 rod internal pressure error - startup data 100

51 Effect of average fuel temperature on FRAP-S3 rod internal pressure error - startup data 101

52 FRAP-S3 predicted versus measured gap closure heat rating 103

53 Effect of gap size on FRAP-S3 gap closure heat rating error 105

54 FRAP-S3 predicted versus measured fuel axial expansion during heatup. 107

55 Effect of average fuel temperature on FRAP-S3 fuel axial expansion error during heatup. 108

56 Effect of gap size on FRAP-S3 fuel axial expansion error during heatup. 109

57 FRAP-S3 predicted versus measured permanent fuel axial deformation. 111

58 Effect of density on FRAP-S3 permanent fuel axial deformation error. 113

59 Effect of burnup on FRAP-S3 permanent fuel axial deformation error. 114

60 FRAP-S3 predicted versus measured permanent cladding hoop strain. 117

61 Effect of gap size on FRAP-S3 permanent cladding hoop strain error 119

62 FRAP-S3 predicted versus measured permanent cladding axial strain 120

63 FRAP-S3 predicted versus measured rod surface corrosion buildup. 123

64 Effect of operating time on FRAP-S3 error in rod surface corrosion buildup. 124

65 Effect of system inlet temperature on FRAP-S3 error in rod surface corrosion buildup. 125

66 FRAP-S3 predicted versus measured cladding hydrogen concentration. 127

67 Effect of operating time on FRAP-S3 cladding hydrogen concentration error. 129

1569 127

23-345

68 Effect of initial fuel moisture concentration on FRAP-S3 cladding hydrogen concentration error. 130

1569 128

LIST OF TABLES

Table		Page
1	Significance of FRAP-S3 Output Parameters for Application to Transient Fuel Behavior Analysis	11
2	FRAP-S3 Comparative Physical Effects	14
3	FRAP-S3 Model Verification - Run Identification and Nominal Input	15
4	Standard Design Analysis Procedures	42
5	Steady State Variables for Standard Design Analysis	43
6	FRAP-S3 Model Verification - Scope of Data Comparison Study	60

23-345

I. SUMMARY AND CONCLUSIONS

Results for several types of data comparisons as well as for power reactor fuel standard design analyses are reported to evaluate capabilities of FRAP-S3[1]*. The model comprises a revised version of a steady-state Fuel Rod Analysis Program under development as a supporting tool for reactor safety analysis. Primary application is in supplying initial conditions for the transient response model, FRAP-T[106].

Comparisons between code predictions and experimental results were made for general categories of fuel behavior indicative of operating rod thermal, pressure, deformation and surface conditions. Other analytical comparisons are used to verify that code performance under standard commercial fuel design and operating conditions is consistent with conclusions based on verification data comparison results.

Analytical Comparison

Standard Design Runs for core average rod PWR and BWR conditions provide a basis for comparison between FRAP-S3 and FRAP-S2[3]. Treatment of fuel relocation and related conductivity effects causes FRAP-S3 to predict lower (BWR) and somewhat higher (PWR) fuel temperature, internal pressure, gas release, and fission product swelling compared with FRAP-S2. Influence of a new fast flux term in the cladding creep model results in FRAP-S3 predicting significantly more negative hoop strain by end-of-life than FRAP-S2. Accounting for strain hardening effects now decreases the creep rate however after the accumulation of

* MOD 003 VERSION 001 (9/14/77), MATPRO MOD 009.

1569 130

about 1% strain. Effective gap size comparisons indicate that soft pellet-cladding contact exists for FRAP-S3 over a much wider range of power and burnup conditions than predicted by previous code versions. With more emphasis on the effect of system fluid conditions, FRAP-S3 predicts similar buildups of cladding surface corrosion for both BWR and PWR rods. Predicted cladding hydrogen concentrations are now more strongly influenced by initial fuel moisture content than by the amount of calculated corrosion.

Realistic variation of design, operating, and model uncertainty parameters provided enough FRAP-S3 output to justify continuing efforts to develop response surface characterizations of Standard Design results. A key application in this area is to define realistic core-wide input ranges appropriate for FRAP-T4 accident analysis at different burnups. Contrary to prior results[3,107], core-wide variation in initial fuel rod thermal conditions can be governed by variation in design and model parameters, in addition to core power distribution. Internal pressure and gap conditions remain less governed by current heat rating than by design and model parameters. The model parameters gain influence with burnup since the effects of prior operation are cumulative, particularly with respect to the creep collapse feedback on crack closure and effective pellet conductivity. The currently calculated distribution of possible initial accident conditions for standard PWR cores is wide enough to warrant further decreases in burnup dependent model uncertainty.

23-346

Data Comparisons

Thermal

The current relocation and pellet conductivity models, coupled with traditional Ross-Stoute gap conductance models, provide a more realistic physical representation of fuel center temperature behavior that the previous cracked pellet model. Comparing measured and predicted pellet temperature drops for a subset of off-center fuel thermocouple experiments, supports use of the current mechanistic thermal model. Incorporation of fuel mechanical deformation and permanent crack healing in subsequent models is expected to further improve temperature results by more actively accounting for irradiation effects on pellet properties and crack disposition.

Fuel center temperature response to varying power and burnup conditions is typically reproduced by the model to within data uncertainty (esti°150C) for a wide range of PWR and BWR design conditions. Up to 15 kW/ft and 15,000 MWD/MTM, the standard error between measured and predicted fuel center temperatures varies between 200 and 250 C based on analysis of some 100 rods from different test programs. For typical design and operating conditions, this result supports the model's best estimate capability for calculating initial pellet stored energy within 20% of experimentally indicated values.

1569 132

Gap conductance data comparisons show qualitative improvement over FRAP-S2 results. Quantitative agreement only reflects more or less consistency between the various experimental heat transfer models used for data reduction and FRAP-S3 relocation, conductivity and gap conductance models. Re-evaluation of gap conductance data accounting for best-estimate gap closure, crack geometry, and pellet conductivity effects is warranted.

Fission Gas

Ability to diagnose performance of the gas release model is a main consequence of more realistic FRAP-S3 fuel temperature predictions. The gas release fraction under moderate operating conditions is generally overestimated by the primarily temperature dependent instantaneous release model. Relatively high release conditions, mainly dominated by temperature effects regardless of burnup, have always been well characterized by the model. The standard error between the predicted and measured gas release fractions is 18.8% for the 180 rod data sample considered.

Analysis of relative influence of temperature, burnup, and associated diffusion parameters on both the gas release data and model error indicate that some basic code improvement is needed. Simply accounting for the cumulative effect of lattice diffusion processes on gas atom disposition with respect to grain boundaries and bubble channeling sites shows promise for adding the required mechanistic dimension to the current, mainly temperature dependent model.

For rods with typical plenum volumes, the heat-up effect on internal pressure conditions during startup is generally represented by the model to within 20% of the data up to 2200 psia. Improvement in predicting burnup conditions, especially for unpressurized rods, hinges on a more realistic representation of fission gas release kinetics in subsequent code versions. The standard error between predicted and measured rod internal pressure for 28 unpressurized and 20 pressurized rods is respectively 96 and 194 psia.

Rod Deformation

Comparing measured and predicted heat rating for initiation of soft gap closure supports use of the initial relocation model for design gap sizes up to 3%. The standard error between measured and calculated initial gap closure heat rating is 4.1 kW/ft for an 80 rod data sample. Performance of this model is a prerequisite for benchmarking improved treatments of pellet deformation and cyclic response still under development. The present simplified gap closure model is mainly limited under operating conditions promoting sustained occurrence of hard PCMI.

Axial fuel thermal expansion during startup ramps was well represented by the model prior to the buildup of significant mechanical interaction effects above 12 kW/ft. The standard error between predicted and measured stack expansion corresponds to .37% of the active length for a 20 rod data sample. The combined effect of calculated fuel densification and swelling was usually within data scatter for the moderate to high burnup stack length change measurements quoted in several experiments. The standard error between measured and predicted permanent fuel deformation is .44% based on analysis of 100 rods with burnups up to 30000 MWd/MTM.

1569 134

FRAP-S3 analysis of cladding diameter changes below 15 kW/ft indicates that creep collapse mechanisms dominate both measured and predicted response. Improvement in modeling cladding creep properties in addition to fuel thermal conditions, contributed to the fact that end-of-life hoop strain predictions were generally within data reproducibilty (±30%) of measured values. The standard error between measured and predicted cladding permanent hoop strain is .58% based on consideration of a 170 rod data sample. The relatively small effect of permanent cladding axial strain was underestimated by the model due in part to as yet incomplete coupling between pellet relocation and mechanical response. The standard error between measured and predicted cladding permanent axial strain is .47% for a data sample of 115 different rods.

Cladding Surface Condition and Impurities

Comparing measured and predicted buildup of cladding surface corrosion shows adequate model capability for characterizing uniform ZrO_2 thickness and hydrogen pickup. The data mainly reflect post-transition corrosion mechanisms for both BWR and PWR system conditions and irradiation times up to 1200 and 900 days respectively. Calculated sensitivity of hydrogen pickup to initial fuel water content, in addition to corrosion, seems appropriate for typical moisture concentrations below 10 ppm. Based on results for a 50 rod data sample, standard errors between measured and predicted end-of-life cladding surface corrosion and hydrogen concentration are respectively .26 mils and 39 ppm.

23-348

II. INTRODUCTION

1. MODEL

FRAP-S3 is the third version of a steady-state fuel rod analysis program. The program has been under development as part of an overall fuel behavior modeling effort in support of reactor safety analysis. The purpose of this volume is to document current predictive capability in key modeling areas. Additional diagnosis of model performance over ranges of fuel design and operating conditions is intended to identify areas of less model applicability and support further development. Other documents describing analytical models[1] and material properties[2] have been prepared by the code developers.

The computer program itself is structured in modular form and is coupled to fuel, cladding and gas material properties supplied by MATPRO[2]. Submodels account for surface heat transfer and corrosion, rod power and temperature distribution, sorbed and fission gas release, gas volume and temperature conditions, fuel swelling and densification, fuel and cladding thermal expansion, fuel relocation, and uniform cladding deformation due to creep, yield and elastic strain. Key input to the code is the fuel design, system operating condition and axial power distribution. The models are then driven by the rod average power history. Results for the input number of rod axial segments are integrated to obtain fission gas composition, length and void volume conditions. Unless sustained gap closure and high fuel temperature are coincident, running time and convergence are usually not limiting considerations. The program description is given in more detail elsewhere[1].

1569 136

FRAP-S is intended to be a realistic analytical tool for extended burnup application. The original core of the model was used previously in industry for steady-state fuel rod design analysis. A major purpose for FRAP-S now, is in supplying the transient fuel rod analysis model (FRAP-T)[106] with initial conditions reflecting operation prior to hypothetical transients.

Importance of steady-state models in conjunction with FRAP-T should not be under-emphasized. Feedback among cumulative burnup effects causes initial conditions for all but initial startup transients to differ considerably from beginning-of-life conditions. Main steady-state outputs of FRAP-S expected to impact transients are those which characterize initial rod temperature distribution, gap size, gas composition, rod internal void volume, gas content, clad strain accumulation and rod surface conditions. These areas are emphasized in model verification analyses.

2. GENERAL VERIFICATION APPROACH

The different types of verification studies and the rational for analyzing results from a large number of runs is described below.

2.1 Types of Analyses

Supporting runs were used to debug the code and evalute the overall effect of changes in the model with respect to the previously documented version, FRAP-S2[3]. The main type of supporting run discussed here falls into the category of Standard Design Analyses. Input rod design and operating condition parameters for these runs are meant to benchmark full-scale application of the program to power reactor fuel from startup through end-of-life. FRAP-S3 Standard Design runs were also meant to establish realistic initial conditions ranges to support potential verification of FRAP-T4 LOCA analysis capability and corresponding input sensitivity[111].

Several types of data comparisions were then performed to evaluate overall capabilities of FRAP-S3 as a predictive tool. The emphasis was necessarily placed on the ability of the code to track 1) fuel temperature and related power level effects on gap, pressure, and thermal expansion, and 2) burnup effects on gas release, internal pressure, and rod dimensional changes. Data comparison results are interpreted with respect to rod operating history and design parameters. The reasons for conducting summary large sample analyses for interpretation of model performance are discussed below.

2.2 Scope of Analyses

The approach used for verification of both FRAP-S and FRAP-T has emphasized use of an increasing number of data comparison results as subsequent code versions are evaluated. These additional tests of the model are performed to enable verification runs to have continued significance for independently benchmarking the predictive capability of successively fine-tuned code versions. This incentive exists particularly for safety analysis codes, because there is always a chance that

1569 138

empiricism in the model based on previous experiments may be misdirected. Such a condition may be undetected by the verification process unless data other than that used for correlation, or data which may reflect as yet unmodeled basic principles are continually added to the sample.

Another reason for maximizing sample size is that the relative importance of modeling any one of a number of potentially significant fuel rod temperature, pressure and deformation mechanisms cannot really be minimized without making as yet unjustified assumptions. This limitation exists due to lack of either data or verified production codes by means of which some relative measure of influence can be assigned with confidence to those parameters describing the fuel condition. Some examples of feedback between various indices of steady state fuel behavior and subsequent transient response are shown in Table 1. The result of interdependence among thermal, mechanical, and chemical fuel behavior mechanisms is that different measurement categories must be considered when benchmarking the integrated code result. Misleading conclusions could be arrived at if the consistency of code performance was not verified for related temperature, pressure, and deformation mechanisms. For each individual data comparison index, identifying the mean, range, and distribution of fuel behavior measurements is dependent on considering many data points applicable to a given design configuration and range of operating conditions. This requirement arises because scatter in the data suggests that the range reflecting reproducibility of fuel rod measurements may be larger in some cases than the model uncertainty range.

23-350

TABLE I

IMPACT OF FRAP-S OUTPUT ON TRANSIENT FUEL BEHAVIOR ANALYSIS

FRAP-S OUTPUT CATEGORY FOR INITIAL CONDITIONS	AREA OF SIGNIFICANCE IN TRANSIENT ANALYSIS
Steady State Temperature Distribution Fuel Stored Energy Fuel Deformation Cladding Deformation Internal Gas Composition Burnup Dependent Fuel Thermal Properties Burnup Dependent Cladding Surface Properties	Transient Temperature Distribution [initial temperature gap conductance fuel thermal conductivity $Zr\text{-}H_2O$ reaction]
	↕ Feedback ⟷ [Surface Heat Transfer] ↕
Internal Pressure Gas Content Fuel Deformation Cladding Deformation Burnup Dependent Fuel Mechanical Properties Burnup Dependent Cladding Mechanical Properties Burnup Dependent Fission Gas Distribution	Transient Cladding Deformation [hydrostatic stress gas flow PCMI stress fission gas release]

1569 140

The final incentive for generating large numbers of data comparisons is based on intended application of the code to power reactor conditions. It is felt that verification conclusions based on measurements from large numbers of rods are more likely to be applicable to the case of typical fuel behavior variation in a large power reactor core with 40 to 50 thousand rods. Variation of fuel behavior throughout the core reflects differences in rod design, fabrication, burnup, heat rating and influence of random phenomena. Scatter in the verification data sample on the other hand is one result of a maximum sample approach. Since the model does not control fuel design, fabrication, or core operating condition, at least some amount of verification data scatter is a necessary corollary to the wide range of core conditions which will exist independently of any model result.

For the most part, differences among experiments in design, operating, and measurement uncertainty, together with the relatively large number of data comparison rods considered (~600), precludes detailed treatment of individual runs in this volume. A summary approach to interpreting verification runs has in the past however usually resulted in trends consistent with both physical expectations and the state of model development. The assumption inherent in considering together data comparison results for many different rods is that both measured and predicted mean fuel behavior responses can be best explained on the basis of parameters describing design configuration and operating conditions. Influence of fabrication variability and non-uniform local effects not considered by the model is assumed to only cause scatter in the data and not determine summary trends or compromise diagnosis of data comparison results.

1569 141

III. VERIFICATION RESULTS

Table 2 shows key predictive areas for the code and the corresponding output parameters where model performance analyses have been required by verification. Two categories of analyses, the results of which are discussed in this section, were conducted to evaluate FRAP-S3 performance in these areas. Letters A and D indicate which modeling areas are addressed respectively by supporting analytical runs and data comparison runs.

1. INPUT

For simplicity, nominal input data and references for all verification runs have been summarized in Table 3. Best estimate values were assumed whenever secondary geometry, system conditions, or fabrication input details were not given in the reference material. Input radial power distributions were based on a Bessel function form for Halden rods[4,22], or reported values for PBF rods[108]. Otherwise, the FRAP-S3 internal models[1] were used: a polynomial fit of LASER output for rods with commerical enrichment and geometry, or an "f" factor (flux depression) relationship for non-Halden test rods with untypical enrichment or geometry. Test rods were axially divided into 3 or 5 intervals. Axial power distributions for data comparison runs were based on in-core instrumentation or in most cases end-of-life gamma scans. Input power histories are consistent with reported irradiation time, average heat rating conditions, and end-of-life burnups.

1569 142

TABLE 2

FRAP-S3 COMPARATIVE PHYSICAL EFFECTS

Output Category	Output Variable	Run Series	
Rod Temperature Distribution	Fuel Center Temperature	A	D
	Fuel Melt Radius	-	-
	Cladding Temperature	A	-
	Gap Conductance	A	D
	Power Distribution	-	-
Cladding Hydrostatic Stress	Rod Internal Pressure	A	D
	Gas Content	A	-
	Gas Composition	A	-
	Gas Release Fraction	A	D
	Void Volumes	A	-
Rod Elastic Deformation	Fuel Thermal Expansion	-	D
	Cladding Pressure Deflection	A	-
Rod Permanent Deformation	Fuel Swelling and Densification	A	D
	Fuel Mechanical Deformation	-	-
	Gap Closure	A	D
	Cladding Creep Col[illegible]se	A	D
	Cladding Tensile Str[illegible]	A	-
Cladding Surface Condition/ Impurity Effects	Corrosion	A	D
	Crud Buildup	-	-
	H_2 Concentration	A	D

LEGEND A Standard Design Study
D Data Comparison Study

TABLE 3. FRAP-S3 MODEL VERIFICATION - RUN IDENTIFICATION AND NOMINAL INPUT

Run No.	Reference	Number Rods	Clad ID* (in)	Diametral Gap (mils)	Fuel Density (%)	Enrichment (%)	Fill Gas† (psia)	Cold Plenum (in)	Dish (%)	Fuel Length (%)	Loop Press. (psia)	Mass Flow (10^6 #/hr-ft^2)	Inlet Temp. (°F)	Peak Power (kW/ft)	Peak/Avg. (axial)	Operating Hours	Output
Standard Design Study																	
Model Comparison																	
46	7 x 7	1	0.4990	12.0	94.0	2.2	15	16.0	0.0	12.0	1035	1.3	533	10.3††	1.4	32000	Standard**
47	8 x 8	1	0.4250	9.0	95.0	2.2	15	12.0	0.0	12.3	1055	1.3	533	8.8††	1.4	32000	Standard**
48	15 x 15	1	0.3740	7.5	94.0	2.8	345	8.8	1.5	12.0	2250	2.5	552	9.8††	1.4	21000	Standard**
49	17 x 17	1	0.3290	6.5	95.0	2.6	300	6.3	1.5	11.9	2250	2.5	552	7.6††	1.4	21000	Standard**
Output Characterization																	
851-80	PWR's	Core	.372-.376	.005-.0098	89.8-97.2	2.8	250-500	5-12	1.5	12.	2250	2.5	552	5.2-10.4	1.2-1.4	21000	Standard**
Data Comparison Study																	
1-6	HPR-80[4]	6	0.4957-0.4961	2.0-6.7	95.2-97.8	5.0	15	1.58	1.3	5.625	406	0.39	446	--	1.3	10,4400	TF, hg
29,30	NECL-4072[5]	2	0.7346	4.3	97.6,95.8	1.4,1.6	15	0.665	2.0	1.8,1.2	1100	2.1	414	20.6,20.2	1.0†††	1810,5,3	ε'_{cr}
31,32	IFA-225[6]	2	0.4952	5.9	95.0	5.9	15	0.827	3.8,0.0	1.736	485	0.35	463	22.6	1.2	2140	ε'_{cr}, ε'_{fx}, ε'_{cx}
33-36	IFA-226[7]	4	0.3743-0.3746	7.9-9.9	91.6-95.9	7.3(U+Pu)	15	5.0-7.0	2.1	2.0-2.15	490	0.36	456,467	12.0,15.0	1.36,1.07	4620	TF, P', ε'_{cx}
37-39	IFA-226[7]	3	0.3737-0.3743	3.6-7.8	94.5	7.3(U+Pu)	15	7.0-7.1	0.9	2.0	490	0.36	460	15.6	1.3	4620	ε'_{cx}
50-52	IFA-226[7]	3	0.3743-0.3746	8.2-8.4	90.6-95.1	7.3(U+Pu)	15	4.8-5.3	0.9	2.14-2.18	490	0.36	467	11.8	1.4	4620	P'
40	HPR-107[8]	1	0.4922	5.9	95.0	5.8	15	1.43	0.0	1.77	490	0.27	467	17.8	1.26	14	ε'_{fx}, ε'_{cx}
41,42	HPR-107[8]	2	0.4921	7.5	95.7	5.8	15	0.57	1.0,0.0	1.76	490	0.33	467	15.8	1.26	14	ε'_{fx}
43-45	HPR-107[8]	3	0.5535	8.4	98.9,97.3	6.0	15	0.39,1.46	1.4	1.77	485	0.32	460	14.7-16.3	1.07	14	TF, ε'_{cx}
53	RISO-269[9]	1	0.4929(SS)	3.9	95.7	1.35	15	0.42	0.0	0.46	2000†††	0.0	375-813***	14.1	1.0†††	3830	TF
54	RISO-415[10]	2	0.5043	7.1	94.0	1.45	15	1.14	2.2	1.04	1000	0.0	563***	20.8	1.2†††	1692	TF
57,59,60	IFA-223[11]	3	0.4980,0.4992	5.9,6.3	94.7	6.0	15	3.66	2.0,0.0	1.98	490	0.36	467,460	21.5,23.8	1.4,1.3	6450,20	TF, ε'_{fx}, ε'_{cx}
58,61	IFA-223[11]	2	0.4992,0.4994	6.5,6.3	94.7	6.0	15	3.66	2.0,0.0	1.98	490	0.36	467,460	21.5,23.8	1.4,1.3	20	ε'_{fx}, ε'_{cx}
62-64	WCAP-2923[12,99]	3	1.2745(SS)	24.5	95.0	0.6,0.8	15	0.5	0.0	0.37	15†††	0.0	150-290***	22.9,25.7	1.0†††	24,30	TF, hg
65-69	IFA-130,131[13]	5	0.5024-0.5035	5.9-12.3	90-94	6.0	15	1.69	0.0	1.52	485	0.39	464	19.4	1.5	20,1500	TF
70,71	IFA-132[13]	2	0.5512	9.9	94.7,94.9	10.0	15	9.45	0.0	1.8	465	0.46	464	32.0,40.1	1.5†††	2740,130	P', ε'_{cx}
73-87	BAW[14]	16	0.370	4.0,8.0	93.5	3.0	15	1.02	0.0	0.24	0	0.0	650***	14.0-26.0	1.02-1.05	1800-18000	GR
88-89	KWO[15]	2	0.3661	8.6	94.3	2.8,3.1	15,329	5.1,9.1	1.5	9.0,8.7	2300	2.5†††	550	7.4†††	1.4†††	25000	ε'_{cr}, ε'_{fx}
90-94	Saxton I[16]	5	0.3635	6.5	95.0	6.1-7.3	15(.78)	0.5	1.9	2.9-3.05	2500	2.6	515	4.2-8.4	1.32	1200-7800	H_2
95A-107	Saxton II[17]	13	0.3444	7.1	94.[illegible]	5.9(U+Pu)	15(.78)	0.8	1.9	3.05	2000,2250	2.7	515,486	8.4-18.3	1.32	2200-10400	ε'_{cr}, ε'_{cx}, GR, ZrO_2, H_2
108-123	Saxton III[18]	16	0.3444	7.1	94.0	5.9(U+Pu)	15(.78)	0.8	1.9	3.05	2000,2250	2.7	515,480	7.2-24.3	1.32	12600-18000	ε'_{cr}, ε'_{cx}, GR, ZrO_2, H_2
124-152	HPR-132[19]	29	0.5740-0.5745	6.1-9.5	95.9-97.0	7.0	15	1.86,1.99	2.4	5.5	406	0.39-0.51	440	8.2-16.8	1.24	900-7700	ε'_{cr}, ε'_{cx}, GR, ZrO_2, H_2
205-212	NECL-[illegible][20]	6	0.7811	33.1	96.6	4.34	15(air)†††	0.01	1.9	.52	1407	0.0	126-328***	19.6-36.[illegible]	1.0-1.13	600	ε'_{cr}, ε'_{cx}, GR
213-217	NECL-[illegible][21]	5	0.8025-0.8044	4.0-8.[illegible]	93.1-9[illegible]	1.86	15(Ar)	0.01-0.16	0.0	.51-1.01	1421	0.0	100-177***	9.5-16.8	1.0	14000	ε'_{cr}, gas, GR
219-221	[illegible]	3	0.5024-0.4969	6.0-6.[illegible]	96.0-96.[illegible]	15.-6.0	15	0.53-0.54	1.5	2.6-5.6	406	0.3-0.46	440	9.3-18.8	1.28	500-1900	TF
232-239	NECL-2230[23]	8	0.64[illegible]-0.6505	7.2-6.[illegible]	95.[illegible]	2.4	15(air)†††	0.062	-	0.50	1100	2.4	486	16.6-17.4	1.0	2800	ε'_{cr}, ε'_{cx}, GR
251-270	GEAP-4264[24]	20	0.5003-0.5103	4.3-8.9	94.[illegible]	1.5-3.8	15	2.1-7.5		2.46-2.85	1000	3.2-6.8	344	27.4-47.3	1.3-1.6	480-1560	GR, ε'_{cr}

* Zircaloy unless otherwise noted

† Helium unless otherwise noted

** Standard Design Package (vs time): centerline temperature, gas release fraction, L_{gas}, internal pressure void volume, g, conductance, gap size, gas helium fraction

†† Core average rod power

*** Clad surface temperature specified

††† Assumed

TF - fuel centerline temperature

ε_{cr} - clad circumferential deformation

ε_{cx} - clad axial deformation

GR - gas release fraction

P - rod internal pressure

hg - gap conductance

GAMOL - gas content

GCOMP - gas composition

VG - void volume

ε_{fx} - fuel axial deformation

ZrO_2 - clad corrosion thickness

H_2 - clad hydrogen concentration

NOTE: prime (') indicates instrumented rod data

1569 144

TABLE 3. FRAP-S2 MODEL VERIFICATION - RUN IDENTIFICATION AND NOMINAL INPUT (cont'd)

Run No.	Reference	Number Rods	Clad ID* (in)	Diametral Gap (mils)	Fuel Density (%)	Enrichment (%)	Fill Gas† (psia)	Cold Plenum (in)	Dish (%)	Fuel Length (ft)	Loop Press. (psia)	Mass Flow (10^6 lb/hr-ft^2)	Inlet Temp. (°F)	Peak Power (kW/ft)	Peak/Avg. (axial)	Operating Hours	Output
273-275	PWR [25-27,29,30]	5	.374	6.0	93.0,94.0	20.	550.,375.	2.0	2.3	3.0	2000.-2200.	.94-2.0	590.,620.	19.9-24.9	1.35	10	TF,ε'_{cx},P',
277-278																	hg',ZrO_2,ε'_{cr}
276,279-281	PWR [28,31]	4	.346	9.9	92.0	9.5	300(He,Ar)	3.0	4.1	2.89	2160.	.61-.236	540.-620.	19.2-20.3	1.32,1.34	23.,33.	TF,ε'_{cx},P',hg
286-288	PRIB [32]	3	.5078	12.0	94.5	1.2	15.	7.0†††	1.1†††	7.38	1050.	1.5†††	500.	9.5-12.1	1.28	5500.-7900	GR,GRMOL, GCOMP,ε_{cr}
289-298	PRIB [32]	10	.505,.5078	12.0	94.5	2.4,2.6	15.	7.0	1.0 1.1†††	4.89	1050.	1.5†††	500.	12.1-21.4	1.28	500.-3260.	GR,GRMOL, GCOMP,ε_{cx},ε_{cr}
299-304	HP(PIE) [33]	6	.7472	3.5,5.1	94.0	4.	15.	.13	1.8	1.56	490.	.96	454.,464.	13.2-19.4	1.08-1.39	5060.	GR
305,306	HP(PIE) [33]	2	.7443	6.3	94.0	4.	15.	.13	2.6	1.58	490.	.96	454.,464.	18.6,19.8	1.04,1.18	7070.	GR
307-309	HP(PIE) [33]	3	.4264	11.7	95.1	10.1	15.	5.6	1.8	4.81	490.	.26	454.	11.3	1.28	5900.	GR
310-313	HP(PIE) [33]	4	.4264	5.8-11.8	95.1	10.1	15.	5.6	1.8,1.9	4.81	490.	.26	454.	11.4,11.6	1.28	9700.	GR
314,315	HP(PIE) [33,34]	2	.4922	3.9,5.9	95.0	5.76	15†††	1.4	0.0,1.2	1.66	490.	.27	454.	20.2,21.0	1.11	2100.	GR,P
316-318	IFA-208 [35]	3	.4992	11.8	94.9	7.0	15†††	3.2	0.0,1.8	4.82	490.	.33	454.	22.8-24.9	1.34	3200.	ε_{cx},ε_{cr},ε'_{fx},ε'_{cx},GR
319,320	IFA-116 [36,39]	2	.5337,.5538	8.6,8.7	96.9,91.3	6.0	5.7,11.4†††	.96,1.01	1.1	1.64	490.	.32	454.	24.1	1.08	4000.	P,TF,GR
321-324	IFA-117 [37,39]	4	.5331-.5539	8.0-8.8	96.9,91.3	6.0	11.4†††	1.06-1.41	1.1	1.64	490.	.32	454.	21.7-26.0	1.04-1.27	4450.	P,TF GR
325	HP(P) [38,39]	1	.6309	8.5	95.9	9.65	15.	5.5†††	2.1†††	1.64	490.	.36	454.	41.8	1.14	1650.	GR
326,327	HP(P) [38,39]	2	.5034,.5036	9.0,12.2	94.0	6.0	15.	1.68	0.0	1.52	490.	.39	454.	20.4	1.03	5440.	GR
328	HP(P) [38,39]	1	.5112	5.9	95.0	10.0	15.	5.0	0.0	2.21	490.	.90	464.	25.2	1.32	4250.	GR
331-334	IFA-178 [40]	4	.5169	11.0	93.8	6.0	15.	1.77	0.0	1.71	490.	.30	454.,464.	16.3-17.1	1.11,1.15	7400.	P',GR
335-339	IFA-181 [41]	5	.4521	11.2	94.0	11.01	15.	2.7,3.2	2.5	4.83	490.	.28	454.	18.5	1.25	5790.	P,ε'_{fx},ε'_{cx},GR
340-345	IFA-162 [42,43]	6	.5039	7.5-13.0	94.8	5.1	15.	3.9	0.0,1.4, 1.8	5.48	490.	.32	454.	16.0	1.25	5280.	ε_{fx},H_2
346,347	IFA-150 [44]	2	.4264	5.9,11.8	95.1	10.1	15.	5.6	1.8	4.81	490.	.26	454.	13.8	1.28	9700.	ε'_{cx}
348	IFA-208 [35]	1	.4992	11.8	94.9	7.0	15.	3.2	0.0	4.82	490.	.33	454.	21.7	1.34	3100.	[illegible]
351	IFA-224 [35]	1	.4992	11.8	90.1	7.0	15.	3.2	3.7	4.82	490.	.34	454.	17.6	1.34	150.	[illegible]
352,353	IFA-230 [35,42]	2	.4992	9.8,13.8	94.9	6.0	15.	3.2	0.0,3.3	4.92	490.	.34	454.	16.3	1.36	60.	ε'_{cx},ε'_{fx}
359-362	WEST [45]	4	.374	7.5	92.	2.0	345.	6.6	1.5	12.	2250.	2.5	552.	5.9,13.7	1.40	5000.,10000.	ε_{fx}
[illegible]5-366	B&W [46]	4	.380	10.0-13.0	92.5-96.5	5.†††	15.	2.†††	2.2	.83	500.†††	0.0	400.	4.5	1.12	1200.,2000.	ε'_{fx}
[illegible]	IFA-166 [42]	1	.4922	5.9	95.	5.8	15.	1.42	0.0	1.66	490.	.27	454.	18.0	1.11	12.	ε'_{fx}
3[illegible]	IFA-116 [36]	2	.5530,.5539	7.9,8.8	91.3,96.9	6.01	15.†††	1.06,2.08	1.1	1.64	490.	.32	464.	13.5,14.5	1.26	15.	TF
372,[illegible]	IFA-142 [40]	2	.[illegible]480	4.7	94.[illegible]	3.	15.†††	.12	2.0,2.2	1.57	490.	.31	465.	20.3	1.14	4180.	P'
381	IFA-186 [47]	2	.5133	9.2	87.3,91.3	11.0	15.†††	1.05	0.0	1.74	590.	.25	454.	20.,20.4	1.11	1070.,10400.	GRMOL,GR
386	IFA-181 [41]	1	.4521	17.2	94.0	11.0	15†††	2.73	2.5	4.83	490.	[illegible]	454.	16.5	1.25	5790.	ε'_{fx},ε'_{cx},P
387-389	IFA-225 [48]	3	.4992	11.8	95.0	5.9	15.†††	.04	3.7	1.60	490.	.35	464.	15.2	1.27	39.	P
390-401	IFA-[illegible] [49]	11	.5080	2.6,13.8	86.8-94.5	7.0	15.	1.4†††	2.[illegible]	.82	490.	.34	454.,464.	12.9,17.5	1.04,1.14	7170.	ε'_{fx}
402-404	IFA-[illegible] [50]	3	.5000	2.4-3.5	94.[illegible]	7.0	15.†††	2.0†††		1.64	490.	.17	454.	17.9	1.08	1640.	ε'_{cr}
405,406	IFA-4[illegible] [51,52]	1	.3913	2.0-6.7	95.0	7.0	15.†††	1.0†††	[illegible]†††	1.31	2000.	.12	491.†††	14.0	1.20	810.	ε'_{fx},ε'_{cr},ε'_{cx}
407	IFA-173 [42]	1	.4921	10.6	93.4	6.1	15.†††	.96	[illegible]†††	1.66	490.	.34	464.	12.9	1.16	36.	ε'_{fx}
408-410	IFA-404 II [50]	3	.4980	2.4	90.1-95.6	7.0	15.†††	2.0†††	2.4	1.64	490.	.17	454.	16.3	1.08	3900.	ε'_{cr}
411-414	MTR [53,54]	4	.2483-.2498	.3,1.0	95.7-97.4	43.0-49.9	15.	.04-.06	10.2,11.9	.41	2000.	.39	516.	13.0-15.6	1.23	285.,320.	ε_{cx},ε_{cr},ε'_{cx},ε'_{cr},GR
415-423	IFA-429 [55]	9	.3[illegible]	8.0	91.-95.	13.	375.	1.0	1.1	.86	490.	.56	464.	7.2-12.0	1.02-1.30	960.	TF,P
424-429	IFA-4[illegible] [56-59]	6	[illegible]	1.9-14.5	92.,95.	10.	15.	.59-.94	0.0	1.86-1.89	490.	.36	464.	5.6-8.2	1.08	17.	TF,hg'

* Zircaloy unless otherwise noted

† Helium unless otherwise noted

** Standard Design Package (vs time): centerline temperature, gas release fraction, h_{gap}, internal pressure void volume, gas abundance, gap size, gas helium fraction

†† Core average rod power

*** Clad surface temperature specified

††† Assumed

- TF - fuel centerline temperature
- ε_{cr} - clad circumferential deformation
- ε_{cx} - clad axial deformation
- GR - gas release fraction
- P - rod internal pressure
- hg - gap conductance
- GRMOL - gas content
- GCOMP - gas composition
- VO - void volume
- ε_{fx} - fuel axial deformation
- ZrO_2 - clad corrosion thickness
- H_2 - clad hydrogen concentration
- NOTE: prime (') indicates instrumented rod data

VERY POOR ORIGINAL

1569 145

23-353

TABLE 3. FRAP-S3 MODEL VERIFICATION - RUN IDENTIFICATION AND NOMINAL INPUT (cont'd)

Run No.	Reference	Number Rods	Clad ID* (in)	Diametral Gap (mils)	Fuel Density (%)	Enrichment (%)	Fill Gas† (psia)	Cold Plenum (in)	Dish (%)	Fuel Length (ft)	Loop Press. (psia)	Mass Flow (10^6 #/hr-ft^2)	Inlet Temp. (°F)	Peak Power (kW/ft)	Peak/Avg. (axial)	Operating Hours	Output
430	PBF[31]	1	[illegible]	9.9	92.	9.5	300.	3.04	1.3	2.89	2160.		540.	13.6	1.349	33.1	TF
431, 432	PBF[60]	2	.4252	7.9	95.	10.	15.	2.17	0.0	2.98	1040.	1.9	401.	11.2,10.6	1.348	2.25,2.0	TF,hg'
433-436	PBF[61]	4	.3740	8.0	93.3	20.	376.,550.	2.0	1.0	2.99	2160.	2.5,2.6	590.	11.3-12.0	1.349	2.0,2.6	TF,hg',P',ϵ'_{cx}
437-440	PBF[62]	4	.3740	8.0	93.3	20.	376.	2.0	1.0	2.99	2220.	2.4	590	12.6-13.7	1.349	2.9,5.0	TF,hg',P',ϵ'_{cx}
441-445	IFA-418,419[63]	5	.3661	9.0	91.6-95.0	6.	614.,323.	4.15	2.7	2.46	490.	2.9	460.	10.1,7.04	1.20	3601,4501	TF
446-449	PBF[64]	4	.3740	7.9	93.3	20.	376.,550	2.0	1.0	3.0	2200.	2.5	590.	11.5-15.5	1.348	3.6	TF,P',ϵ'_{cx}
450-453	PBF[65]	4	.4248	8.7,3.9	97.,95.	10.	374.(Xe,He,Ar)	2.17	0.0	3.0	1040.	.14-.63	510.	10.9-11.8	1.348	6.0	TF,hg'
454-457	PBF[66]	4	.3443	3.7,13.6	94.	12.5	363.-390.(Xe)	2.26	1.3,1.4	2.89	2205.	1.3-3.6,1.6	630.	6.3-15.7	1.348	22.5-39.	TF,hg'
458,459	PBF[67]	2	.3444	8.6	94.	12.5	389.,377(Xe)	2.0	1.6	2.89	2206.	1.6	540.	4.8,4.4	1.348	3.5	hg'
460A-463A	PBF[68]	4	.3443,.3444	3.3-3.9	94.	12.5	1204.,377(Xe)	2.0	1.3	2.89	2205.	3.6,1.6-3.1	630.	8.2-14.9	1.348	10-12	TF,P',ϵ'_{cx}
464A	PBF[69]	1	.3445	8.7	92.	12.5	175.(Xe)	2.0	1.4	2.89	2206	1.6	540.	5.0	1.348	1.5	hg'
460-462	SAXTON[70]	3	.3435	7.5	92.	12.5,9.5	314.	3.0	1.33	2.88	2250	2.7	480.	6.16-6.7	1.49	13571	ϵ_{cr},VO,GCOMP,P
463-465	SAXTON[70]	3	.3435	7.5	92.	12.5	12.9(Air)	2.0	1.33-1.41	2.97	2250.	2.7	480.	6.02-6.54	1.49,1.42	13571	ϵ_{cr}
466,467	SAXTON[70]	2	.3435	7.5	92.	9.5,12.5	385.,314.	3.0	1.41	2.88	2250	2.7	480.	5.54,6.06	1.42	13571	ϵ_{cr}
468	SAXTON[70]	1	.3435	7.5	92.	12.5	12.9(Air)	2.0	1.41	2.97	2250.	2.7	480.	6.2	1.37	13571	ϵ_{cr}
469-472	SAXTON[70]	4	.3435	7.5	92.	12.5	314.	3.0	1.41	2.88	2250.	2.7	480.	6.15-6.45	1.37	13571	ϵ_{cr}
473-475	SAXTON[70]	3	.3435	7.5	92.	12.5	12.9(Air)	2.0	1.41	2.97	2250	2.7	480.	6.48-6.77	1.37,1.43	13571	ϵ_{cr}
476-478	SAXTON[70]	3	.3435	7.5	92.	12.5	314.	3.0	1.41	2.88	2250	2.7	480.	6.65-6.92	1.43	13571	ϵ_{cr}
479-481	SAXTON[70]	3	.3435	7.5	92.	12.5	12.9(Air)	2.0	1.41	2.97	2250	2.7	480.	6.77-6.99	1.36-1.43	13571	ϵ_{cr},VO,GCOMP,P
482-489	SAXTON[70]	8	.3445	6.5	94.	5.7	12.9(Air)	1.8	1.42	3.0	2250	2.7	480.	1.23-3.11	1.22-1.28	13571	ϵ_{cr}
490, 491	SAXTON[70]	2	.3430, .3435	9.0, 9.5	94.	12.5	385.,430.	3.0	1.41	2.92	2250	2.7	480.	2.73,5.78	1.42,1.28	13571	VO,GCOMP,P
492-499	MAINE YANKEE[71]	8	.3880	8.5	92.2-93.3	2.4	14.7	5.8	1.37	11.4	1866	2.3	525.	6.90-7.35	1.191	11821	GR,ϵ_{fx},ϵ_{cr},VO,GCOMP
500-507	MAINE YANKEE[71]	8	.3880	8.5	92.3-93.6	2.4	14.7	5.8	1.37	11.4	1866.	2.3	525.	6.63-7.34	1.191	11821	GR,ϵ_{fx},ϵ_{cr},VO,GCOMP
508-514	MAINE YANKEE[71]	7	.3880	8.5	91.7-93.6	2.01	14.7	5.8	1.37	11.4	1866.	2.3	525.	6.18-6.71	1.91	11821	GR,ϵ_{fx},ϵ_{cr},VO,GCOMP
515-521	MAINE YANKEE[71]	7	.3880	8.5	92.7-94.0	2.95	14.7	5.8	1.37	11.4	1866.	2.3	525.	5.20-6.07	1.91	11821	GR,ϵ_{fx},ϵ_{cr},VO,GCOMP
522-542	H.B.ROBINSON[72-80]	21	.3734	6.5	92.0	3.1	275.	6.83	1.47	11.98	2250.	2.3	536	7.00-7.65	1.135	19177	ϵ_{fx},ϵ_{cr},VO,GCOMP,P
543-548	BIG ROCK POINT[81,82]	6	.4825	11.5	[illegible]	1.92-2.29	14.7	5.60	2.86,0.0	5.72	1350.	1.2	540.	9.0-10.6	1.19-1.33	6468,13420	GR,ϵ_{fx},ϵ_{cr},ϵ_{cx},GCOMP
549,550	EPRI[83]	2	.5256,.5145	11.6,3.5	95.	2.98	4.4	.246	0.0	.463	50.	[illegible]	172.,162.	21.58,16.06	1.00	1689	GR
551,552	EPRI[83]	2	.5456	9.6	97.8	4.5	14.7(Ar,He)	.058	1.49	.53	1120.	2.6	471.,463.	15.22,21.33	1.29,1.39	2815.	ϵ'_{cr},ϵ_{cx},ϵ'_{cx}
553	[illegible][83]	1	.3660	12.0	96.	6.0	320.	4.0	2.17	2.45	490.	.29	460.	[illegible]	1.04-1.07	5936	TF
555	[illegible]	1	.4205	8.3	94.4	2.05	14.7	5.5	[illegible]	1.67	1160.	3.4	491	16.37	1.22,1.23	1817	TF,GR
556-5[illegible]	[illegible][84]	30	.3803-.3808	6.3-6.8	94.-96.	2.76-3.49	14.7	1.90		3.00	1017.	1.2	528.	4.53-7.45	1.10-1.48	28167-47350	GR,ϵ_{cr},ZrO_2,H_2,GCOMP,VO,ϵ_{cx}
586	IFA-206[85]	1	.5941	11.4	95.	6.0	14.7	4.27	2.06	5.05	490.	.84	460.	14.51	1.22	6576	TF
587	IFA-208[85]	1	.4992	11.8	94.5	7.0	14.7	3.15	0.0	4.82	490.	.33	460.	18.7	1.22	2706	TF
588,589	IFA-211[85,95]	2	.4992	11.0	94.3	6.0	14.7	5.20	1.06	4.92	490.	.34	460.	17.67	1.22	10285	TF,GR
590A,590B	IFA-224[85]	2	.4992	11.8	89.3	7.0	14.7	3.15	0.0	4.82	490.	.34	460.	16.15	1.22	2556	TF
591	IFA-230[85]	1	.4992	9.8	95.9	6.0	14.7	5.20	0.0	4.92	490.	.34	460.	17.67	1.22	9596	TF
592-594	IFA-410[85]	3	[illegible]	7.9-15.6	94.0	7.09	14.7	1.75									

* Zircaloy unless otherwise noted

† Helium unless otherwise noted

** Standard Design Package (vs time): centerline temperature, gas release fraction, h_{gap}, internal pressure void

†† Core average rod power

††† Clad surface temperature specified

‡‡‡ Assumed

TF - fuel centerline temperature

ϵ_{cr} - clad circumferential deformation

ϵ_{cx} - clad axial deformation

GR - gas release fraction

P - rod internal pressure

hg - gap conductance

GRMOL - gas content

GCOMP - gas composition

VO - void volume

ϵ_{fx} - fuel axial deformation

ZrO_2 - clad corrosion thickness

H_2 - clad hydrogen concentration

NOTE: prime (') indicates instrumented rod data

VERY POOR ORIGINAL

1569 146

TABLE 3: FRAP-S3 MODEL VERIFICATION - RUN IDENTIFICATION AND NOMINAL INPUT (cont'd)

Run No.	Reference	Number Rods	Clad ID* (in)	Diametral Gap (mils)	Fuel Density (%)	Enrichment (%)	Fill Gas† (psia)	Cold Plenum (in)	Dish (%)	Fuel Length (%)	Loop Press. (psia)	Mass Flow (10^6 #/hr-ft^2)	Inlet Temp. (°F)	Peak Power (kW/ft)	Peak/Avg. (axial)	Operating Hours	Output
595,598,599	IFA-411[85,86]	3	.4249	6.8	94.8	7.09	14.7	5.2	0.0	4.92	490.	.34	460.	13.4	1.22	3491-5496	TF, ϵ'_{fx}, ϵ'_{cx}
596,597	IFA-410[85]	2	.3661	12.2	95.7	12.,6.	323.	3.97	1.47	2.46	490.	.29	464.	15.24,13.25	1.06	1686,2800	TF
600-602	IFA-409 II[86]	3	.4252	9.1	92.6-92.9	2.73,2.89	14.7	6.0	1.93	.82	490.	.24	460.	6.56	1.07	4525	ϵ'_{fx}
603-605	IFA-418[87]	3	.3661	12.2,9.0	95.7,92.1	12.,6.	514.	4.0	1.47	2.46	490.	.29	460.	10.06-15.54	1.05	6631	ϵ'_{fx}
606,607	IFA-419[87]	2	.3661	9.0	91.2,94.3	6.	323.	4.0	1.47	2.46	490.	.29	460.	7.01	1.05	5341	ϵ'_{fx}
608-610	IFA-427[87]	3	.3661	7.4,12.2	93.0	3.95,12.	323.,514.	4.0	1.47	2.46	490.	.29	460.	9.14	1.05	2001	ϵ'_{fx}
611	IFA-207[88]	1	.5941	11.4	95.	6.	14.7	4.27	2.85	5.05	490.	.84	460.	13.7	1.22	2785	TF
612,613	IFA-263[86,97]	2	.4992,.4988	6.3,5.9	94.7	6.01	14.7	3.66	0.0,2.02	1.98	490.	.36	460.,465.	22.41,17.67	1.26,1.45	5925,10720	TF
614A-615B	TMECO I, II[89]	4	.6929	3.9	95.7	1.35	14.7(XE)	.44	0.0	.46	500.	0.0	205.-880.	20.0	1.00	2870,16725, 16705	TF
616A,616B	IFA-227 I[91]	2	.5520	8.7,2.8	96.6	2.4	14.7	.28	0.0	1.72	490.	.20	460.	17.45	1.15	59.4	ϵ'_{cr}
617B	IFA-227 II[90]	1	.5522	3.0	96.5	2.4	14.7	.28	.33	1.72	490.	.26	460.	19.5	1.15	45.6	ϵ'_{cr}
618A,618B	IFA-227 III[90]	2	.5520	2.8	96.6	2.4	14.7	.28	26,0.0	1.72	490.	.20	460.	13.62	1.15	38.8	ϵ'_{cr}
619A,619B	IFA-227 IV[90]	2	.5512	2.8	90.,95.	2.4	14.7	.59	.45	1.61	490.	.26	460.	11.43	1.08	32.6	ϵ'_{cr}
620-628	IFA-106[92]	9	.4252	5.2,7.2	94.6-95.5	10.02	14.7	3.31	0.0	2.38	490.	1.2	464.	9.02-14.32	1.31,1.15	9506	TF, P', GR, ϵ'_{fx}, ZrO_2, ϵ'_{cx}
629-632	IFA-107[92]	4	.4252	5.2,7.2	94.8,95.5	10.02	14.7	3.31	0.0	2.38	490.	1.2	464.,460.	9.46-15.26	1.35,1.08	3375	TF, P', GR, ZrO_2
633-639	IFA-138[93]	7	.7480	7.1,4.3	93.9	3.0	14.7(XE)	.20†††	2.14	1.43	490.	.31	460.,464.	15.43-18.49	1.21,1.23	11960	GR
640-644	IFA-142[93]	5	.7480	4.7	94.3	3.0	14.7(XE)	.20†††	2.16,2.02	1.43	490.	.31	464.,460.	16.3-21.41	1.15,1.20	8900	GR
645,646	IFA-206[93]	2	.5941	11.4	95.	6.0	14.7	4.27	2.85,0.0	5.05	490.	.84	460.	12.26,13.12	1.22	6560	GR
647-650	BRP(MO_2)[94]	4	.4820-.4824	9.8-12.4	90.7-94.6	1.92-2.29	14.7	5.59-5.80	2.84,0.0	5.70	1350.	1.2	540.	6.90-9.23	1.28	27811	ϵ'_{fx}, ϵ'_{cr}, ϵ'_{cx}
651-657	BRP(MO_2)[94]	7	.4820	11.0	92.0	2.16-8.86	14.7	5.7†††	0.0	5.64,5.70	1350.	1.2	540	8.96-11.55	1.37	21343	ϵ'_{fx}, ϵ'_{cr}, ϵ'_{cx}
658-665	IFA-118 I[95]	8	.5522-.5525	1.5-4.1	95.7	6.0	14.7	1.53	0.0,.712	1.64	490.	.28	465.,460.	15.7-19.4	1.35,1.20	1728	ϵ'_{cx}
666-669	IFA-118 II[95]	4	.5522-.5525	3.8-4.1	96.0	6.0	14.7	1.57-1.90	0.0-1.02	1.64	490	.28	465.,460.	12.4-15.7	1.34,1.10	1344	ϵ'_{cx}
670-675	IFA-118 III[95]	6	.5521-.5528	1.3-3.9	96.[illegible]	6.0	14.7	1.52-1.70	0.0,.714	1.64	490.	.28	465.,460.	14.1-16.7	1.30,1.20	2736	ϵ'_{cx}
676-686	IFA-402[96]	11	.500	2.4-9.6	94.6,99.0	7.0	14.7	2.95	2.38,2.37	1.64	490.	.34	460.	9.3-9.75	1.17,1.16	70	ϵ'_{cx}
687-691	IFA-215[100]	5	.5502	4.0	96.0	6.0	14.7	2.9†††	.711	1.64	490.	.32	465	10.06-14.66	1.30,1.20	78	ϵ'_{cx}
692,693	IFA-216[101]	2	.5126	6.7	90.1,94.8	9.7	14.7	2.9†††	0.0	1.64	490	[illegible]	465.,466	20,14.26	1.30,1.20	193,137	ϵ'_{cx}
694-697	IFA-413[38]	4	.4988	2.3-9.8	95.6	7.0	14.7	1.5†††	0.0,2.38	1.64	490.	.34	460.,465.	8.23-10.42	1.17,1.16	98	ϵ'_{cx}
698,699	IFA-410[38]	2	.489	7.9	94.6,96.9	7.09	14.7	1.75†††	0.0	1.64	490.	.33	464.	12.19	1.12	50	ϵ'_{cx}
700-702	IFA-411[38]	3	.4249	6.8	94.[illegible]	7.09	14.7	5.2†††	0.[illegible]	4.92	490.	.34	460.	12.19	1.22	50	ϵ'_{fx}, ϵ'_{cx}

* Zircaloy unless otherwise noted

† Helium unless otherwise noted

** Standard Design Package (vs time): centerline temperature, gas release fraction, h_{gap}, internal pressure void volume, gas abundance, gap size, gas helium fraction

†† Core average rod power

*** Clad surface temperature specified

††† Assumed

- TF - fuel centerline temperature
- ϵ_{cr} - clad circumferential deformation
- ϵ_{cx} - clad axial deformation
- GR - gas release fraction
- P - rod internal pressure
- hg - gap conductance
- GRMOL - gas content
- GCOMP - gas composition
- VO - void volume
- ϵ_{fx} - fuel axial deformation
- ZrO_2 - clad corrosion thickness
- H_2 - clad hydrogen concentration
- NOTE: prime (') indicates instrumented rod data

VERY POOR ORIGINAL

1569 147

2. STANDARD DESIGN STUDY

Steady-state fuel behavior calculations were performed with FRAP-S3 for standard design commerical fuel rods. Considerations of Standard Design Studies within the scope of both FRAP-S and FRAP-T verification is a continuation of previously reported analyses[3,107,109,110]. The main objectives here have always been 1) to establish model performance characteristics for both normal and off-normal power reactor design and operating conditions, and 2) to provide realistic parameter ranges by means of which apparent model capabilities inferred from test rod analysis can be interpreted.

Revised thermal models incorporating the initial pellet relocation, crack closure, and effective thermal conductivity feedbacks were used to generate the FRAP-S3 standard design results discussed below. Comparisons between FRAP-S2 and FRAP-S3 runs precedes a section discussing response surface characterization of FRAP-S3 output.

2.1 Model Comparison

Analytical comparisons were performed between FRAP-S3 and previously reported[3] FRAP-S2 results so as to establish the cumulative effect of model changes on code output. Predictions for key thermal, mechanical, and surface condition parameters are compared versus burnup and power for representative 7 x 7 and 15 x 15 fuel designs. Previous results[3,107] have shown that output trends for more recent 8 x 8 and 17 x 17 design

1569 148

types are consistent with those identified for the incumbant fuel, differing only in magnitude due to lower heat rating, fuel temperature and sensitivity to burnup.

The comparison runs represent steady operation of core average PWR and BWR rods at full reactor power. The results correspond to typical output characteristics of the code, and as such are suitable for scoping overall differences between code versions. Ramp cases were also investigated at beginning, middle, and end-of-life. Rod average discharge burnup is about 32000 MWd/TU for high burnup runs. The axial peaking factor is 1.4. Respectively, rod average heat rating is 23 and 24.3 kW/m for 15 x 15 and 7 x 7 runs. All local results presented here, such as fuel temperature, gap size and cladding deformation, will correspond to the axial peak power location.

Figures 1 and 2 compare FRAP-S2 and FRAP-S3 calculated center temperature versus operating time for 7 x 7 and 15 x 15 rods. The fact that relocation increases gap conductance while decreasing pellet thermal conductivity, results in different trends between unpressurized and pressurized rods.

Higher FRAP-S3 gap conductance for the BWR rod outweighs the effect of lower pellet conductivity. The net results relative to FRAP-S2 are lower center temperature, stored energy and internal pressure (gas release), as seen in Figures 1, 3, and 4. These are desirable trends given the previously identified[3] conservative temperature history and rapid pressure buildup calculated by FRAP-S2. BWR thermal conditions

1569 149

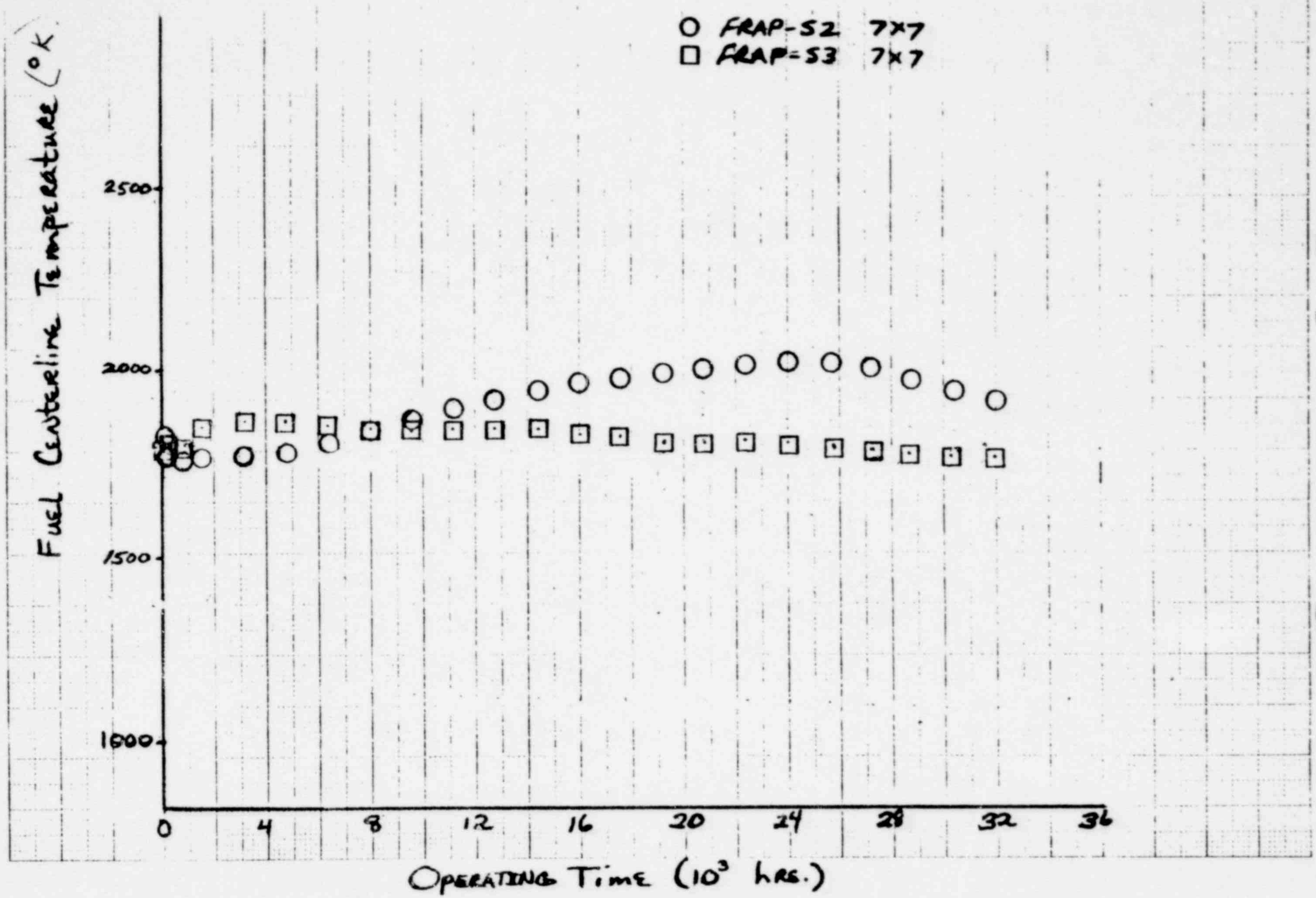

FIGURE 1 : FRAP-S2 AND FRAP-S3 CENTER TEMPERATURE HISTORIES FOR A CORE AVERAGE 7x7 ROD

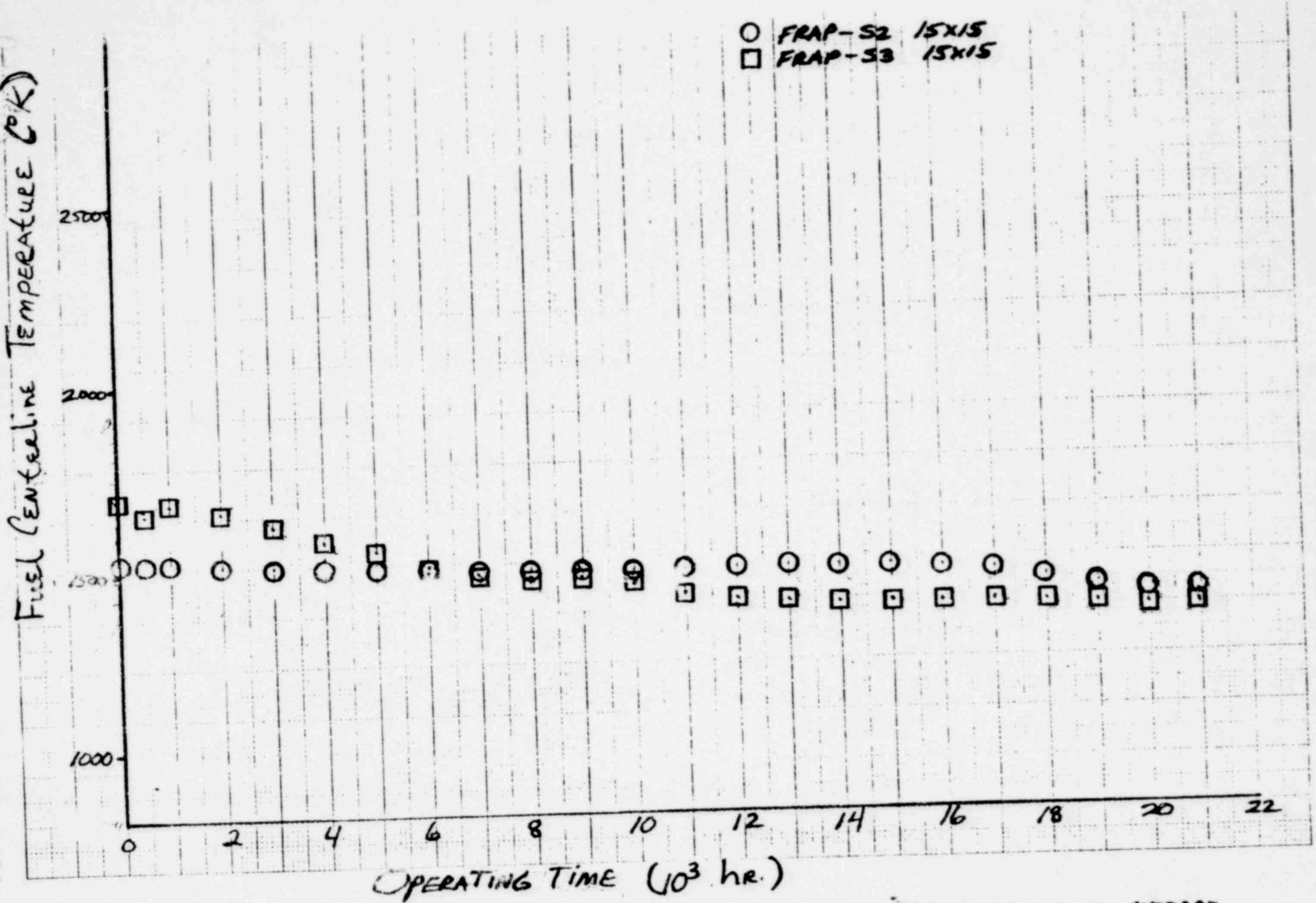

Figure 2 : FRAP-S2 AND FRAP-S3 CENTER TEMPERATURE HISTORIES FOR A CORE AVERAGE 15X15 ROD

1569 151

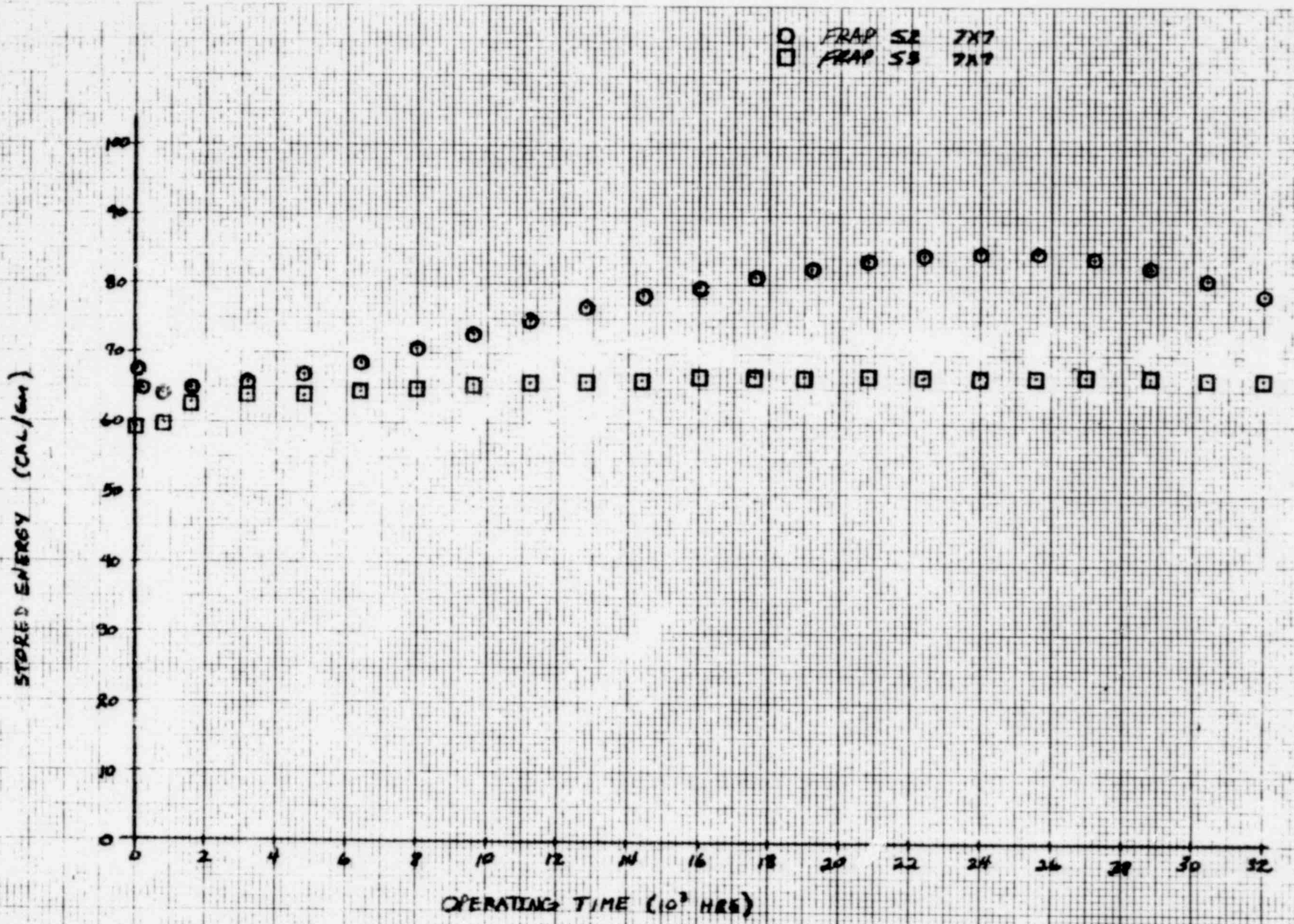

FIGURE 3 FRAP-S2 AND FRAP-S3 STORED ENERGY HISTORIES FOR A CORE AVERAGE 7X7 ROD

1569 152

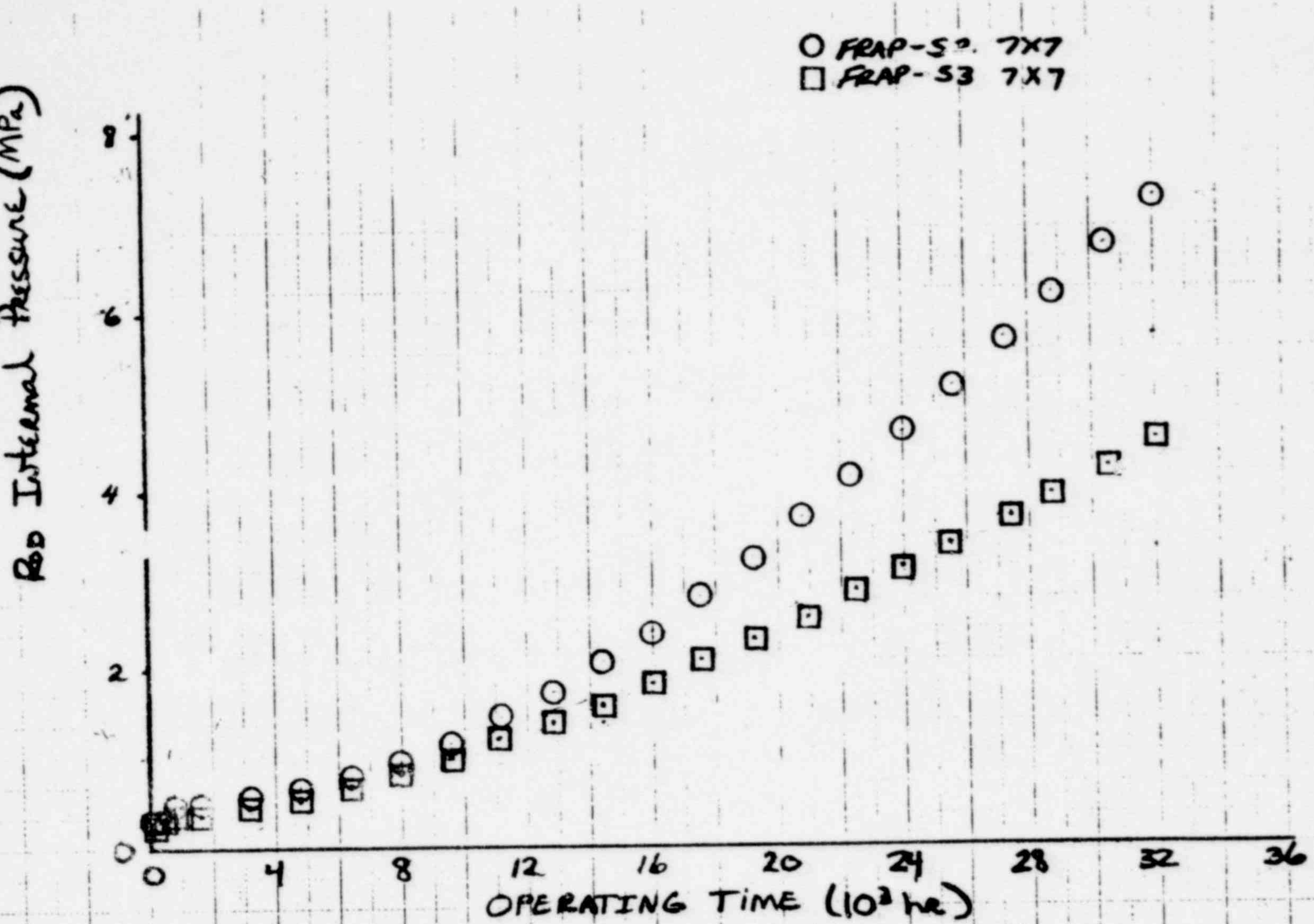

FIGURE 4 : FRAP-S2 AND FRAP-S3 INTERNAL PRESSURE HISTORIES FOR A CORE AVERAGE 7X7 ROD

are calculated by FRAP-S3 to be relatively stable as burnup increases. The effect of negative cladding strain on pellet thermal conductivity (due to crack closure) is almost balanced against the cumulative effect of degraded gas mixture conductivity. The effect of revised FRAP-S3 thermal models can be stronger under lead rod operating conditions as seen in the Figure 5 stored energy comparison for beginning of life ramp cases. It should be noted however that subsequently discussed thermal data comparison results indicate that existence of open, fission gas filled pellet cracks can increase calculated stored energy relative to previous models.

The effect of relocation on the pressurized rod temperature history in Figure 2 is to initially increase temperatures relative to FRAP-S2. This trend is consistent with previously identified modeling needs based on the underprediction of pressurized rod thermocouple data[3,110]. The corresponding stored energy histories for core average 15 x 15 rods are shown in Figure 6. Calculated FRAP-S3 thermal conditions are observed to decrease with burnup. Unlike the BWR case, the effect of more cladding creep collapse under PWR conditions helps the resultant pellet conductivity increase outweigh the relatively small gas release effect. Differences in PWR thermal conditions between FRAP-S2 and FRAP-S3 are not enough to cause significant changes in the rod pressure levels shown in Figure 7, again since gas release calculated by either model is low for PWR rods.

Significant differences in hot gap dimension between FRAP-S2 and FRAP-S3 can be noted for both 7 x 7 and 15 x 15 rods shown in Figures 8

1569 154

175

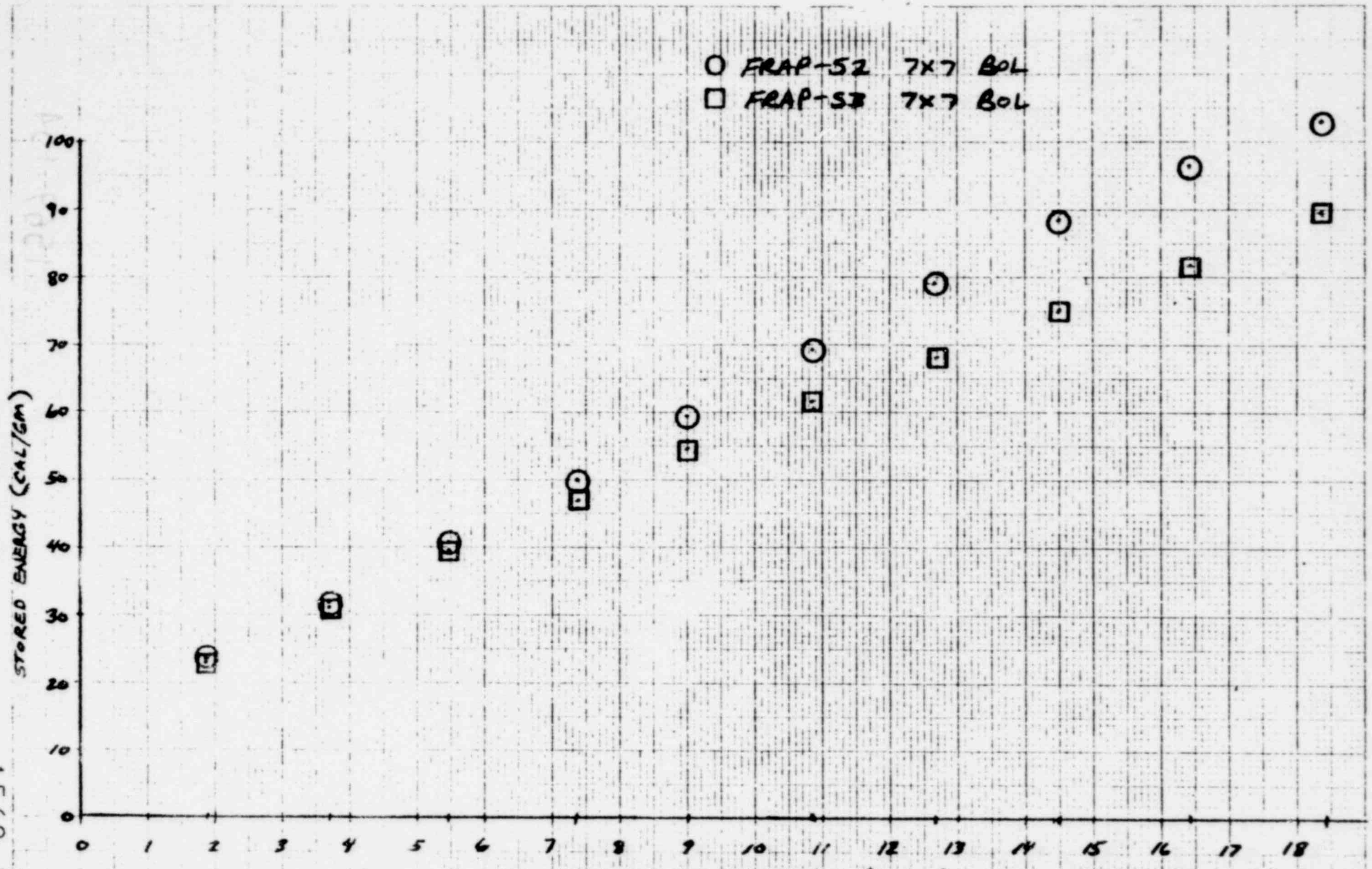

FIGURE 5 : FRAP-S2 AND FRAP-S3 STORED ENERGY VS. HEAT RATING FOR A 7X7 ROD
AT BEGINNING OF LIFE

1569 155

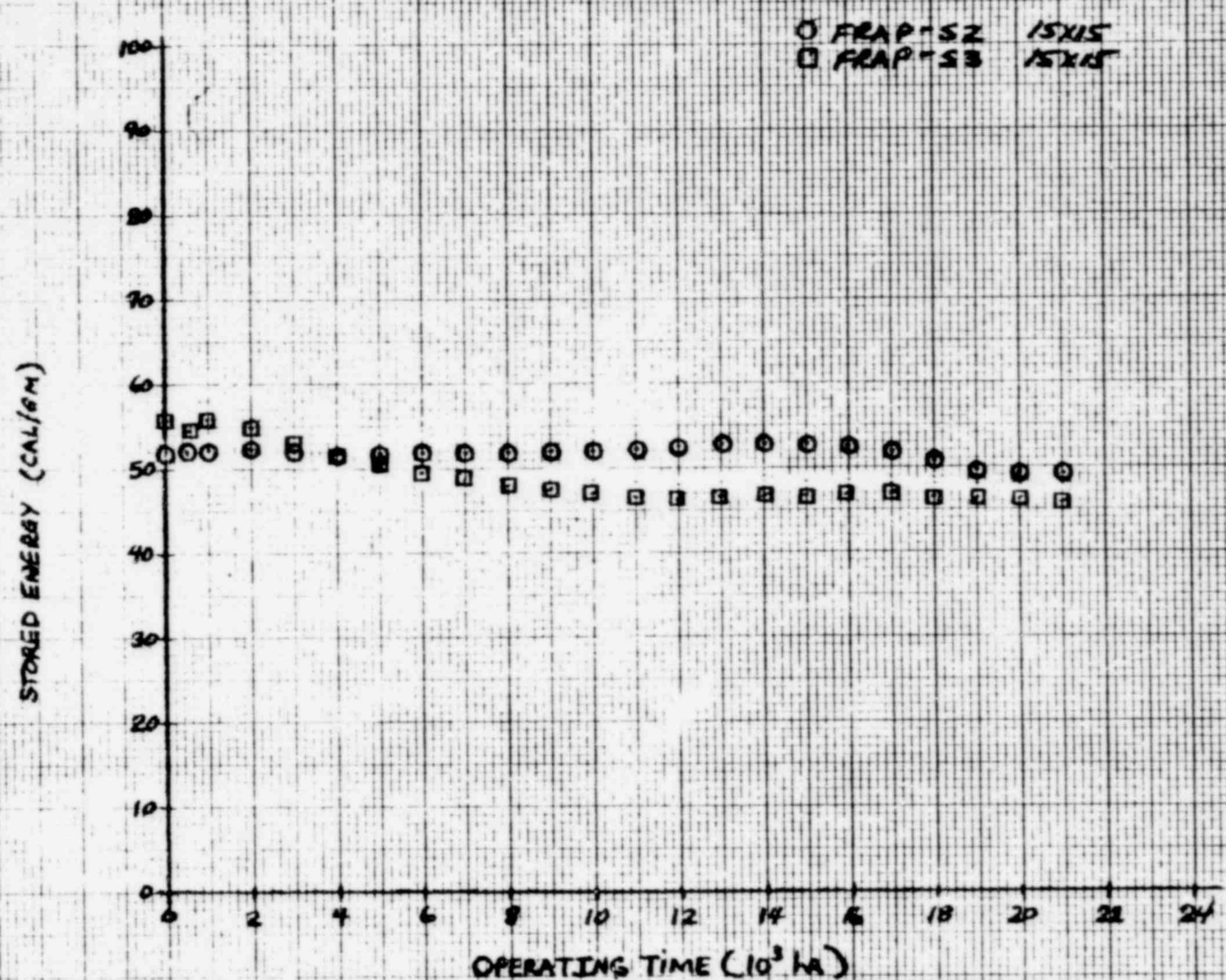

FIGURE 6 : FRAP-S2 AND FRAP-S3 STORED ENERGY HISTORIES FOR A CORE AVERAGE 15X15 ROD

1569 156

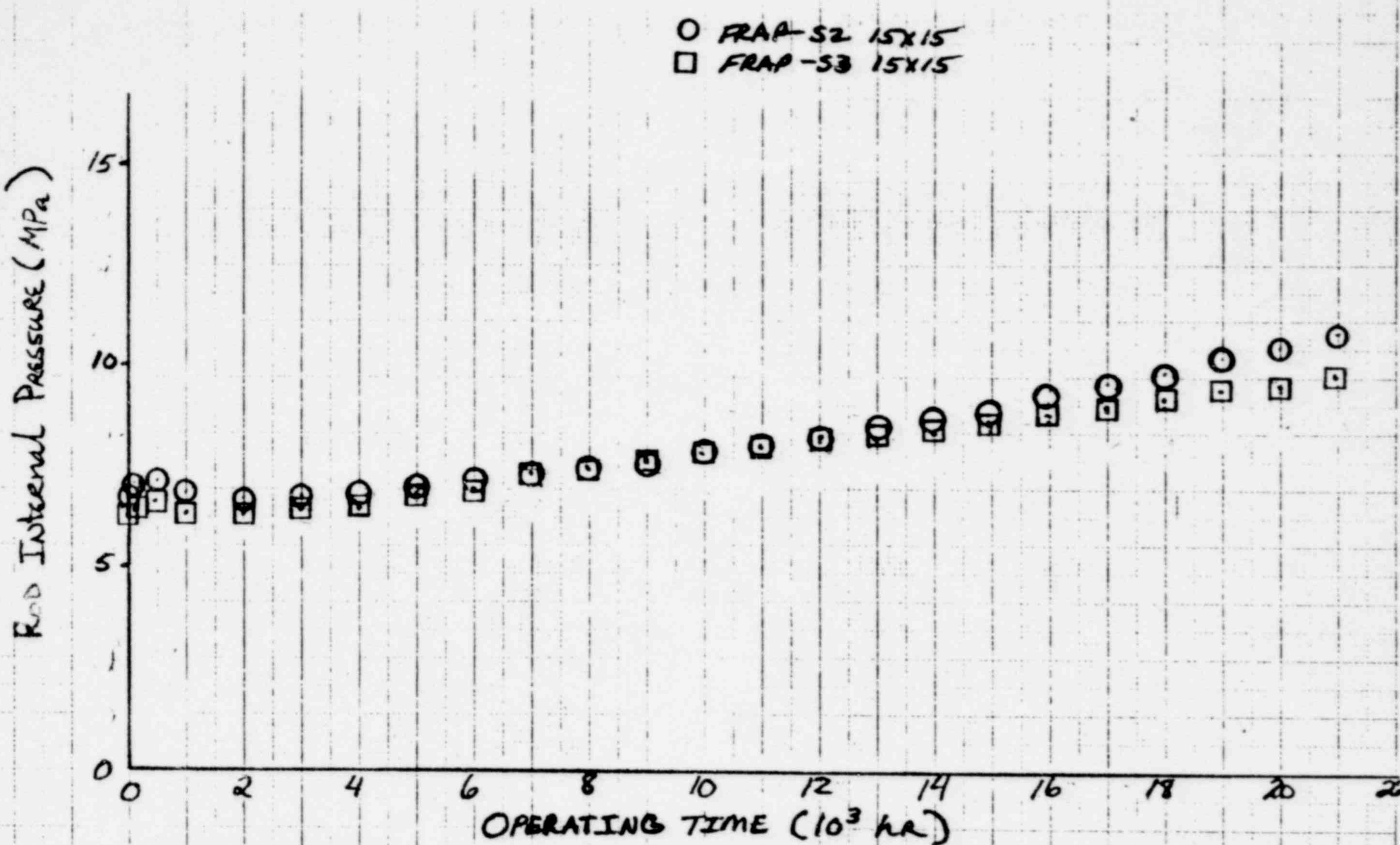

FIGURE 7: FRAP-S2 AND FRAP-S3 INTERNAL PRESSURE HISTORIES FOR A CORE AVERAGE 15X15 ROD

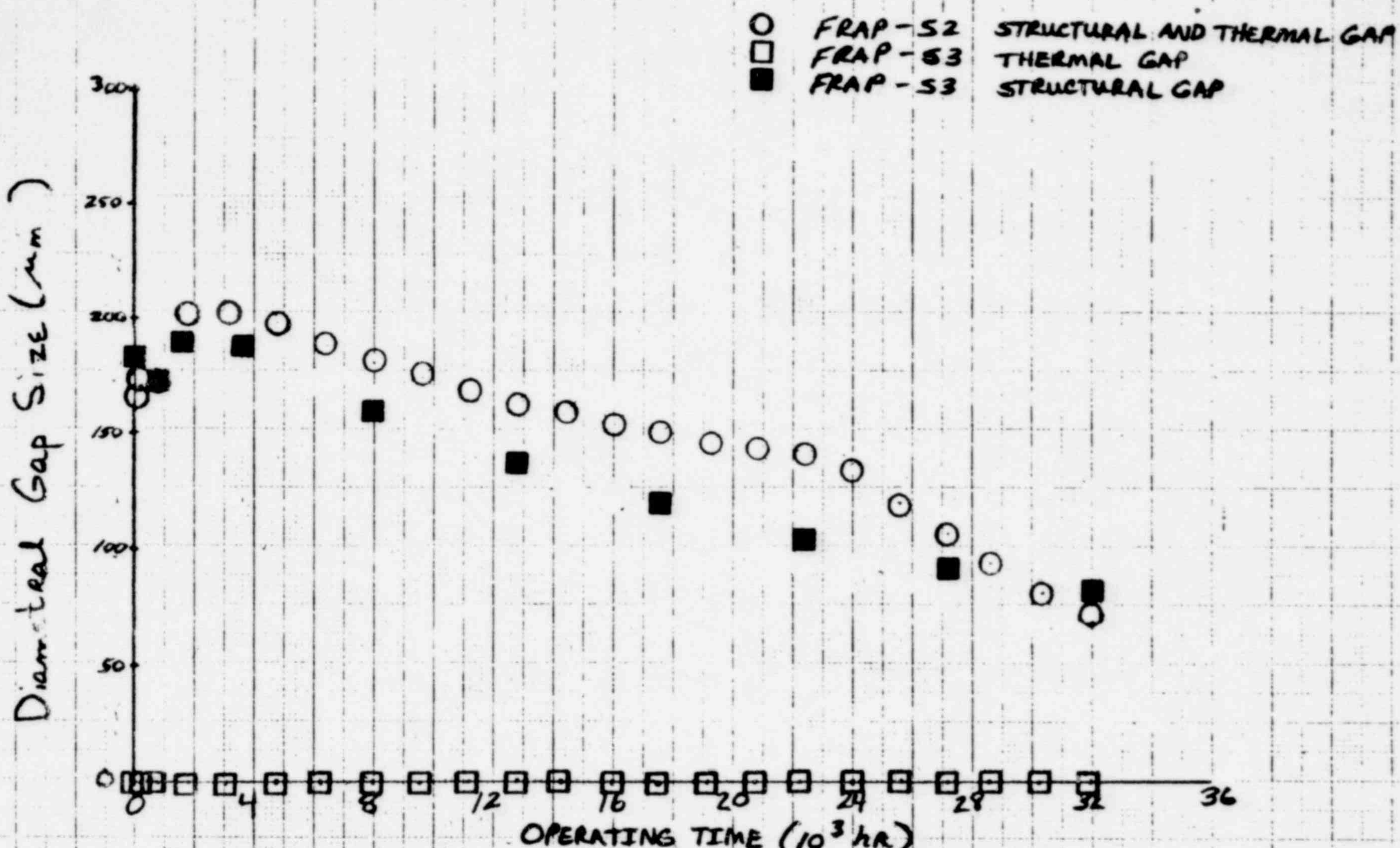

Figure 8: FRAP-S2 AND FRAP-S3 GAP HISTORIES FOR A CORE AVERAGE 7x7 ROD

1569 158

and 9. The gaps used in FRAP-S2 for both structural and thermal analysis are essentially the same, differing by virtue of the originally used "repack" factor by only about .1 mils. FRAP-S3 incorporates a much more active pellet relocation concept in its thermal analysis as indicated by the zero gap history predicted for both fuel designs. Soft gap closure conditions are calculated to exist even at the moderate power levels reflected in a core average irradiation history. It should be noted that positive cladding stresses are not calculated by FRAP-S3 until the structural gap closes. Full coupling between relocation and deformation models requires treatment of pellet mechanical strain in subsequent code versions.

The currently indicated structural gap differences between FRAP-S2 and FRAP-S3 are not consequences of the new relocat... model, but rather the result of other changes in cladding creep properties. The effect of implementing a new creep model with a fast flux enhancement term, in addition to revised cladding temperature and stress dependence, is shown for 15 x 15 and 7 x 7 rods in Figures 10 and 11. FRAP-S3 hoop strain for the 7 x 7 rod in Figure 11 includes the effect of a larger rod/system pressure difference (previously shown in Figure 4), in addition to the effect of higher cladding creep rate. The cladding strain history for the PWR rod shown in Figure 10 indicates a strain hardening effect on creep rate after the accumulation of about 1% deformation. The initiation of a positive strain rate near end-of-life corresponds to the incidence of structural gap closure previously shown in Figure 9. Figure 12 illustrates how structural gap differences between current and previous models also changes both the calculated onset of PCI and the related cladding strain range consequences of hard gap closure.

1569 159

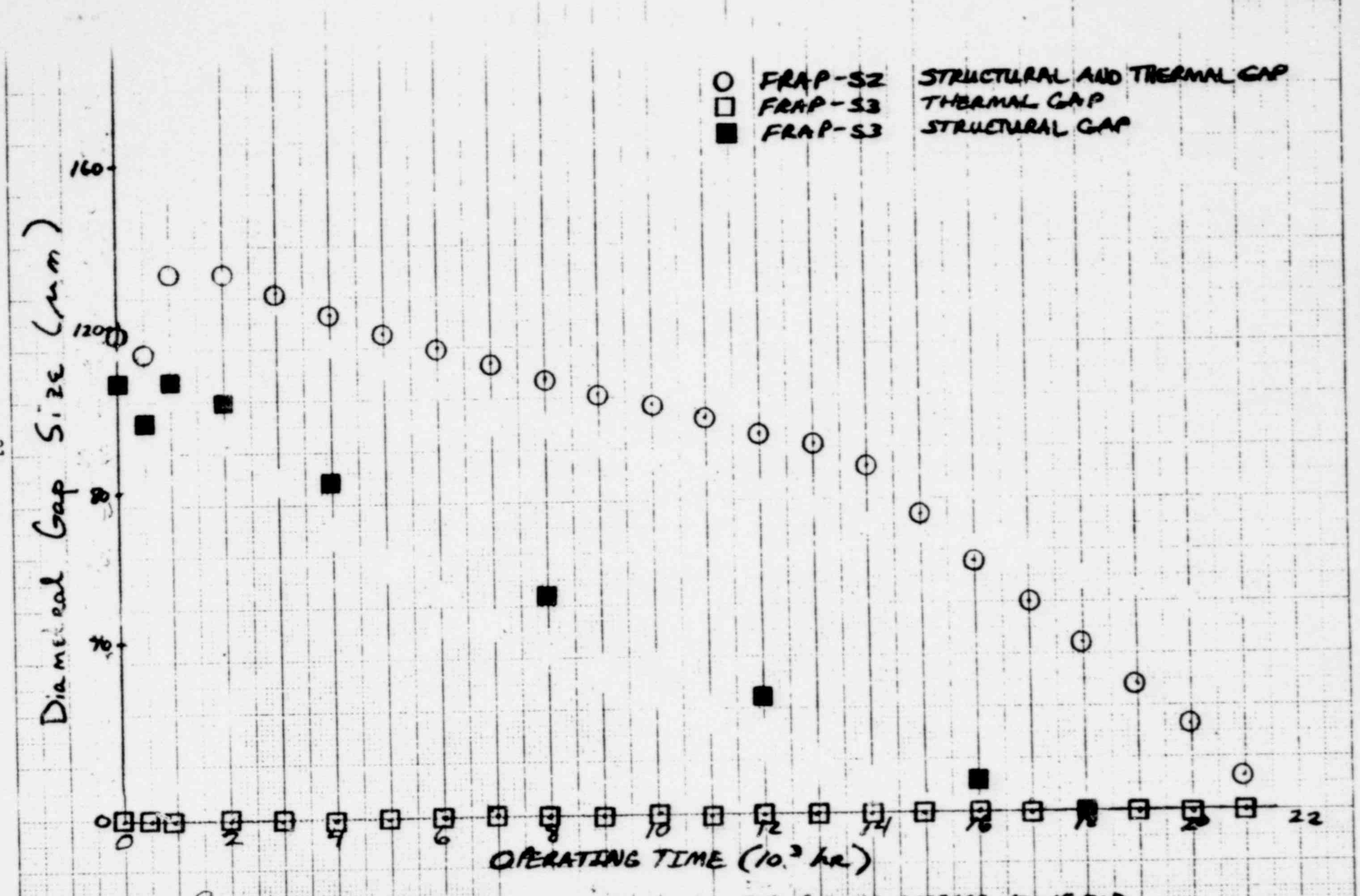

Figure 9 : FRAP-S2 AND FRAP-S3 GAP HISTORIES FOR A CORE AVERAGE 15x15 ROD

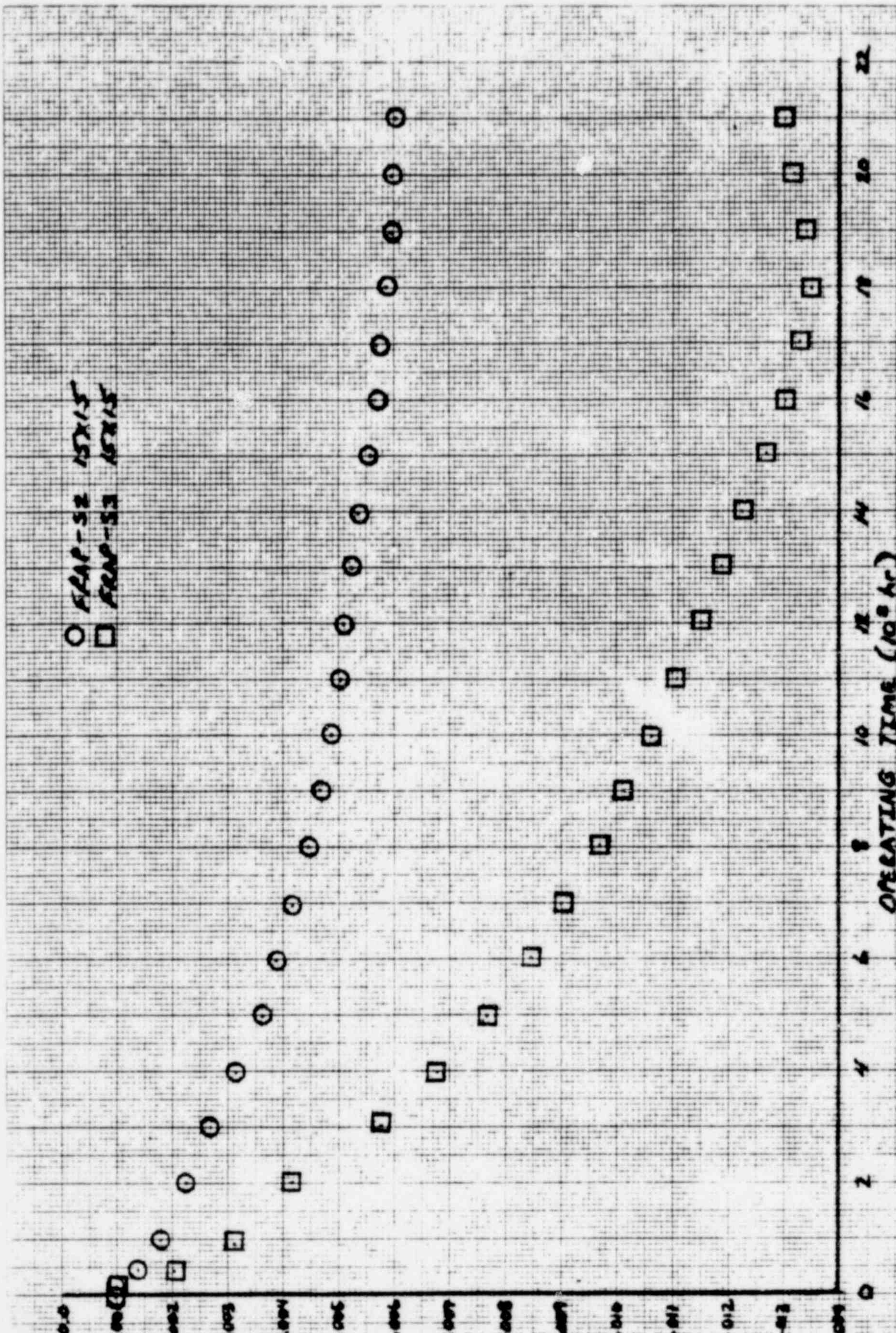

Figure 10 : FRAP-S2 AND FRAP-S3 CLADDING HOOP STRAIN HISTORIES FOR A CORE AVERAGE 15X15 ROD

SD1

23-361

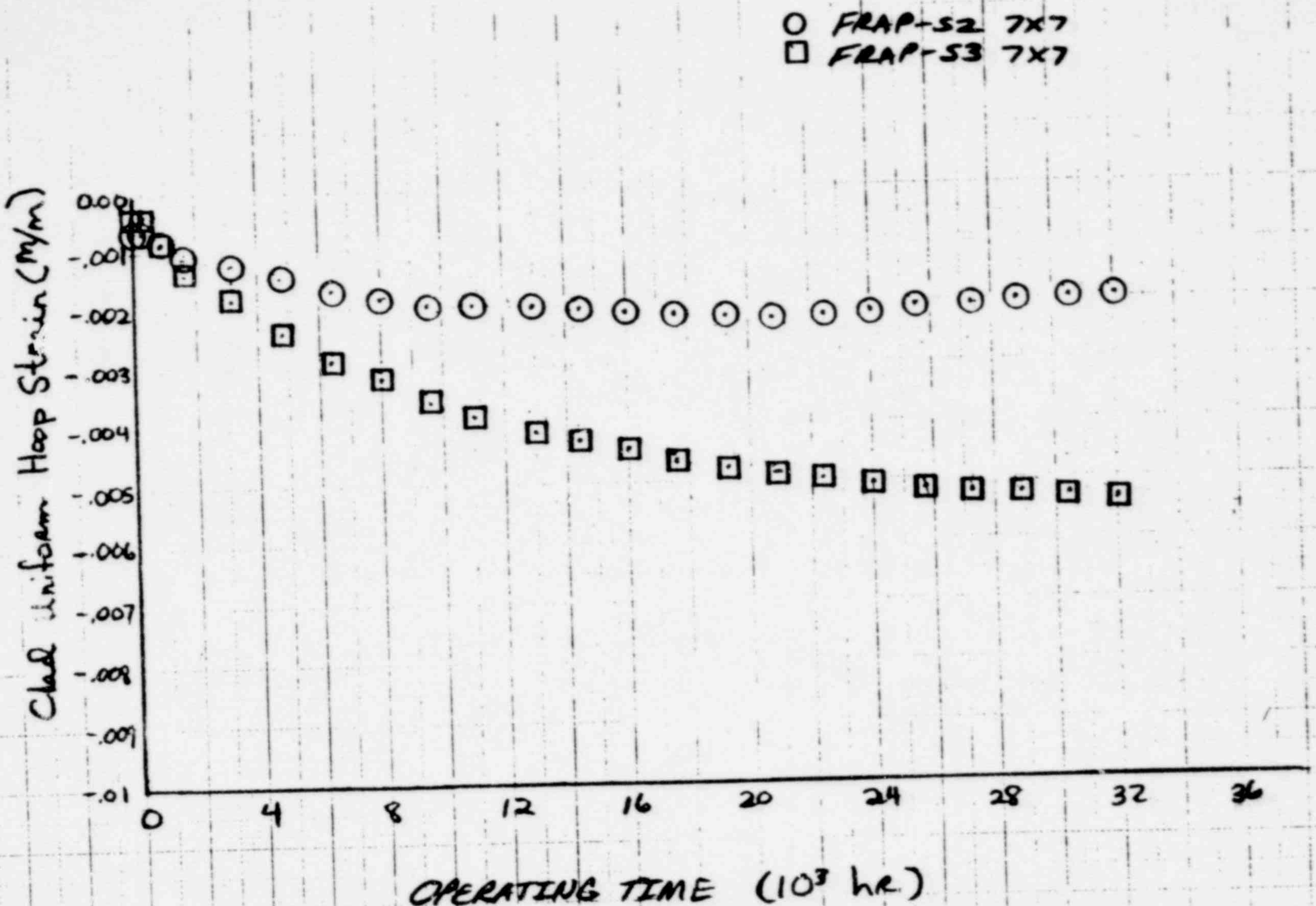

FIGURE 11 : FRAP-S2 AND FRAP-S3 CLADDING HOOP STRAIN HISTORIES FOR A CORE AVERAGE 7X7 ROD

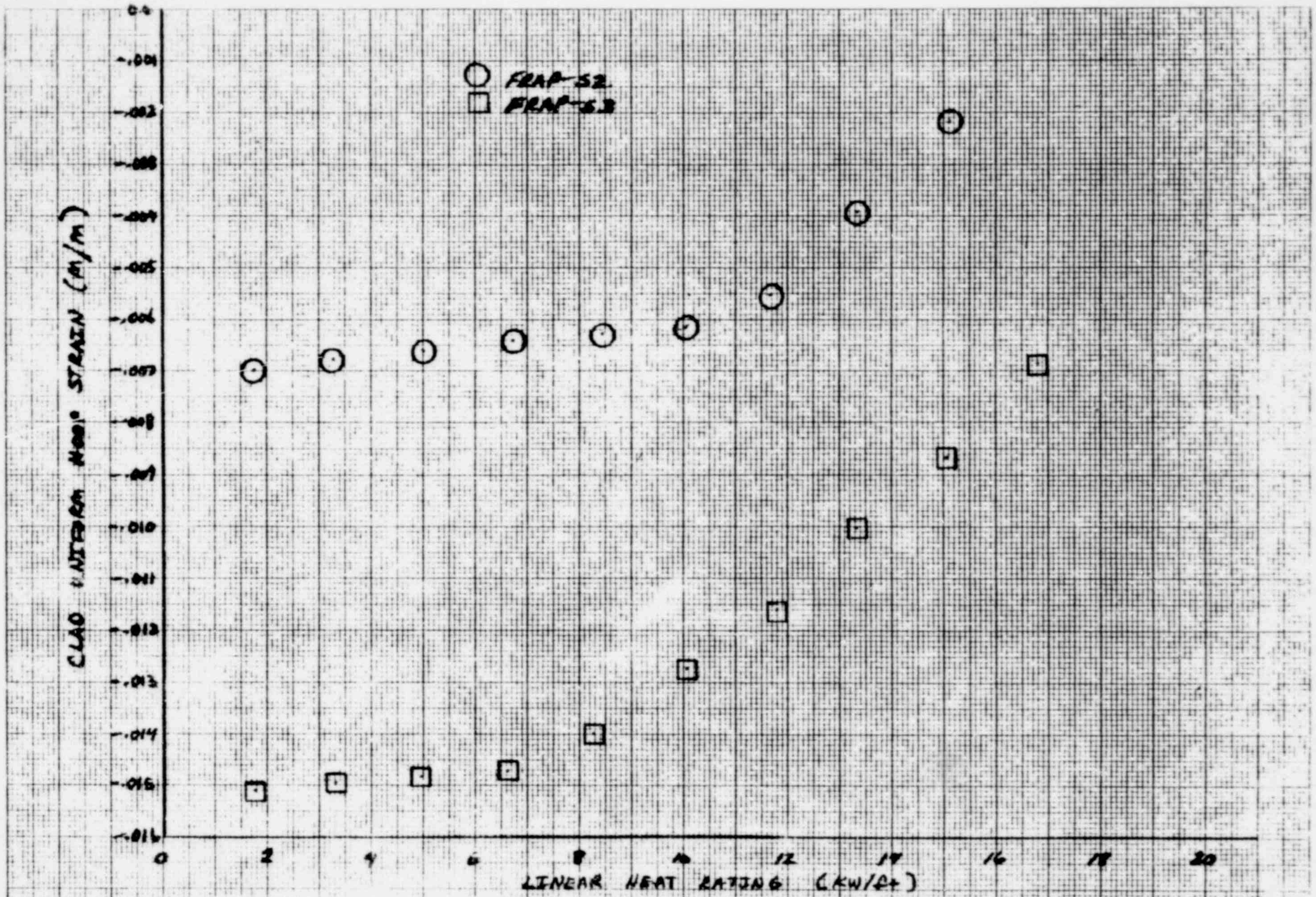

FIGURE 12 : FRAP-S2 AND FRAP-S3 CLADDING HOOP STRAIN VS. HEAT RATING FOR A CORE AVERAGE 15X15 ROD AT END OF LIFE

The final area addressed by FRAP-S2/FRAP-S3 model comparison runs relates to the calculated buildup of cladding surface corrosion and the related absorbtion of hydrogen by the cladding. Figures 13 and 14 show corrosion layer thickness versus operating time respectively for 7 x 7 and 15 x 15 rods. MATPRO models used by FRAP-S3 have been revised to represent system chemistry differences more explicitly than the user input corrosion rate acceleration term used by FRAP-S2. Nominal BWR results for the current model, shown in Figure 13 are very comparable to the FRAP-S2 run in which an acceleration factor of 10 had been applied to the lab correlation. Figure 14 shows that FRAP-S3 predicts less corrosion than FRAP-S2 under PWR conditions. FRAP-S2 corrosion rates were mainly dependent on cladding temperature. Current results indicate that system chemistry effects (in this case relative lack of oxygen radicals in the absence of boiling) are calculated to outweigh the effect of higher PWR cladding temperatures.

Hydrogen uptake comparisons are shown in Figures 15 and 16, again for BWR and PWR rods. The model treats initial fuel moisture content in addition to surface corrosion as a potential source of hydrogen. This fact explains why FRAP-S3 predicts so much more hydrogen absorption than FRAP-S2 for the BWR case, despite close agreement in corrosion results. For the same reason, FRAP-S3 predicted hydrogen buildup in the PWR cladding ends up being more comparable with FRAP-S2 results than the corrosion comparison would indicate.

1569 164

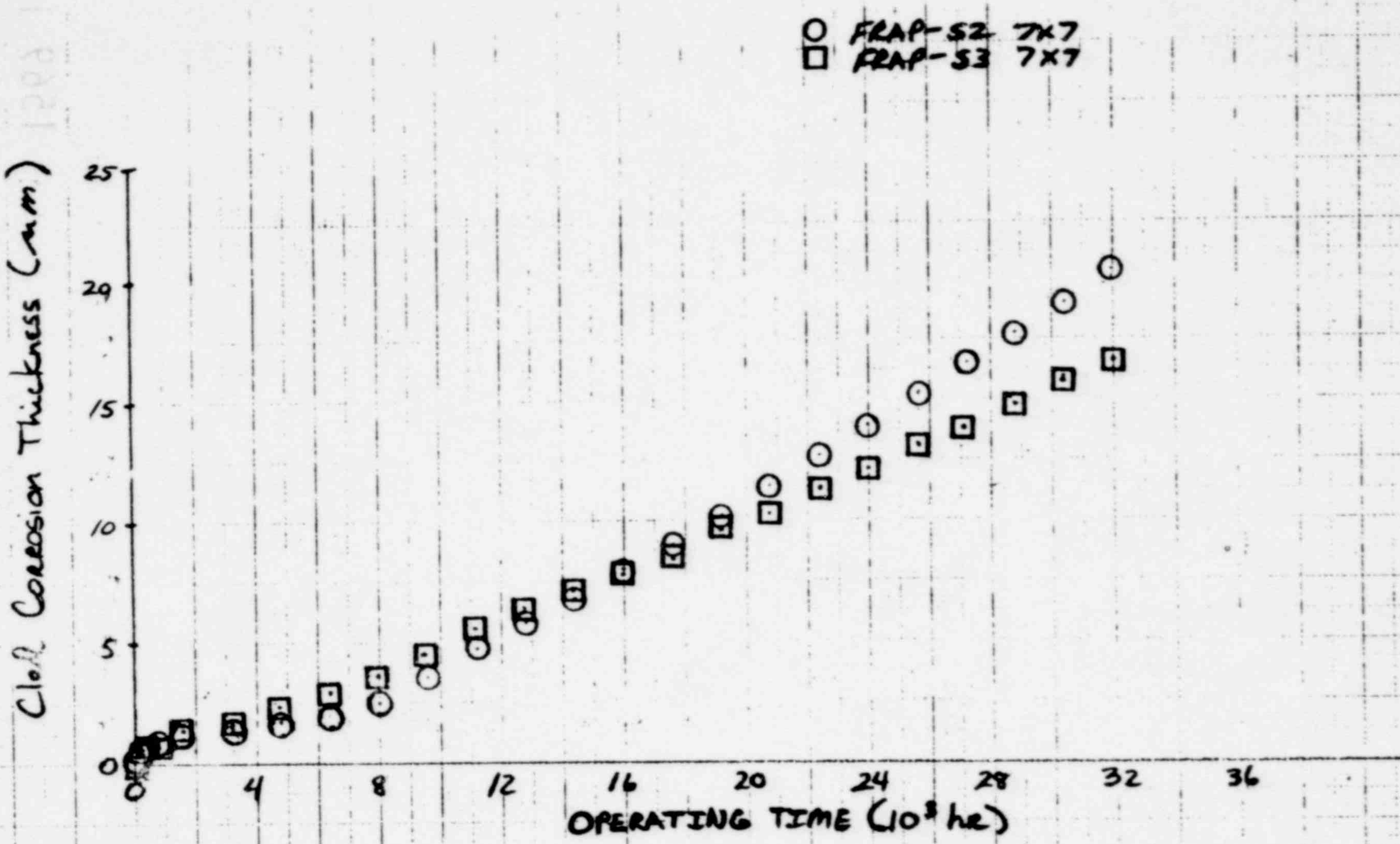

FIGURE 13: FRAP-S2 AND FRAP-S3 CLADDING SURFACE CORROSION BUILDUP FOR A CORE AVERAGE 7x7 ROD

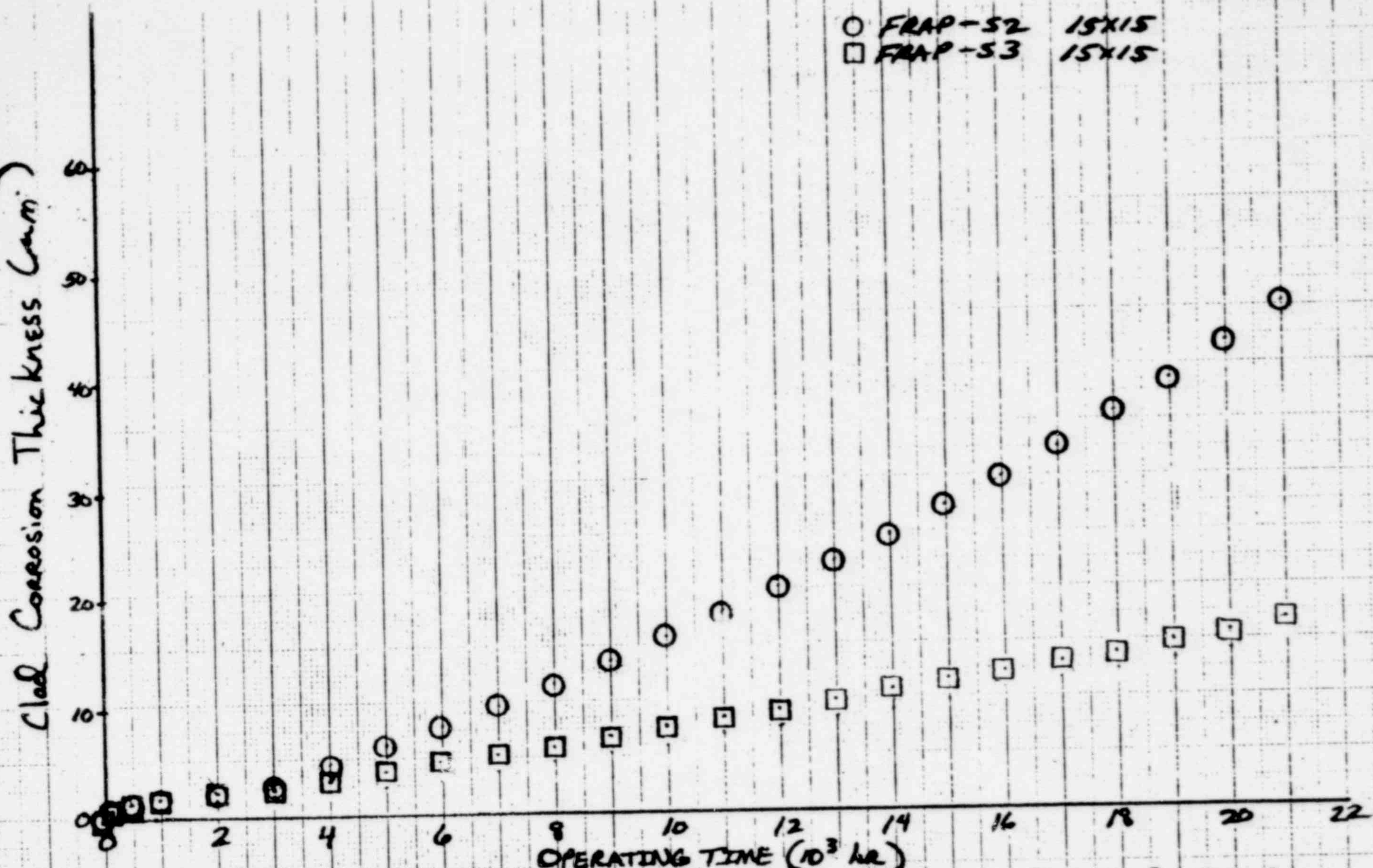

FIGURE 14 : FRAP-S2 AND FRAP-S3 CLADDING SURFACE CORROSION BUILDUP FOR A CORE AVERAGE 15X15 ROD

5412

23-363

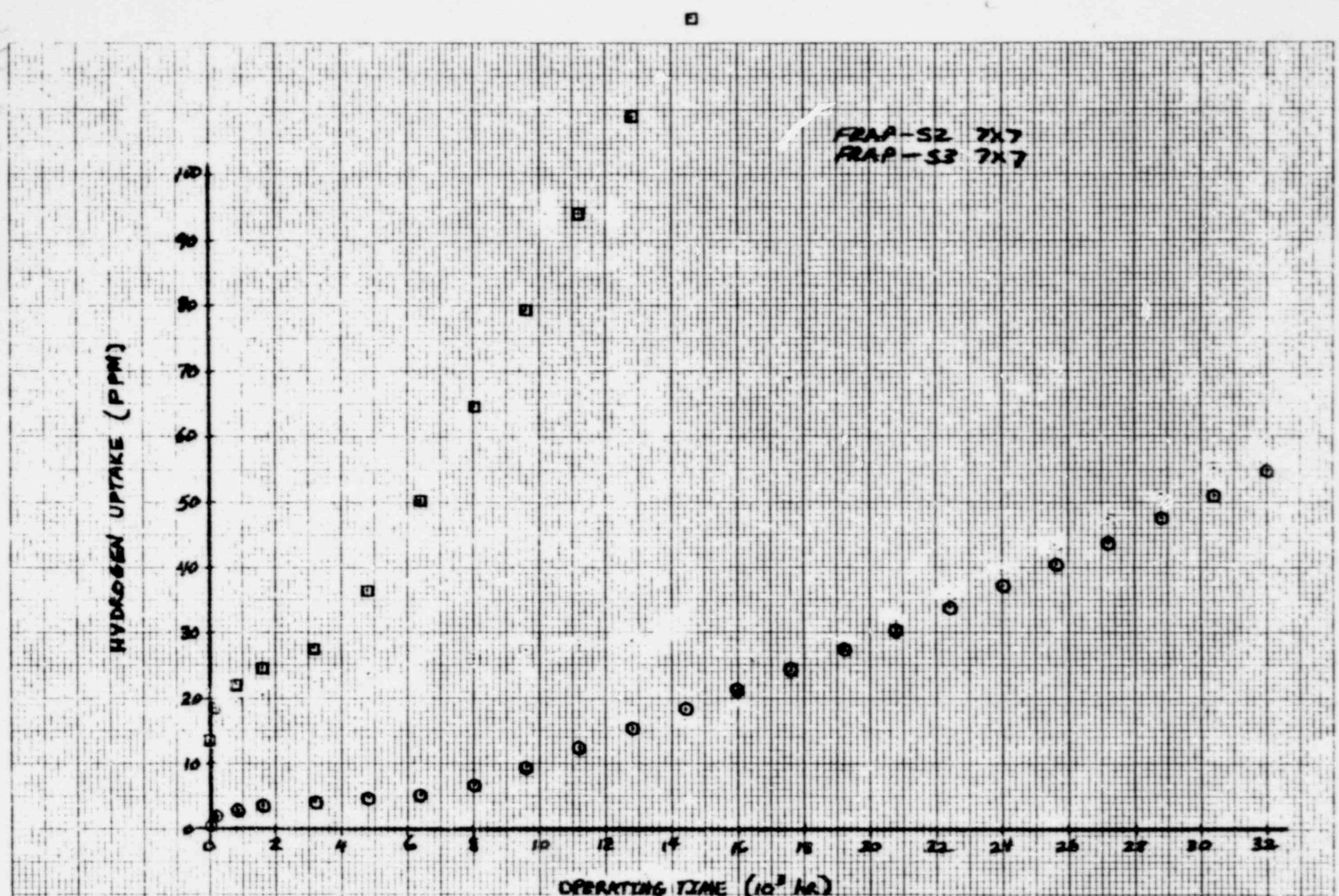

FIGURE 15 : FRAP-S2 AND FRAP-S3 CLADDING HYDROGEN CONCENTRATION FOR A CORE AVERAGE 7X7 ROD

1569 167

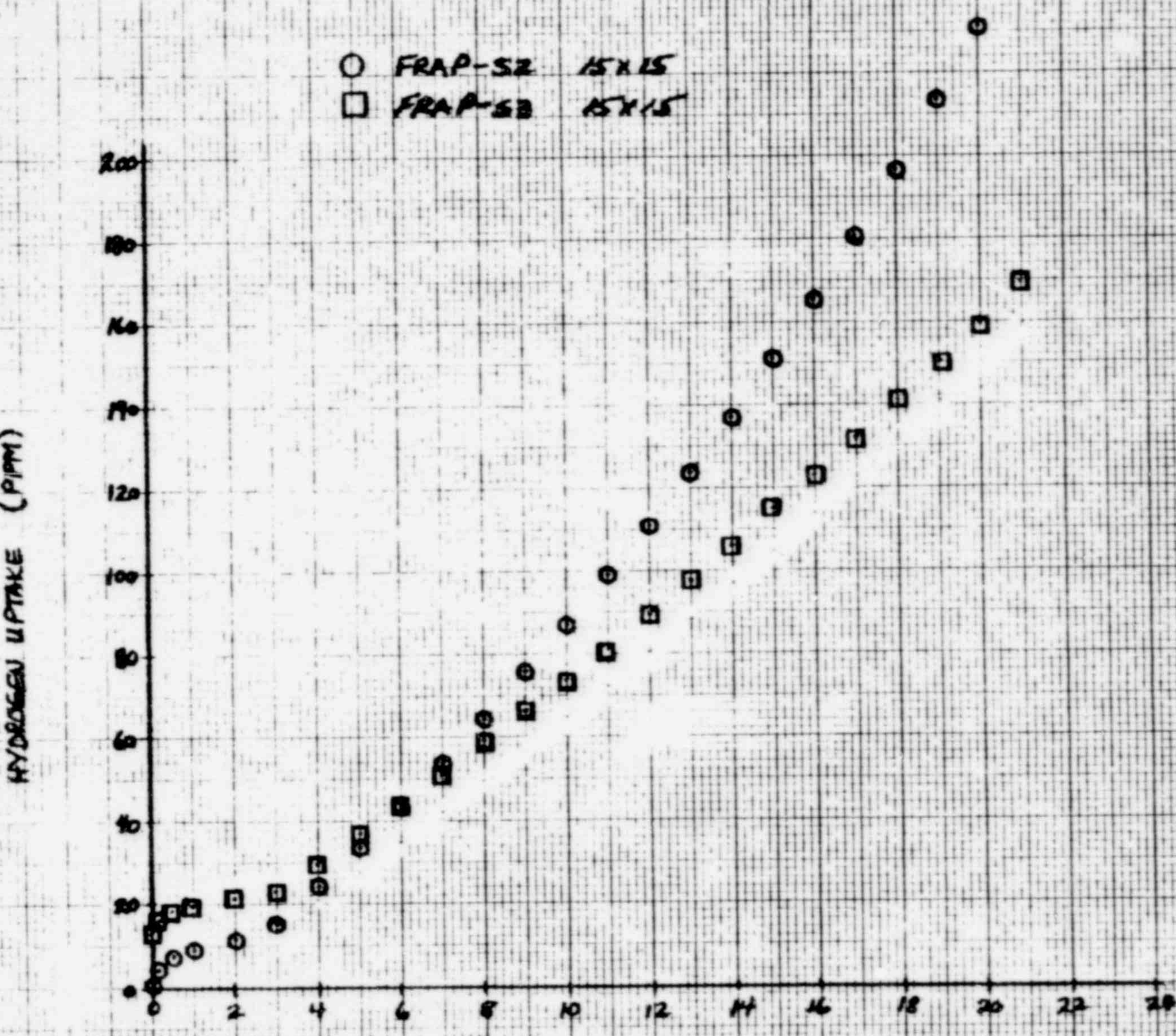

FIGURE 16: FRAP-S2 AND FRAP-S3 CLADDING HYDROGEN CONCENTRATION FOR A CORE AVERAGE 15X15 ROD

2.2 Output Characterization

As stated before, a major purpose of FRAP-S3 is to supply FRAP-T with best estimate initial conditions reflecting operation prior to hypothetical transients. The burnup effects currently considered by FRAP-T reflect variation in rod geometry, gas content, gas composition, void volume, cladding material properties, and surface conditions from the as-built state. As an extension of prior statistical Standard Design Studies[107], these and related steady state output parameters are being analyzed in more detail for typical PWR design and operating conditions. Developement and demonstration of methods by which to extrapolate fuel rod model capability to a representation of core behavior is required to verify model performance for full scale applications.

2.2.1 Applications. FRAP-S3 results for the general PWR analysis can be used to define initial condition distributions for various postulated accidents. Using the present results as input data, FRAP-T4 studies could characterize core geometry and activity release during the course of a hypothetical loss-of-coolant accident (LOCA). A response surface characterization of steady state conditions could be applied to generating initial transient conditions for any specific set of design and operating parameters within the broad ranges considered here. Other results of this study will eventually include a quantitative evaluation of the relative influence of design, model, and power history variability on computed steady state output.[111]

1569 169

2.2.2 Procedures. Table 4 illustrates current Standard Design Analysis procedures for both FRAP-S3 and FRAP-T4. Detailed description of applying response surface techniques to FRAP-S and FRAP-T is given elsewhere[111]. The handling of input and output parameters is summarized below.

2.2.2.1 Input Parameters. In order to obtain realistic distributions and ranges of steady-state output parameters at different burnups, distributions of relevant FRAP-S3 input parameters must be defined. These parameters not only reflect differences in PWR design and operating conditions but also FRAP-S3 model uncertainties. Results of previous verification studies[107] showed that the effect of design and model uncertainty could sometimes outweigh the effect of power history on initial gap, gas composition and internal pressure. The variables specified as main contributors to FRAP-S output variability are listed in Table 5.

2.2.2.1.1 Design. The variation in design parameters results from two sources: 1) differences in nominal fuel design between cores or core regions, and 2) differences between design and as-built values. Distributions of nominal design values were based on various Safety Analysis Reports. The distributions of as-fabricated parameters about the nominal values were obtained from several pretest fuel characterization programs.[111] The documented nominal design values were found to be consistent with those used in past Standard Design Analyses[107]. Due to the more general nature of the present study however, parameter ranges represent a broader design spectrum than previously considered.

TABLE 4

STANDARD DESIGN ANALYSIS PROCEDURES

Steady State Analysis

Input	Output	Method
General PWR design variables - 8 Model uncertainties - 8 Operating parameters - 3	Response equations as a function of burnup for: . gas content . void volume . local rod geometry . fission gas fraction . rod surface condition	Response surface for generating equations Second order error propagation for obtaining response distributions

Transient Analysis

Input	Output	Method
Steady state output variables impacting transients Best estimate distributions for: . decay heat . surface heat transfer or core flow history	Response equations as a function of time for: . internal pressure . clad temperature . rod geometry Use FRAIL for prediction of: . flow blockage . failure . activity release	Response surface for generating equations Second order error propagation for obtaining response distributions

23-366

TABLE 5

STEADY-STATE VARIABLES FOR

STANDARD DESIGN ANALYSIS

Variables	Range
Design/State Parameters	($\pm$ 3σ limits)
Cold plenum length	5 - 12 in.
Cladding thickness	.0215-.0282 in.
Diametral gap	5.0 - 9.8 mils
Fuel Density	89.8-97.2% T. D.
Fill gas pressure	250 - 500 psi
Clad effective coldwork	0 - .20
Fuel grain size	3 - 10 μm
Fuel sintering temperature	1400 - 1800°C
Model Parameters	
Corrosion	$\pm$ 30%
Fuel thermal expansion	$\pm$ 10%
Creep collapse	$\pm$ 50%
Densification	$\pm$ 40%
Gas release	$\pm$ 60%
Fuel swelling	$\pm$ 40%
Fuel thermal conductivity	$\pm$ 10%
Gap conductance	$\pm$ 50%
Operating Parameters	($\pm$3σ limits)
Region 1 power	2.47 - 9.85 Kw/ft
Region 2 power	3.91 - 9.19 Kw/ft
Region 3 power	1.30 - 8.50 Kw/ft

1569 172

2.2.2.1.2 Model Uncertainty. Model uncertainties in FRAP-S were characterized using both previous[3] and anticipated results of model verification data comparision studies. The model uncertainty was assumed to correspond to the mean difference between model predictions and those data reflecting the moderate operating conditions of interest. In estimating the model uncertainty, it was taken into account that FRAP-S3 is expected to have somewhat less thermally dependent error than FRAP-S2 in gas release, gap, and rod deformation conditions due to incorporation of best estimate relocation and conductivity models.

2.2.2.1.3 Operating History. PWR core power distributions reflect differences in fuel management techniques among the various utilities. Most of the utilities employ an inward fuel shuffling scheme. Decisions concerning individual assembly placement are often not made however until the shuffling outage. In this study, the assumption is made that the basic first core configuration will apply through a reactor operating history made up of several cycles. Referring to Figure 17, this assumption implies that assemblies of type 1 will be discharged at the end of cycle 1; type 2 assemblies will be moved to locations previously held by type 1; type 3 assemblies are shuffled to type 2 locations; fresh fuel is loaded into type 3 locations.

The core is divided into 3 power regions, each region being characterized by a distribution of rod average power within the region. These distributions were obtained from physics design calculations reported in

23-367

			3	3	3	3
		3	3	2	1	3
	3	1	2	1	2	1
3	3	2	1	2	1	2
3	2	1	2	1	2	1
3	1	2	1	2	1	2
3	3	1	2	1	2	1

Fuel Type

Fig. 17 First core loading arrangement for FRAP-S3 standard design study . . . .

1569 174

various Safety Analysis Reports. An example of a typical core power distribution is shown in Figure 18. The mean heat ratings and standard deviations are plotted versus region number. Total core power is constant. Figure 18 may also be interpreted as a cumulative power history for a group of assemblies over 3 cycles. Abrupt power changes are the result of fuel shuffling operations.

Because of differences in fuel management and design techniques, a given fuel type power history may differ markedly from that shown in Figure 18. For example, a utility may employ a shuffling scheme in which a group of assemblies are moved into regions of successively higher power. In this study, local power levels have been treated as independent variables, thereby accounting for any dependence of initial transient conditions on cumulative power history effects. Both axial and regionwise power distributions are represented as local power effects on the code output.

2.2.2.2 Statistical Method. Statistical standard design analyses have been conducted by verification[107] using previous versions of FRAP-S. At that time, a Monte Carlo sampling technique was employed. This method results in quantifiable distributions of output parameters, but the relative influence of each input variable cannot be distinguished. For this reason, a response surface technique was applied to further expand interpretation of Standard Design results.

In contrast to the Monte Carlo technique, the response surface input variables are not randomly sampled, but are chosen through an

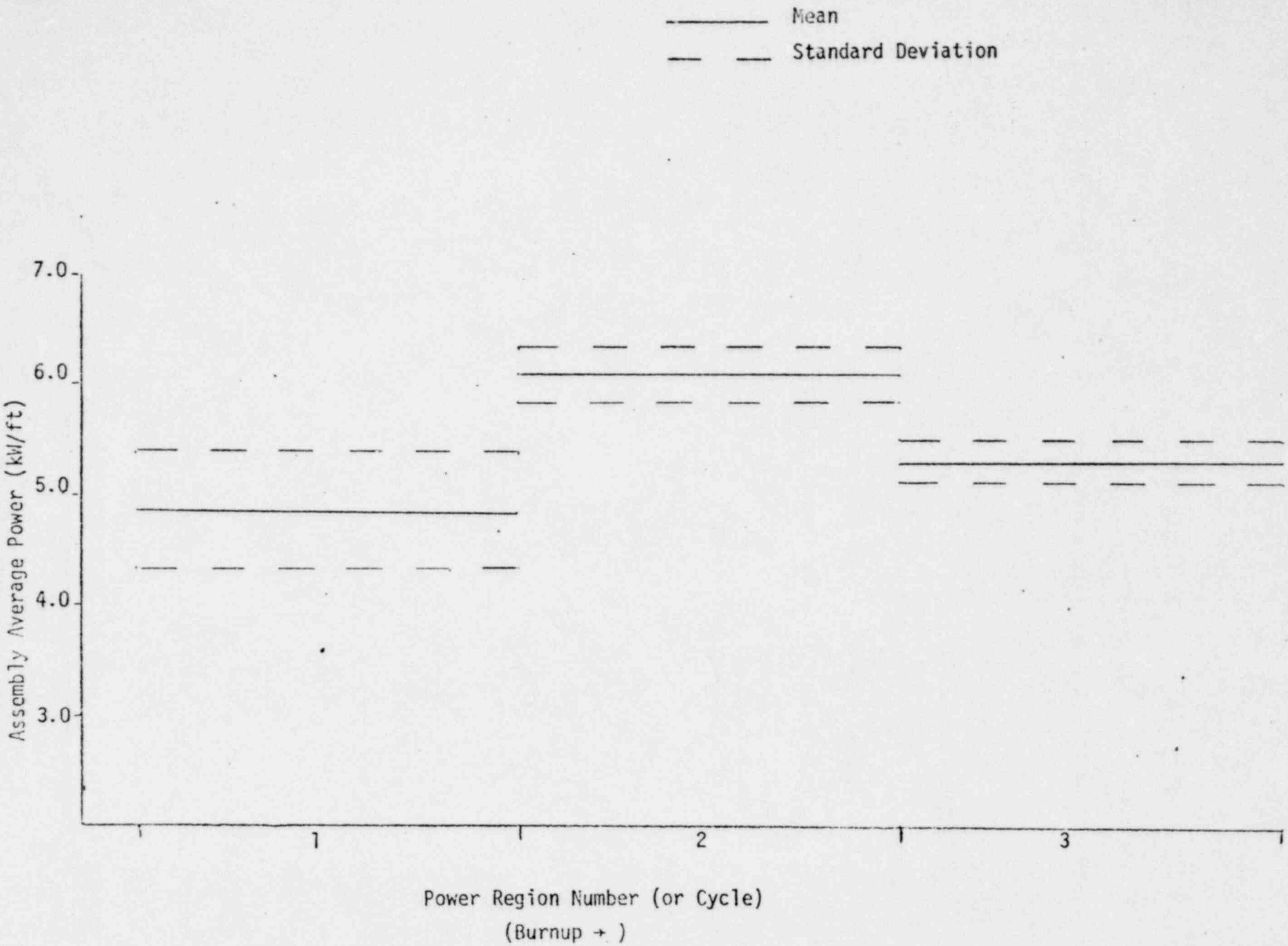

Fig. 18 Range in region wise core power distributions for FRAP-S3 standard design study. . . . .

experimental design. The design chosen for this study is of the central composite type. This design has shown sufficient capability and resolution for interpreting multiparameter studies of this sort. Eighty runs were required to define first and second order terms as well as interaction terms.

From the total set of computer runs, 80 values of the main FRAP-S3 output variables were obtained for each of 20 timesteps and 5 axial nodes. The following output variables were selected for further examination: gas content, gas composition, rod geometry, burnup, stored energy, internal pressure, gap size, and surface conditions. A system of equations was constructed for each output value of the form.

$$y = a_0 + \sum_i a_i x_i + \sum_{i,j} a_{ij} x_i x_j \qquad (1)$$

where

y = output variable

x = input variable x (listed in Table 5) or time

a = coefficients of the polynomial

This system of equations was then solved for the coefficients, a, of the polynomials. The response (y) at any time may be found by inserting appropriate values for the x_i and time parameters. This equation represents FRAP-S output for PWR's with design and operating conditions within the ranges shown in Table 5.

1569 177

Once the response surface equation is obtained, a distribution of response (y_i) may be found. Using an error propagation technique, only the distributions of the x_i need be specified. The computer code (SOERP)[111] is used for this part of the analysis. The distributions of the x_i need not be the same as those used to develop the response equation. Distributions constructed from either core-wide or assembly-wide parameters may be used. The only restriction is that the distribution limits cannot lie outside of the range which was used to construct the response equation. This constraint does not limit planned analyses since the original constructing range encompasses a number of PWR designs.

Power history effects are eliminated by solving two sets of response equations for each of the three power (burnup) groups identified in Figure 19. The first set of response equations are of the form:

$$y_{in} = y_{in} (x_j, t_K) \qquad (2)$$

where

y_i = output variable i used as input to transient analysis of region n

x_j = input variable j

t_K = operating time since last fuel shuffling.

In the first region (cycle), the distributions of the x_j used in Equation 2 are simply the same as those listed in Table 5. In the second and third regions (cycles), the rod state parameters of Table 5 now have values

1569 178

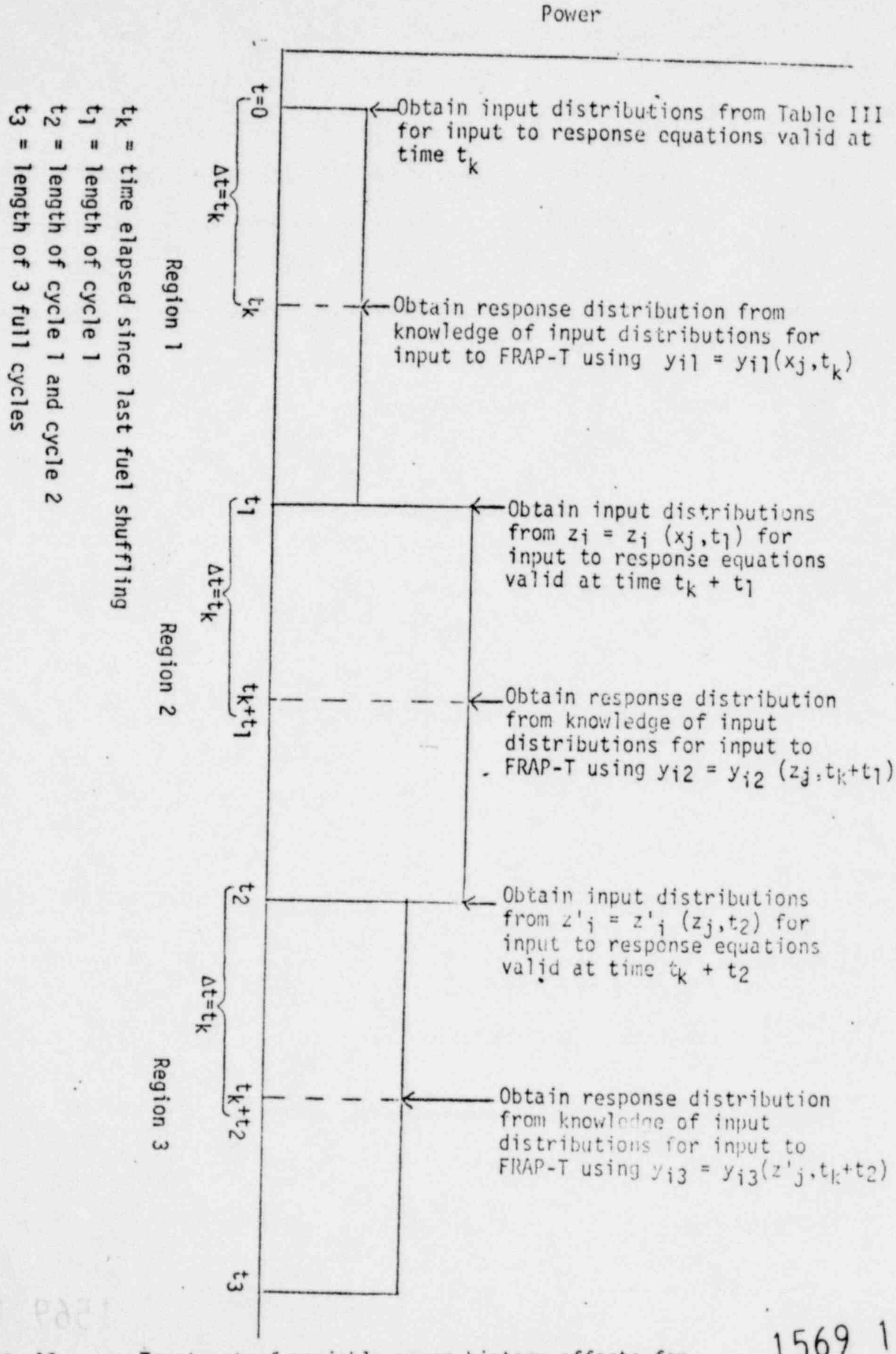

1569 179

Fig. 19 Treatment of variable power history effects for FRAP-S3 standard design study. . . . .

23-370

which reflect previous burnup. The burnup-dependent values for these variables are found from the second set of response equations for Region 1 and are of the form:

$$z = a_o + \sum_i a_i x_i + \sum_{i,j} a_{ij} x_i x_j \qquad (3)$$

for region (cycle) 2, and,

$$z' = b_o + \sum_i b_i z_i + \sum_{i,j} b_{ij} z_i z_j \qquad (4)$$

for region (cycle) 3, where

z = value of state parameter at time t_1 (used as input to the cycle 2 response equation)

z' = value of state parameter at time t_2 (used as input to the cycle 3 response equation)

a,b = coefficients

The distributions of each of the z_j and z'_j are then found using linear error propagation techniques[111] on Equations 3 and 4. The distributions of the z_j and z'_j describe input distributions which are used to solve for the distributions of the Y_{i2} and y_{i3}, respectively. Model uncertainties are assumed to remain constant through all three cycles.

1569 180

2.2.3 Output. As of this writing, statistical analysis of current standard design output is still in progress. The eighty FRAP-S3 runs required for sufficient resolution of the experimental design have been completed. Regression analyses of pressure gap, stored energy, gap conductance, and center temperature conditions have been performed for each burnup step. The main effects contributing to the output response in these areas involve many interaction terms between the parameters listed in Table 5. Coefficients have been obtained for both time independent and time dependent forms of the response surface equation describing rod internal pressure buildup. An initial series of comparisons indicate good agreement between FRAP-S3 and response surface calculated pressure conditions. Only FRAP-S3 results will be discussed at this time. The complete response surface analysis will be presented in subsequent documentation[111].

Figures 20, 21, and 22 show standard design PWR distributions of internal pressure, stored energy, and gap conditions calculated by FRAP-S3 at beginning, middle and end-of-life. Variation in the results reflects systemmatic selection of code input data across the entire range of PWR design and operating parameters previously given in Table 5. As such, the FRAP-S3 output ranges shown only represent distributions used for constructing standard PWR response surfaces and do not always constitute expected conditions for a given core configuration. For example, nominal output values should not occur with as much frequency as normally expected in analysis of physical systems. In other words, the experiment design places emphasis on uniformly defining FRAP-S3

1569 181

23-371

FIGURE 20 FRAP-S3 CALCULATED DISTRIBUTIONS OF ROD INTERNAL PRESSURE USED FOR GENERATING STANDARD PWR RESPONSE SURFACES AT BEGINNING, MIDDLE, AND END OF LIFE.

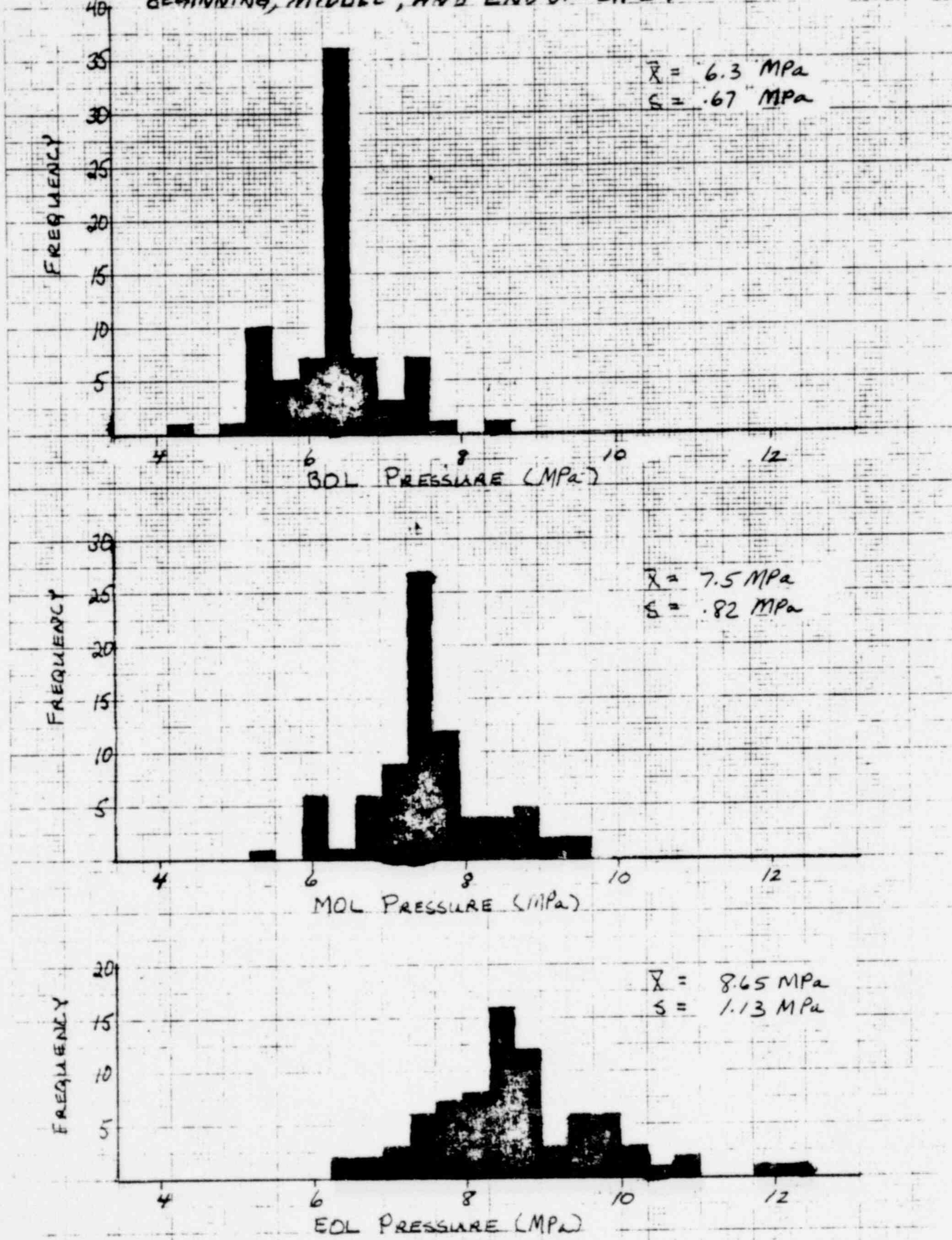

1569 182

FIGURE 21 FRAP-S3 CALCULATED DISTRIBUTIONS OF FUEL STORED ENERGY USED FOR GENERATING STANDARD PWR RESPONSE SURFACES AT BEGINNING, MIDDLE, AND END OF LIFE

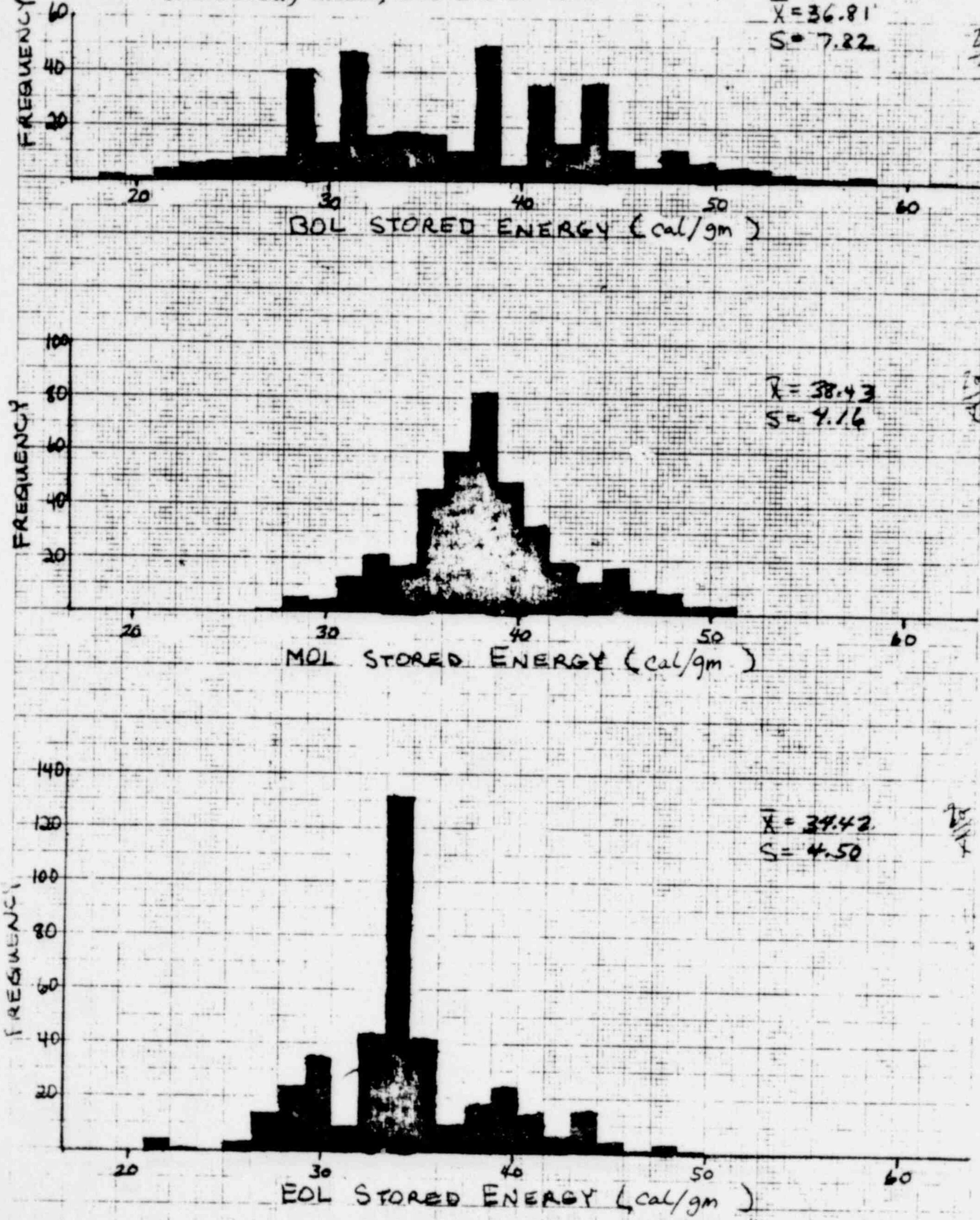

23-372

FIGURE 22 FRAP-S3 CALCULATED GAP POROSITY DISTRIBUTIONS USED FOR GENERATING STANDARD PWR RESPONSE SURFACES AT BEGINNING, MIDDLE, AND END OF LIFE

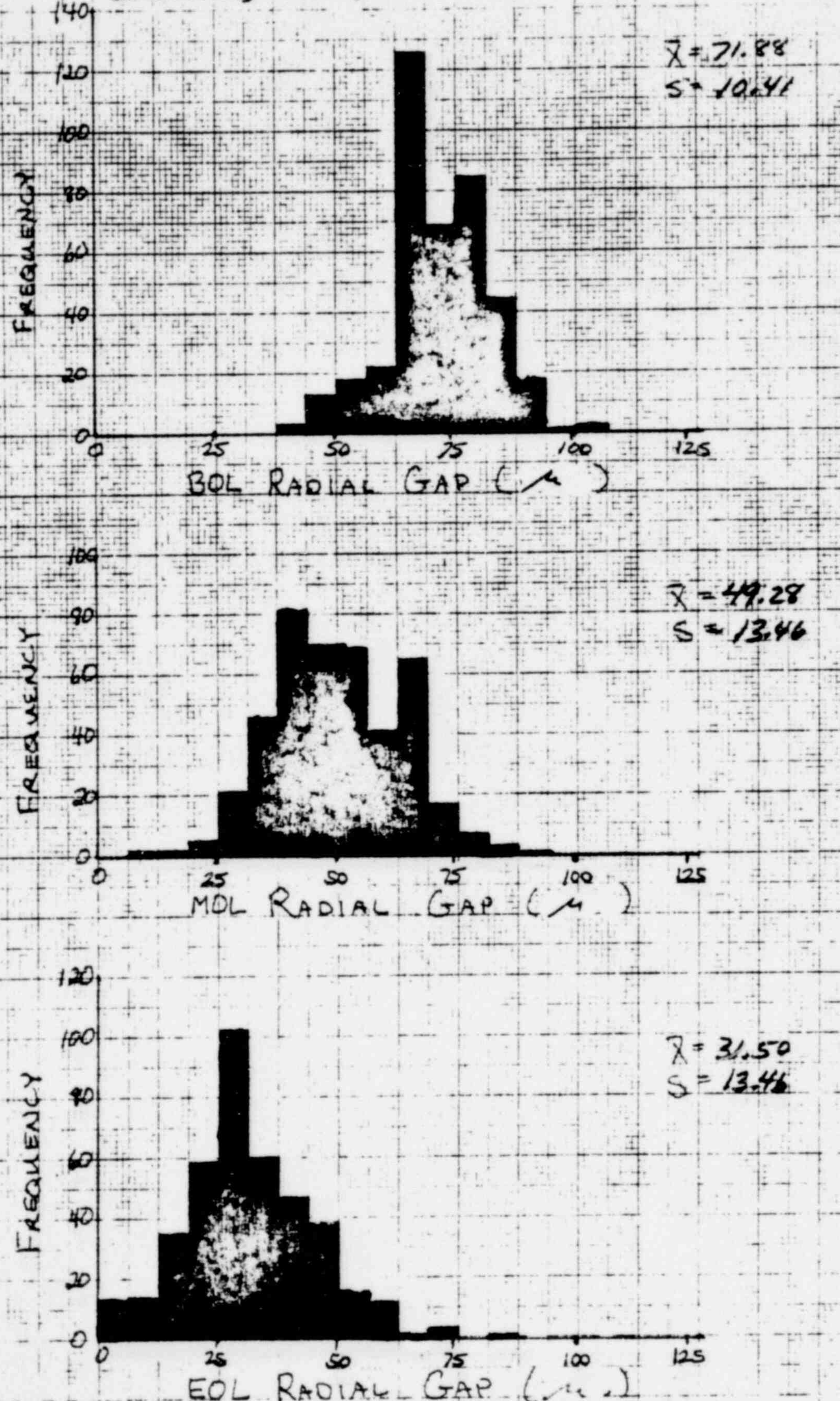

1569 184

output across a ±3σ range of input conditions. It is only in future applications of the response surface itself that mean values will be specified to occur with greater frequency. The fact that peaked output distributions are observed at all in the figures reflects relative insensitivity of the results to variations of the input data. In any event the absolute range of code results, as well as dependence of output trends on burnup should be representative of typical PWR conditions.

Figure 20 shows how cumulative burnup effects act to expand the range of initial pressure conditions for accident analysis. The influence of gas release is reflected by increasing mean pressure values. The burnup effect on pressure conditions however has less influence on absolute pressure level than fill gas condition. Extremes in the distributions are found to reflect ±3σ levels for initial backfill pressure. The existence of well defined mean values suggests that relatively few design and operating parameters have strong influence on internal pressure. The total range of operating pressure conditions for standard design PWR rods extends between 4 and 12 MPa. Based on a FRAIL[106] calculated 50% failure probability, these pressure values correspond to cladding burst temperatures ranging between 730 and 850 C.

Figure 21 indicates that the range of FRAP-S3 calculated PWR stored energy conditions is strongly dependent on burnup in addition to heat rating. Beginning of life peaking at 5 different levels reflects local power conditions at the axial nodes considered. Distributions about these values mainly reflect variation in design parameters and material properties. The effect of

1569 185

23-373

local heat rating becomes less strong as burnup increases. This tendency reflects smaller region-wise power variation over cycles 2 and 3 (Figure 18) in addition to the damping influence of burnup effects on axial fuel temperature gradients. The effect of crack closure and increasing pellet conductivity are more active in reducing fuel temperatures at the peak power node (peak cladding temperature and fast flux) due to more creep collapse. The 2σ variation in PWR stored energy conditions ranges between 20 and 40% of the mean values depending on burnups. This variation can be considered the absolute maximum amount applicable to a given core, since the input data spanned the range of design and operating parameters representing all typical PWR conditions. Variations in initial stored energy on the order of 5 to 10% have been shown to result in significant changes in calculated peak cladding temperature and strain response under hypothetical LOCA conditions. Subsequent response surface analysis for specific core configurations could establish realistic stored energy distributions for refining estimates of core wide accident response.

Figure 22 shows that PWR gap size distributions are also calculated by FRAP-S3 to be strongly burnup dependent. The gap results refer to structural gap conditions. All thermal expansion and deformation mechanisms with the exception of pellet relocation are incorporated in the structural gap values. The term "gap porosity" has been applied here since the structural gap really exists as some combination of gap and crack space. This space can be considered as being available for gas flow or to accommodate pellet expansion prior to occurrence of high

1569 186

stress during hard PCMI. Mean gap porosity decreases with burnup since the effects of creep collapse and fuel swelling are calculated to outweigh the effect of fuel densification. The beginning of life gap s ze range indicates that as built geometry variations contribute significantly to the burnup dependent variation. The overall range of possible PWR gap size conditions would indicate that considerable core-wide differences can exist in susceptibility to PCMI and gas flow effects.

In summary, response surface characterization of how initial transient conditions are distributed for given core types can aid in establishing a quantitative basis for statistically evaluating large scale consequences of off-normal events. Preliminary inspection of the FRAP-S3 results used to construct the response surface indicate that statistical representations of core-wide conditions will be meaningful both for making best estimate calculations and for evaluating the degree of conservatism resulting from evaluation model assumptions.

3. DATA COMPARISON STUDY

Certain verification data processing requirements exist as a result of conducting large sample comparisons between analytical and experimental results. Some preliminary data processing functions have been applied here to making systemmatic comparisons between FRAP-S3 and experimental results. Physically significant trends have been graphically established as have some quantitative bases for interpreting summary results. The main criterion used to demonstrate adequate performance of basic physical models remains their ability to represent the mean measurement response over typical ranges of design parameters and operating conditions such as power or burnup.

1569 187

23-374

Table 6 summarizes the number of rods, types of data and main sources of information for each comparison index investigated with FRAP-S3. Differences between FRAP-S3 sample sizes and those analyzed in previous verification studies reflects the following benchmarking considerations: (1) emphasis on fuel thermal, gas release, pressure, and gap closure response due to strong influence of initial fuel relocation and effective conductivity models in these areas, (2) the need to better represent commerical fuel operating conditions in terms of moderate duty, extended burnup effects on creep collapse, gas release, stack geometry, and corrosion, (3) elimination of all stainless clad data and rods with center melting due to untypical cladding strength, contact conductance and fuel plasticity effects, and (4) the statistical incentive for a maximum sample size approach which arises from the verification objective of quantifying model performance capability

3.1 Thermal Model

3.1.1 Fuel Centerline Temperature. Fuel temperature results will be discussed first due to governing influence of temperature distribution on FRAP-S3 gas release, rod internal pressure, and deformation models.

3.1.1.1 Duplicate Comparison Study. Prior verification results[107] established that the original cracked pellet gap conductance model represented fuel temperatures better than an annular gap approach. Subsequent results[3,110] in both thermal and mechanical areas established need for improvement and recommendations for a more

1569 188

TABLE 6

FRAP-S3 MODEL VERIFICATION: SCOPE OF DATA COMPARISON STUDY

COMPARISON INDEX	DATA CATEGORY	SAME SIZE (RODS)			MAXIMUM OPERATING HOUR	TEST PROGRAM
		S1	S2	S3		
Fuel Temperature	*	30	52	106	16725	HPR, RISO, WCAP, PBF
Gap Conductance	Δ/PIE	-/27	18/27	37/-	BOL/ -	AECL, HPR, PBF
Fuel Melt Radius	PIE	94	94	-	2500	AECL, GEAP
Fuel Axial Elongation	*/PIE	8/18	35/22	58/64	9000/28000	HPR, KWU, B&W, W, BRP, MAINE YANKEE, H. B. ROBINSON
Rod Internal Pressure	*	17	50	53	12000	HPR, AECL, PBF
Gas Release Fraction	PIE	104	159	199	44000	HPR, SAXTON, B&W, W, AECL, PRTR, GEAP, VBWR, DRESDEN, MAINE YANKEE, H. B. ROBINSON, BRP, CEA
Gas Composition	PIE	-	8	45	44000	PRTR, H. B. ROBINSON, SAXTON, MAINE YANKEE, BRP, VBWR, DRESDEN
Gas Content	PIE	-	10	35	10000	HPR, PRTR
Void Volume	PIE	-	-	46	44000	VBWR, DRESDEN, MAINE YANKEE, H. B. ROBINSON, SAXTON
Cladding Axial Elongation	*/PIE	13/82	28/92	96/126	9500/44000	HPR, SAXTON, AECL, PRTR, MTR, PBF GEAP, BRP, VBWR, DRESDEN
Cladding Circumferential ε	*/PIE	4/132	16/132	26/175	2100/44000	HPR, AECL, GEAP, SAXTON, KWU, PRTR, MTR, VBWR, DRESDEN, MAINE YANKEE, H. B. ROBINSON, BRP
Cladding Corrosion	PIE	30	30	61	44000	HPR, SAXTON, VBWR, DRESDEN, MAINE YANKEE, H. B. ROBINSON, BRP
Cladding H_2 Concentration	PIE	30	36	46	44000	HPR, SAXTON, VBWR, DRESDEN, MAINE YANKEE, H. B. ROBINSON, BRP

* - instrumented rod data
Δ - inferred from instrumented rod data
PIE - post-irradiation exam

complete fuel relocation treatment with associated pellet conductivity feedback. Initialization errors were then found in the original cracked pellet model[110] and subsequently corrected. A series of duplicate fuel temperature comparisons were performed by verification to determine whether use of the more physically based relocation/$k_{effective}$ model introduced unforseen thermal anomalies or in any way compromised calculated temperature conditions more than the corrected cracking model. Adequate representation of fuel temperatures was found earlier[3] to be a prerequisite for interpreting both measured and predicted fission gas release and cladding deformation.

About 700 data points, representing measured center temperature histories for some 90 rods, were analyzed using both thermal models. For each comparison point, design and operating con ' ions (power, burnup, system conditions) were consistent with reporte_ alues. The difference between predicted and measured temperature based on the corrected original cracking model was compared to that obtained using the relocation/$k_{effective}$ model.

The total sample results shown in Figure 23 se... nconclusive. Comparison points occupying the cross-hatched area i dicat cases for which better temperature agreement is obtained using the relocation/ $k_{effective}$ model. This situation exists for only 50% of the comparison points. Respectively, the relocation model and corrected cracking model have tendencies of similar magnitude to either overpredict underpredict center temperatures.

1569 190

FIGURE 23 - COMPARISON BETWEEN PREDICTED - MEASURED FUEL CENTER TEMPERATURES USING FRAP-S3 WITH AND WITHOUT RELOCATION/$k_{effective}$ MODELS

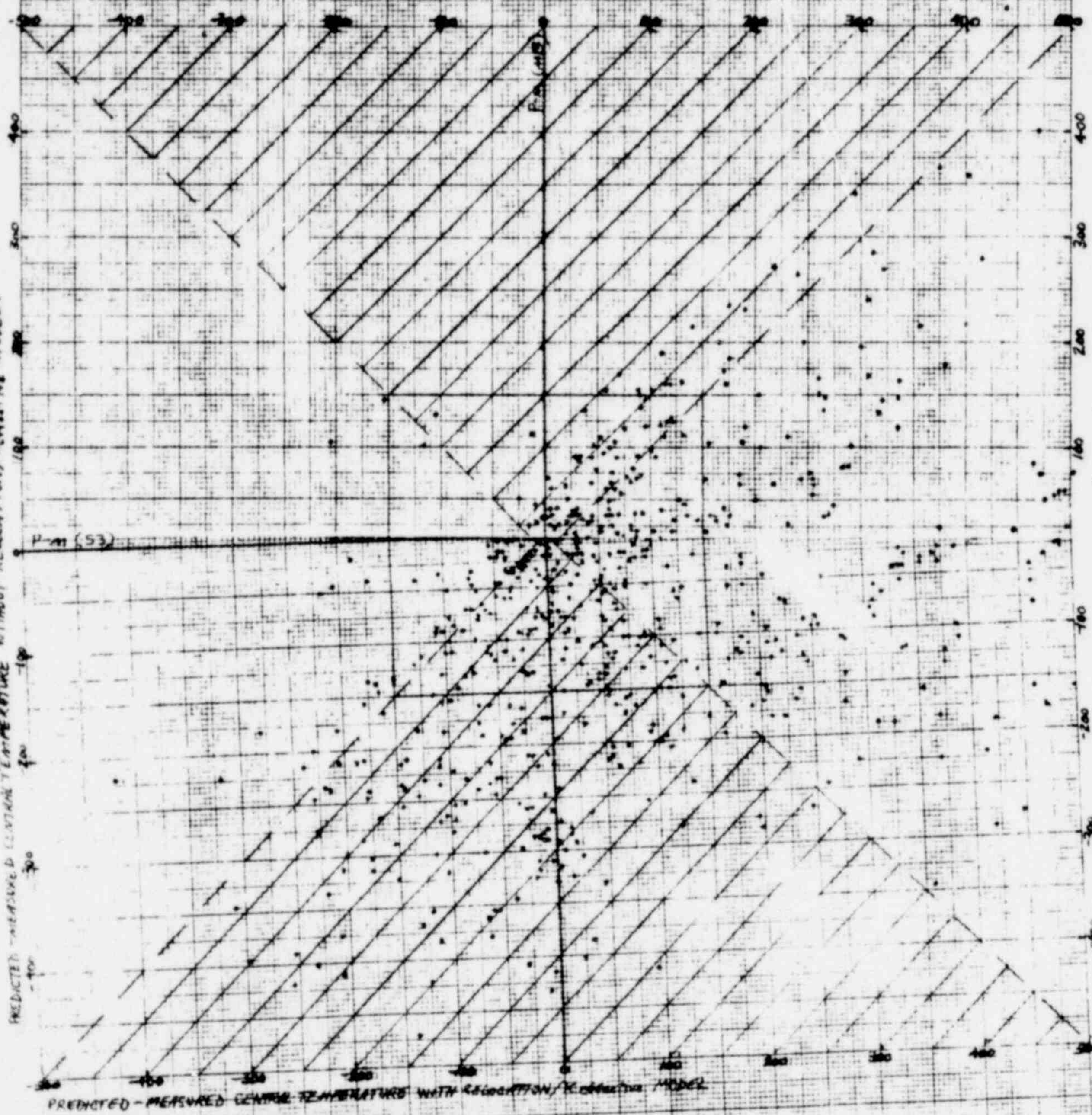

The thermal model comparison in Figure 23 can be analyzed further by evaluating differences in the error distribution obtained from both sets of runs. Figures 24 through 26 compare the frequencies with which differences between predicted and measured center temperatures fall within 50 degree error intervals between -500 and +500 C. Consideration of the total sample in Figure 24 indicates that certain design and operating conditions cause a concentration of overpredictions to occur in the right hand tail of the relocation model error distribution. Separating early life pressurized rod data in Figure 25 shows better performance for the relocation model in terms of both distribution shape and coincidence of the mean with zero error. Since unpressurized rod thermal conditions are typically more sensitive to operating mechanisms causing fuel and cladding deformation, or changes in pellet and gas conductivity, it seems as though some irradiation effect is either currently not accounted for or needs to be handled differently in subsequent thermal models. This point can be illustrated by plotting the model error frequency for burnup data comparisons as shown in Figure 26. Burnup results should be preferentially affected if there are deficiencies in the way the model treats irradiation effects on crack disposition and gap conditions. Tendency of the relocation model to overpredict burnup temperatures supports the contention that additional irradiation effects, such as permanent crack healing or fuel deformation induced crack closure need to be considered.

Since center temperature results provide only partial demonstration of stored energy predicitve capability, the error in characterizing pellet temperature distribution was compared, again between the corrected

COMPARISON BETWEEN CENTER TEMPERATURE ERROR FREQUENCIES USING FRAP-S3 WITH AND WITHOUT RELOCATION/$k_{effective}$ MODELS

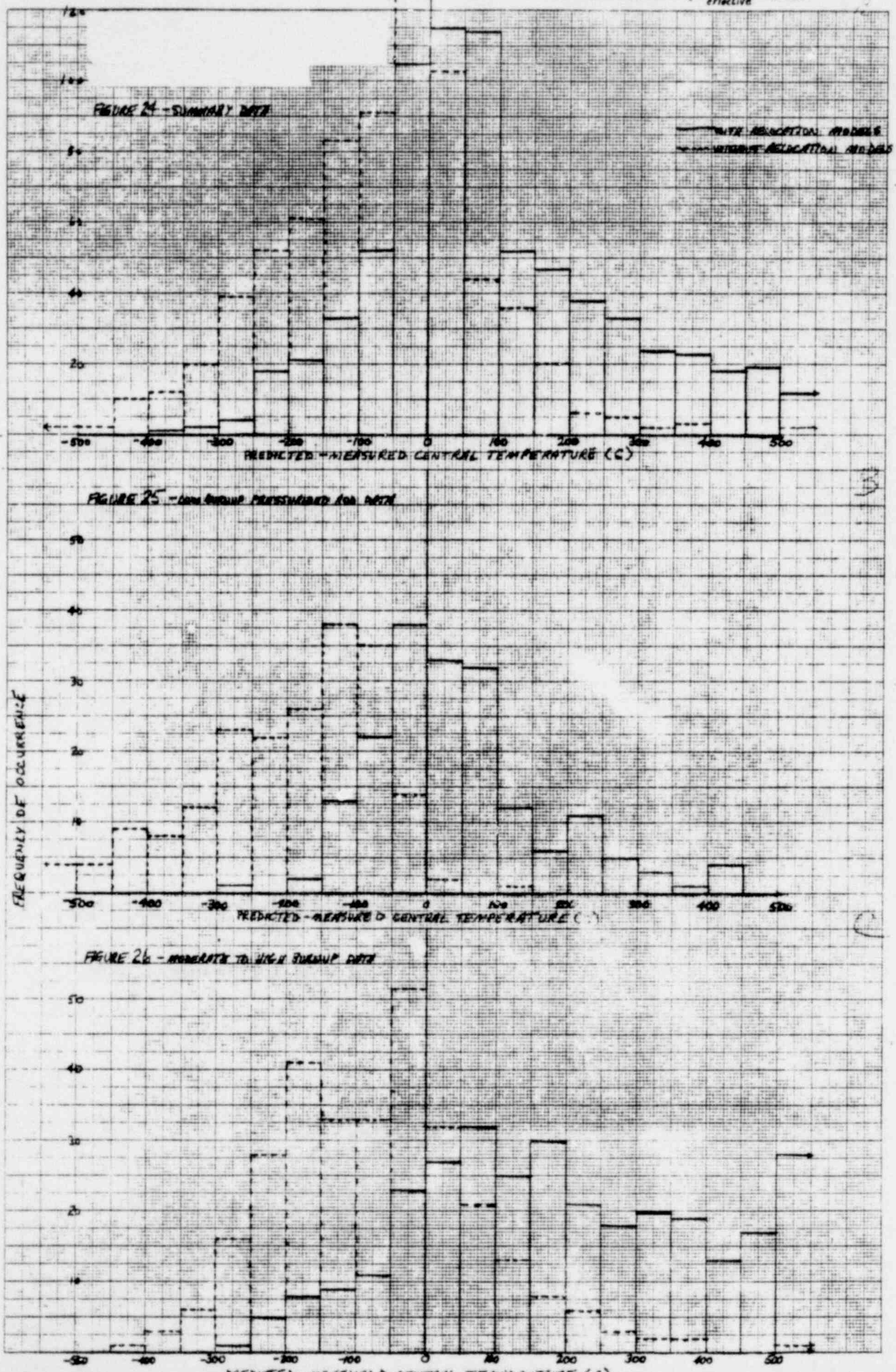

1569 193

23-377

cracking model and the current relocation model. The results shown in Figure 27 correspond to a subset of fuel temperature experiments having both central and radially distributed pellet thermocouples. The fact that the relocation model represents pellet temperature drops better than the cracking model supports the calculated relocation effect on fuel thermal conductivity at least for startup conditions.

Figures 28 and 29 compare the measured and calculated effects of gap size on pellet temperature distribution using FRAP-S3 with and without the relocation model. Gas composition is the same for both pressurized rods. For each rod, the models predict essentially the same fuel surface temperature. The pellet temperature profiles calculated without considering cracking effects on thermal conductivity are also quite comparable. The relocation model however predicts that more cracking tendency exists for the larger gap rod at these power and burnup conditions. The effective pellet conductivity is consequently lower and the temperature gradient higher in this case than that calculated for the small gap rod. Pellet conductivity reflects differences in gap and crack conditions, then, even at the same fuel temperature.

Figures 30 and 31 compare the measured and calculated effects of gas composition on fuel temperature for two rods with similar gap sizes, again using FRAP-S3 with and without the relocation model. The pellet temperature difference predicted without using relocation is insensitive to gas composition. The relocation model however calculates a lower effective fuel conductivity for the argon-filled rod as indicated by the steeper temperature gradient in this case. Crack conductivity then, in addition to availability of relocation gap space, is calculated to change the effective pellet conductivity.

1569 194

FIGURE 27 - COMPARISON BETWEEN PREDICTED - MEASURED PELLET TEMPERATURE DROP USING FRAP-S3 WITH AND WITHOUT RELOCATION/$k_{effective}$ MODELS

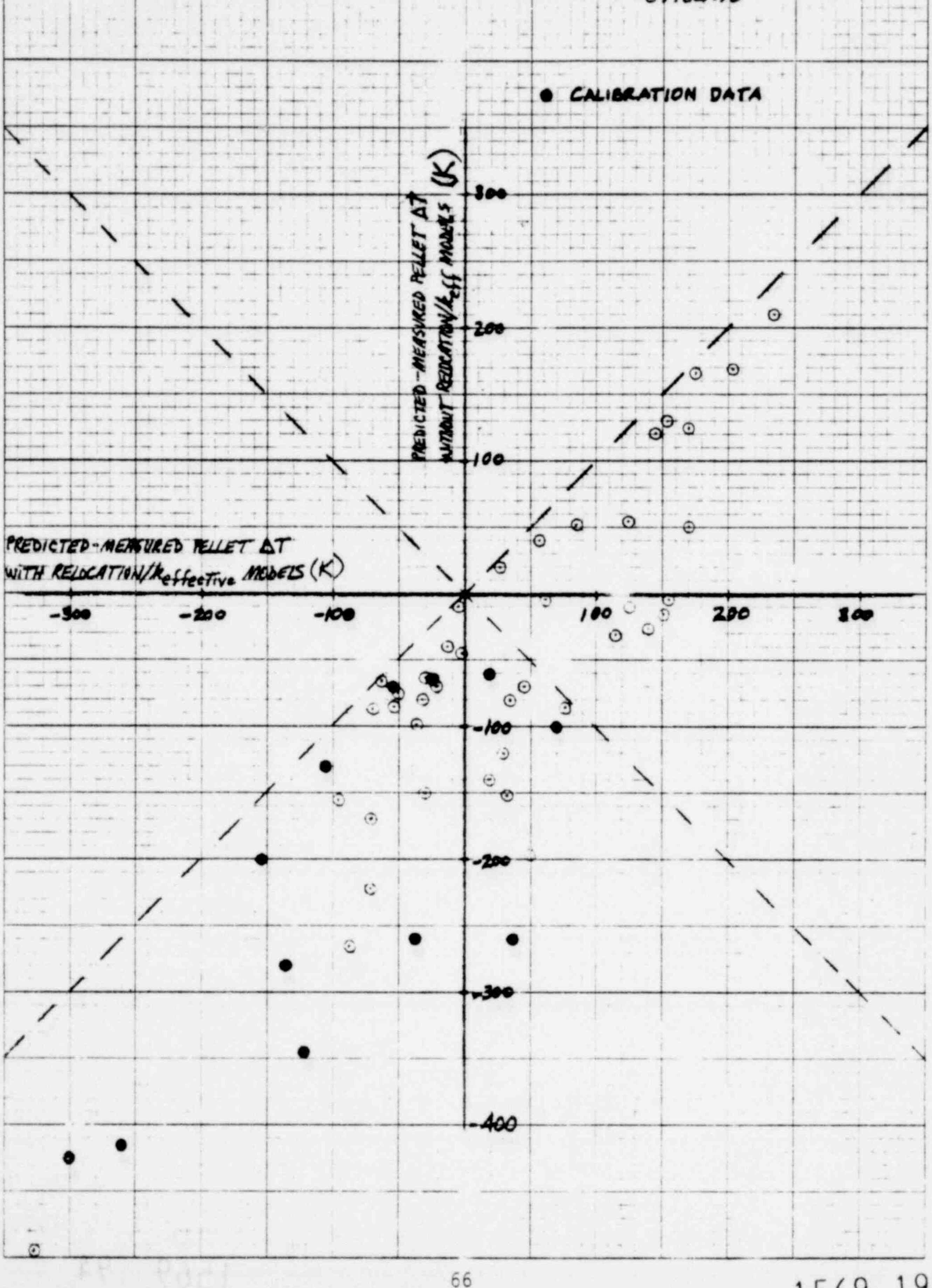

1569 195

23-378

46 0780

FIGURE 28 - SMALL GAP ROD

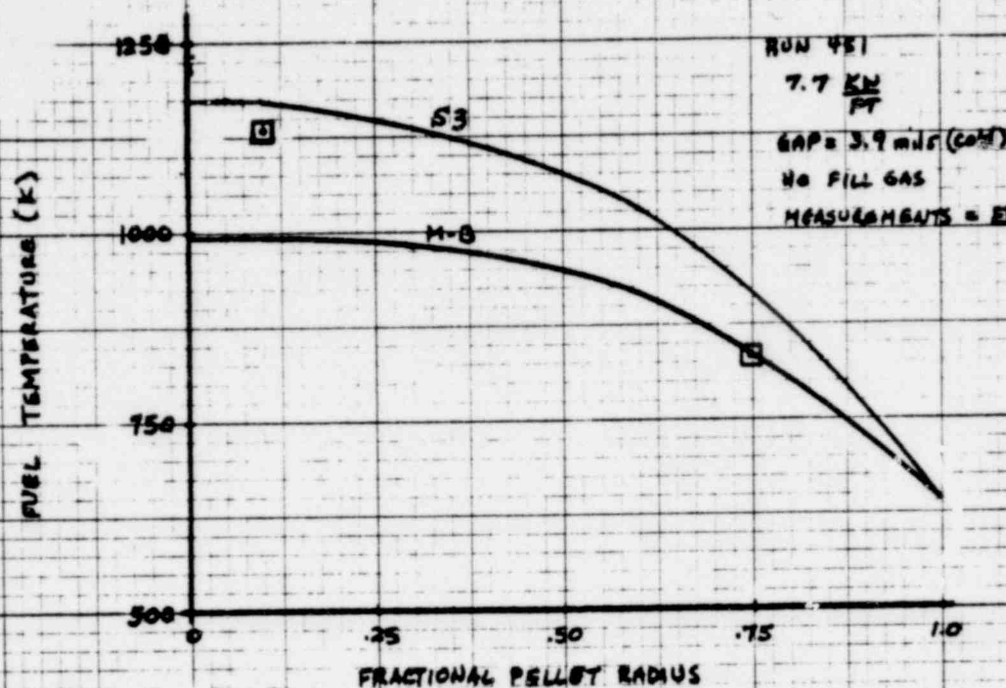

FIGURE 29 - LARGE GAP ROD

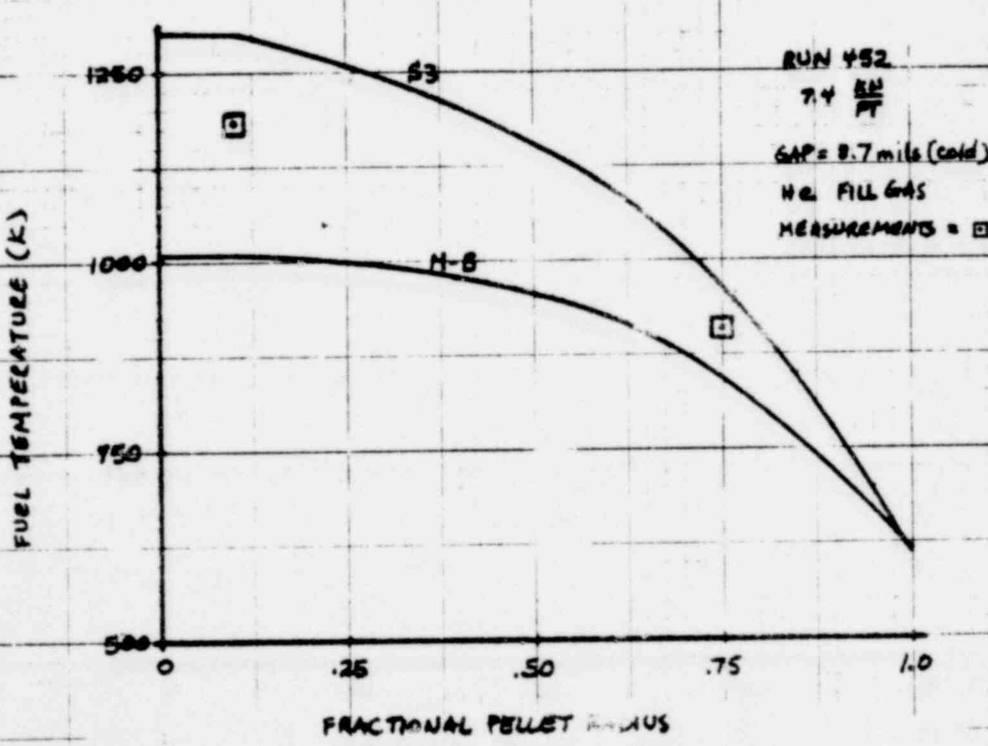

COMPARISONS BETWEEN MEASURED AND PREDICTED PELLET TEMPERATURE DISTRIBUTION V[illegible] [illegible] WITH AND WITHOUT RELOCATION/$h_{effective}$ MODELS

1569 196

FIGURE 30
HELIUM FILL GAS

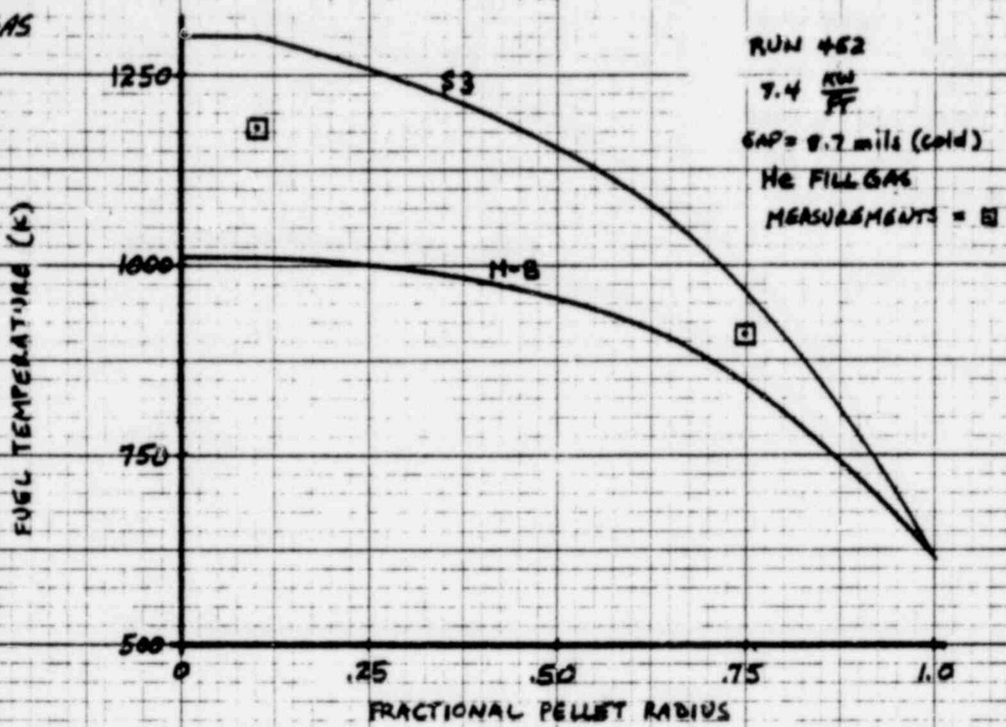

FIGURE 31
ARGON FILL GAS

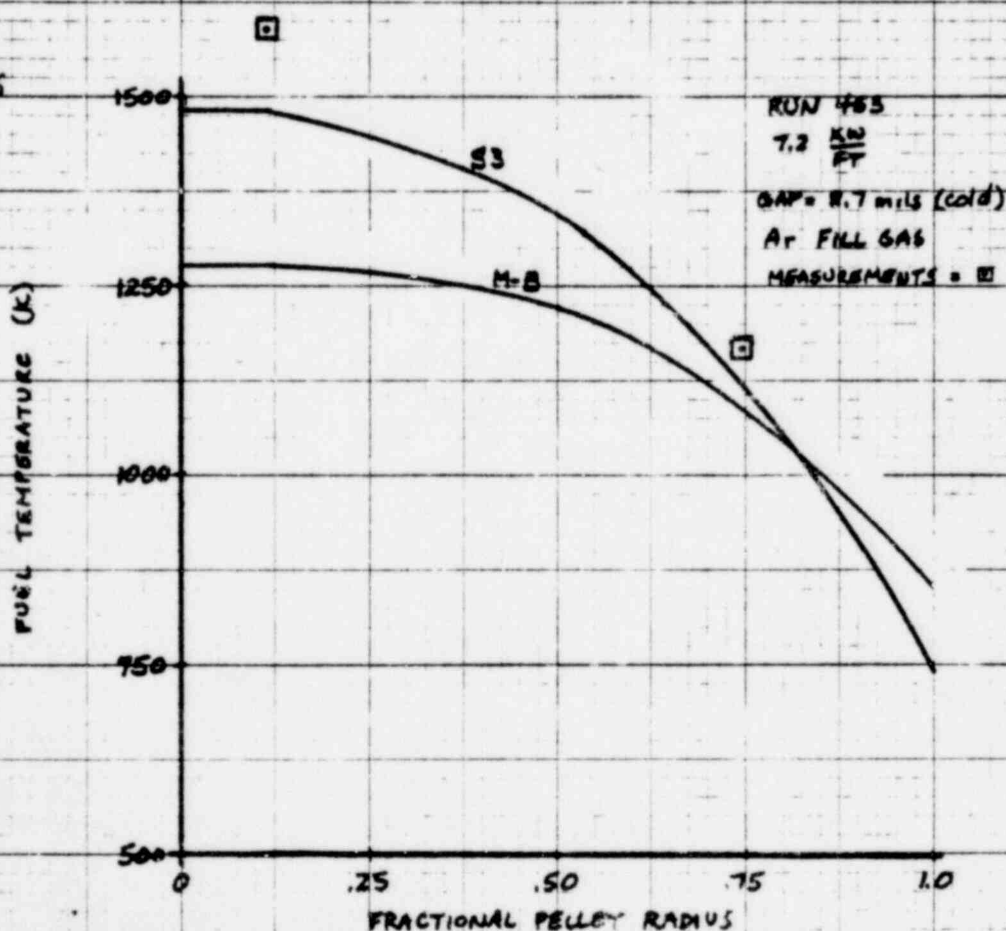

COMPARISONS BETWEEN MEASURED AND PREDICTED PELLET TEMPERATURE DISTRIBUTION USING FRAP-S3 WITH AND WITHOUT RELOCATION/$k_{effective}$ MODELS

In summary, the decision was made to perform the balance of verification runs using a finalized FRAP-S3 version with pellet relocation, effective fuel conductivity and Ross-Stoute gap conductance as active models. Based on results of many different fuel temperature as well as cladding deformation experiments, it was felt all along that the basic form of the relocation model is physically sound. Along with its associated gap and crack condition feedbacks, the model incorporates more realistic concepts of hot state rod geometry and internal heat transfer than those used in previous FRAP code versions. Moreover, the evidence indicated that relocation 1) provides a better representation of pellet temperature drop and PWR center temperature conditions than the alternate cracking model and 2) has no less capability, from a center temperature standpoint, than previous thermal models analyzed by verification. An operational relocation model was also needed to provide gap closure conditions for benchmarking revised calculations of pellet mechanical deformation in FRAP-T4. It was hoped that shortcomings qualitatively identified in the initial relocation model via duplicate temperature comparisons could be diagnosed with more certainty by conducting a complete verification effort. In this way, other fuel performance areas exhibiting sensitivity to thermal conditions, could be analyzed in addition to temperature itself. Large sample analysis could then provide enough resolution to identify areas in the new thermal model which warranted further improvement.

3.1.1.2 Summary Fuel Temperature Results. This section presents summary fuel center temperature results for the complete pellet thermocouple sample of some 100 rods, representing over 800 data comparison points.

Figures 32 and 33 compare measured and predicted center temperatures for unpressurized and pressurized rods respectively. The standard error between measured and predicted fuel temperature is 198C based on Figure 32 data and 254C based on Figure 33 data. Results for unpressurized rods are more representative of different fabrication, design, and operating conditions due to availability of a larger measurement sample. For the same reason, interpretation of the unpressurized rod data comparisons is less affected by differences in systematic error between the experiments considered. Any tendency to overpredicted pressurized rod temperatures in Figure 33 for example, is mainly based on adjusted burnup measurements from one test program and cannot be interpreted as a general result until more data are considered. The fact that unpressurized rod center temperatures are often overestimated by the relocation model is expected in light of duplicate comparison results discussed in the previous section (Figure 26). Subsequent graphical diagnosis of trends in temperature results will attempt to establish which thermal parameters contribute most to the model error. The consistent occurrence of certain data points at the extreme limits of the error distribution also provides some insight into which data should be verified for accuracy or perhaps given less weight in statistical evaluations of model performance.

Figures 34 through 37 relate fractional model error for all center thermocouple data points to the expected first order design and operating parameter effects, in this case, gap size, local power, fuel density and local burnup. It is not likely that underestimating gap conductance is a significant source of systematic error, as shown in Section 3.1.2.

23-380

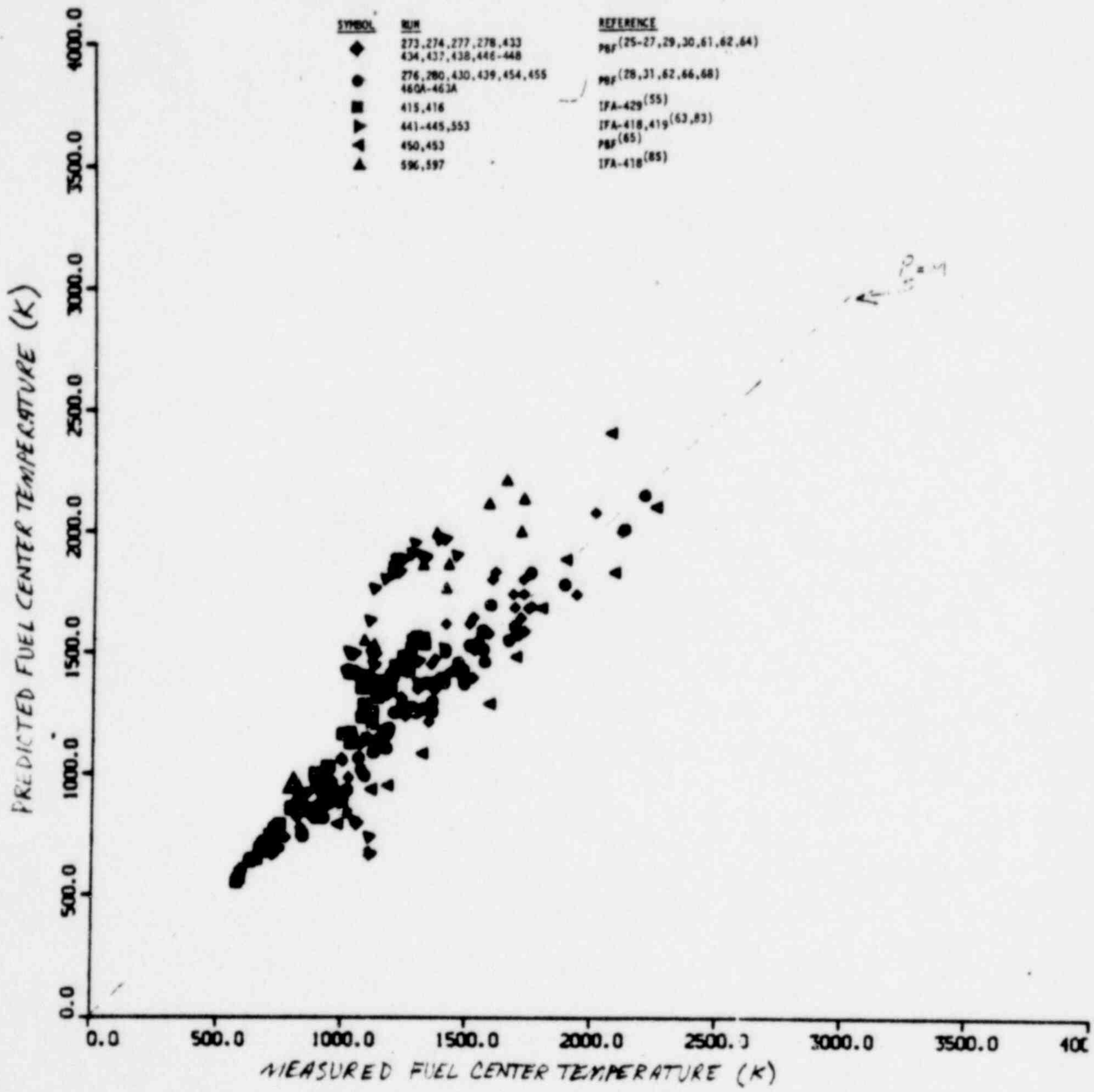

FIGURE 33 FRAP-S3 predicted versus measured center temperatures for pressurized rods . . . .

1569 200

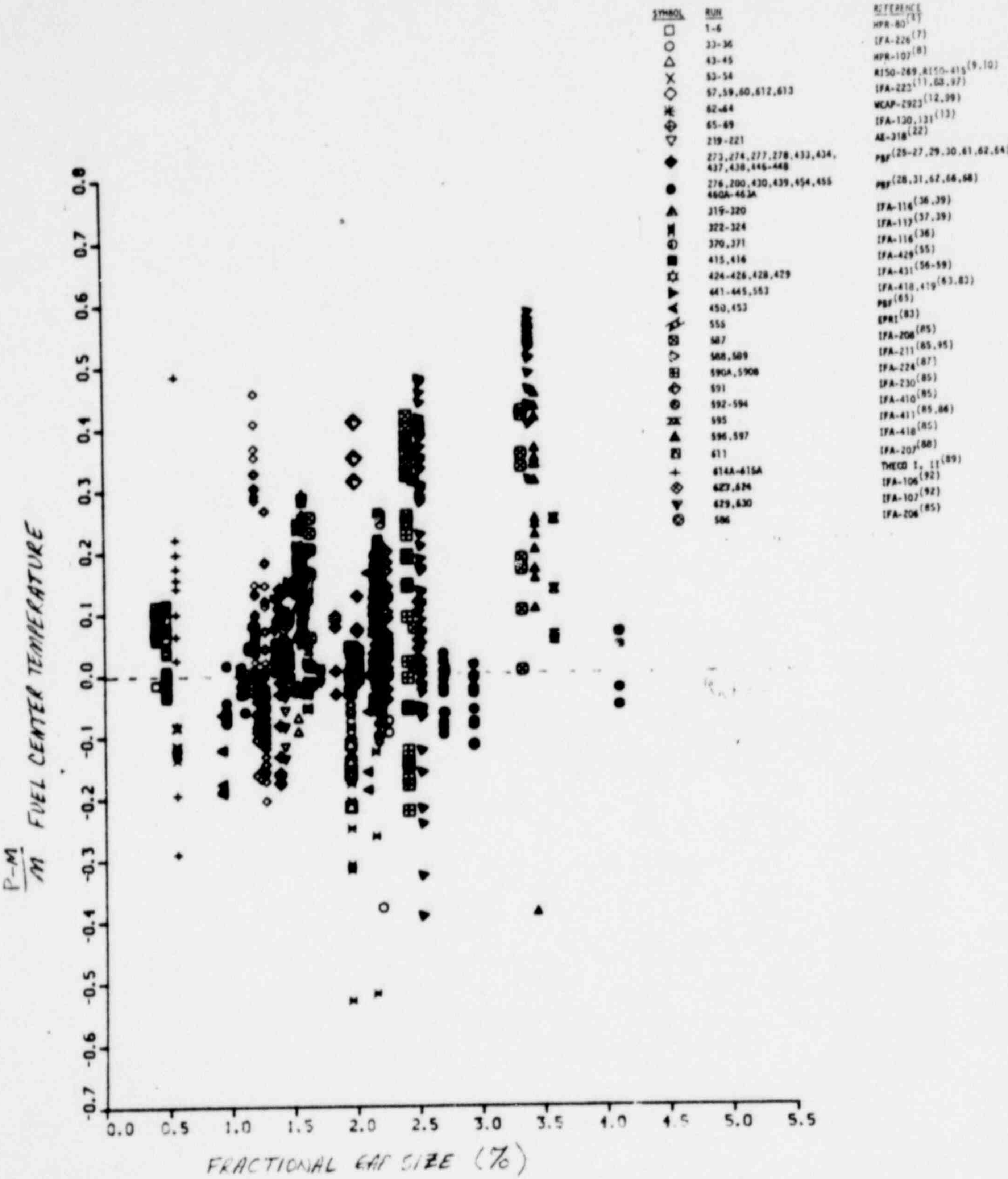

FIGURE 34 Effect of gap size on FRAP-S3 center temperature error. . . . .

1569 201

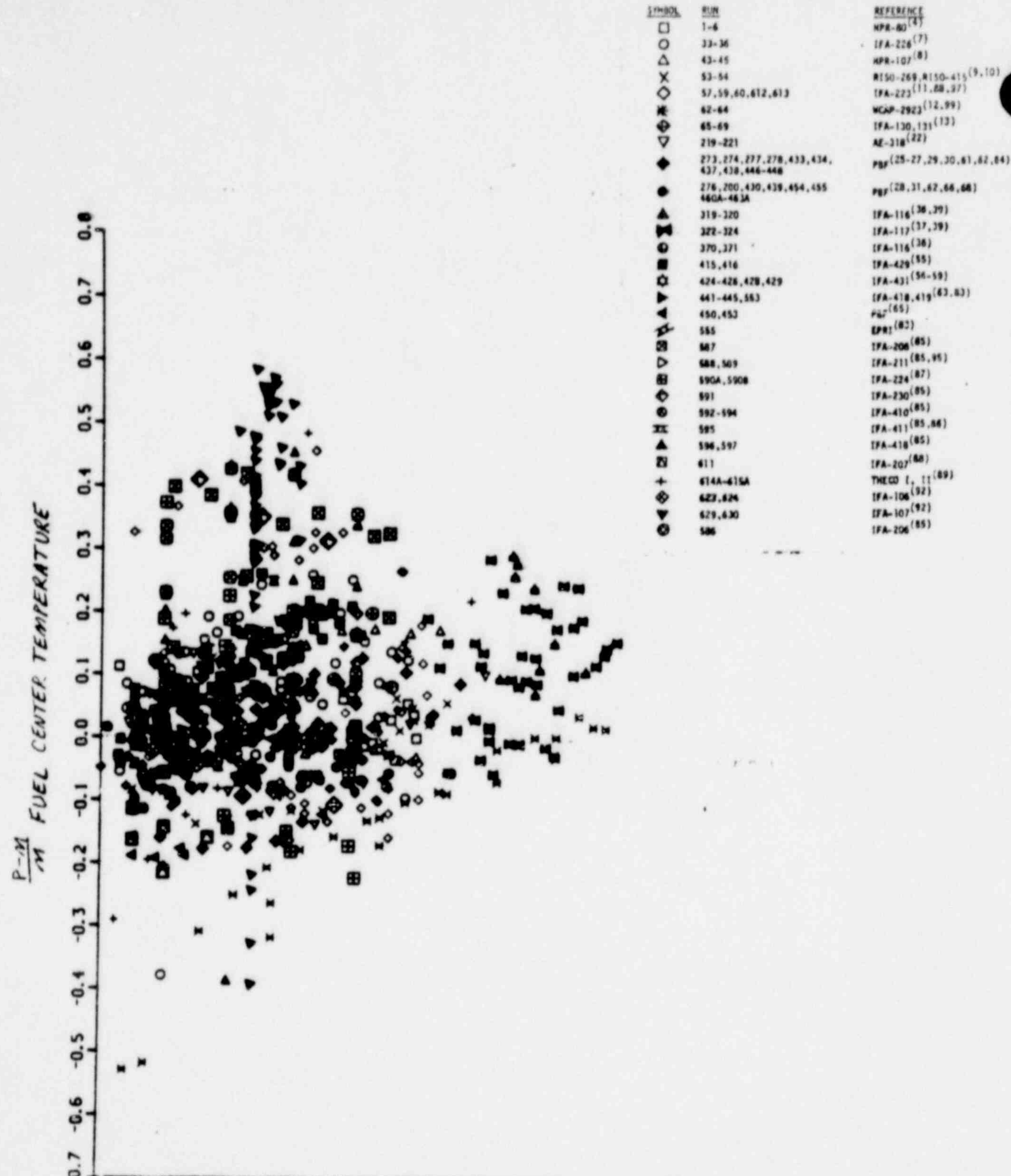

FIGURE 35 Effect of local heat rating on FRAP-S3 center temperature error. . . . .

1569 201

1569 202

23-382

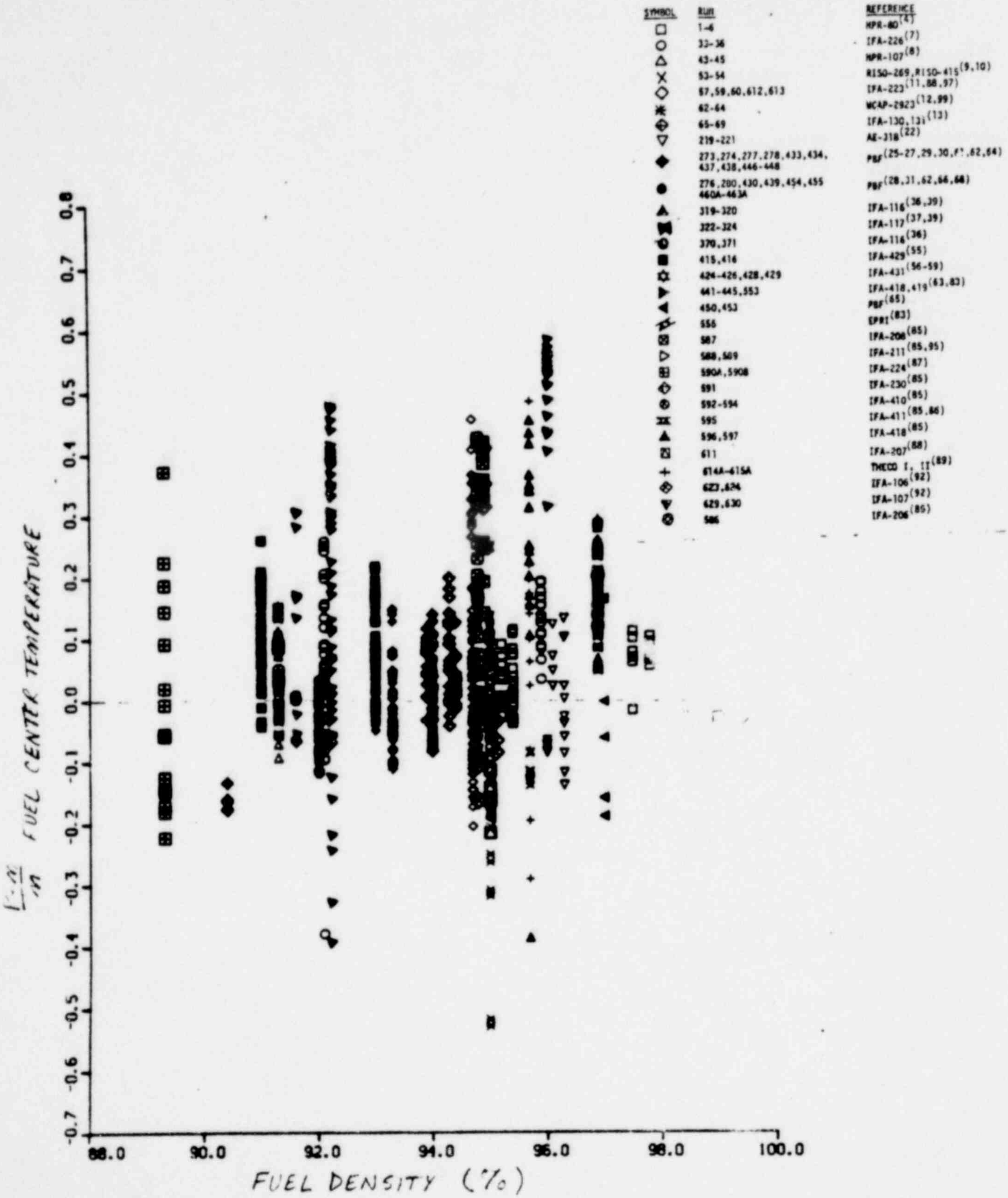

FIGURE 36 Effect of fuel density on FRAP-S3 center temperature error. . . . .

1569 203

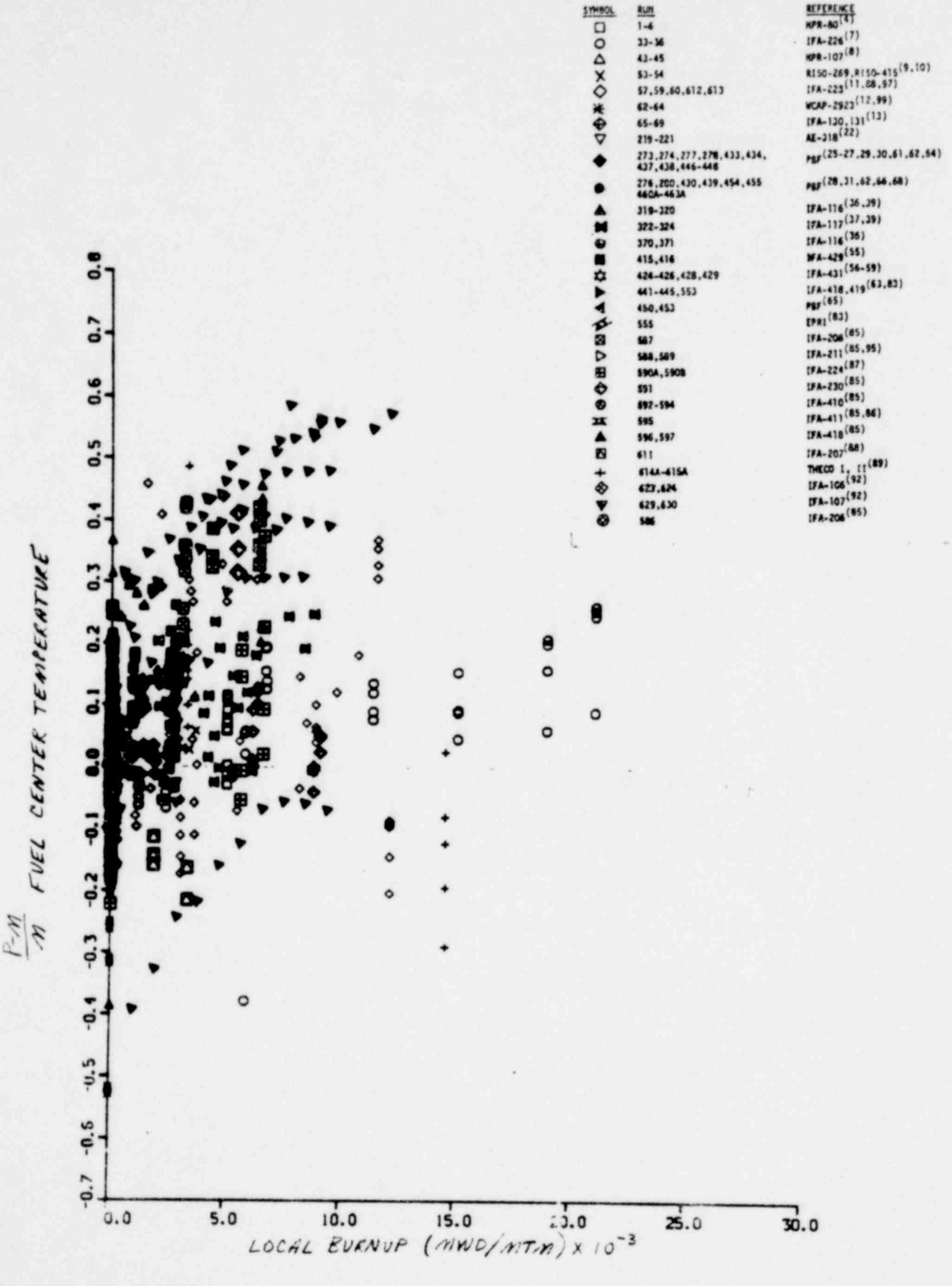

FIGURE 37 Effect of local burnup on FRAP-S3 center temperature error. . . . .

1569 204

Figure 34 indicates somewhat more tendency to overpredict fuel center temperature for gaps greater than 2%. Relocation effects may be more limited under large gap conditions than the currently applied floor on fractional thermal conductivity of .45 would suggest. It may be necessary to allow a limit on the amount of relocation to more directly moderate thermal conductivity adjustments, rather than to apply a constant minimum value to the adjustment itself.

Figure 35 relates fractional error in calculated center temperature to local heat rating conditions. The fact that overpredictions occur more consistently above 10 kW/ft is an argument for completely closing peripheral pellet cracks under moderate to hard PCI conditions. The current model assumes that a minimum 10% reduction in thermal conductivity will always exist in the outer, unhealed fuel annulus.

The effect of fuel density on the fractional model error parameter shown in Figure 36 is not entirely clear. Prior verification results[110] suggested that density had no effect on the pellet diameter increase due to relocation. Center temperature error in Figure 36, however seems to increase for pellet densities below or above 93 to 94%. Either the current density effect is confounded by other influences or some effect of relocation on thermal conductivity is unaccounted for when fuel density is much different than that reflected in the relocation model calibration data (93-95%). It is known that the previously used porosity effect on pellet conductivity is not actively coupled in the current model to the often larger cracking effect on conductivity.

Even though relatively few fuel temperature measurements are available over extended operating periods, more tendency to overpredict low to moderate burnup temperatures is indicated in Figure 37. The fact that crack healing is not currently treated as a permanent restructuring/ deformation related phenomenon is likely to be at least partly responsible. Overprediction of fission gas release or the underestimation of pellet crack conductivity may also contribute to the observed trend. It is noteworthy that component gas conductivities used to calculate gas mixture and therefore crack conductivity have not always been measured or benchmarked against model predictions at the local fuel temperature conditions now imposed by the relocation model. In any event, all but a few of the burnup data points reflect unpressurized rods whose thermal response is most sensitive to calculated fission gas release and internal heat transfer geometry effects.

3.1.2 Gap Conductance. Gap conductance values have been analytically inferred for various experiments based on thermal model agreement with measured fuel temperatures, or cladding temperature phase lag during programmed power oscillations. Significant data scatter arises due to the geometric sensitivity and steep temperature gradients inherent in analyzing gap heat transfer conditions. Relative agreement between FRAP-S3 results and inferred experimental values is strongly affected by similarity in material properties and analytical assumptions. In this case, whether or not the experimental method considers a relocated pellet geometry and effective conductivity feedbacks, will determine the degree to which FRAP-S3 results match the gap conductance data. FRAP-S2 had previously shown a tendency[37] to overpredict gap conductance for pressurized rods. Unpressurized rod results were scattered due to the higher thermal model sensitivity accompanying a lower gap conductance level.

Figures 38 and 39 compare "measured" and calculated gap conductance for pressurized and unpressurized rods respectively. Physically identifiable trends are not very evident since the comparison is now dominated by the net degree of consistency between FRAP-S3 and the experimental gap conductance model. With the exception of a few data points representing initially fission gas filled rods, the calculated gap heat transfer level is always in excess of 1000 BTU/hr-ft^2-F. Most of the measured values are overpredicted by the model. The relocation model allows high gap conductance to exist under soft (open cracks) as well as hard gap closure conditions.

The effects of gap and power on relative gap conductance model error are shown in Figures 40 and 41 for all of the data considered. The trends in both cases indicate more consistency between measured and calculated values for operating conditions promoting hard gap closure, ie small initial gap sizes or high heat ratings. This observation is not unexpected since the effects of differences between FRAP-S3 and the experimental heat transfer model are minimized when FRAP-S3 calculates pellet cracks to be closed. Under open or soft gap closure conditions, the inferred experimental values are overpredicted by factors of 2 to 10. It is worthwhile for experimentally derived pellet relocation and effective conductivity concepts to be incorporated in gap conductance

1569 207

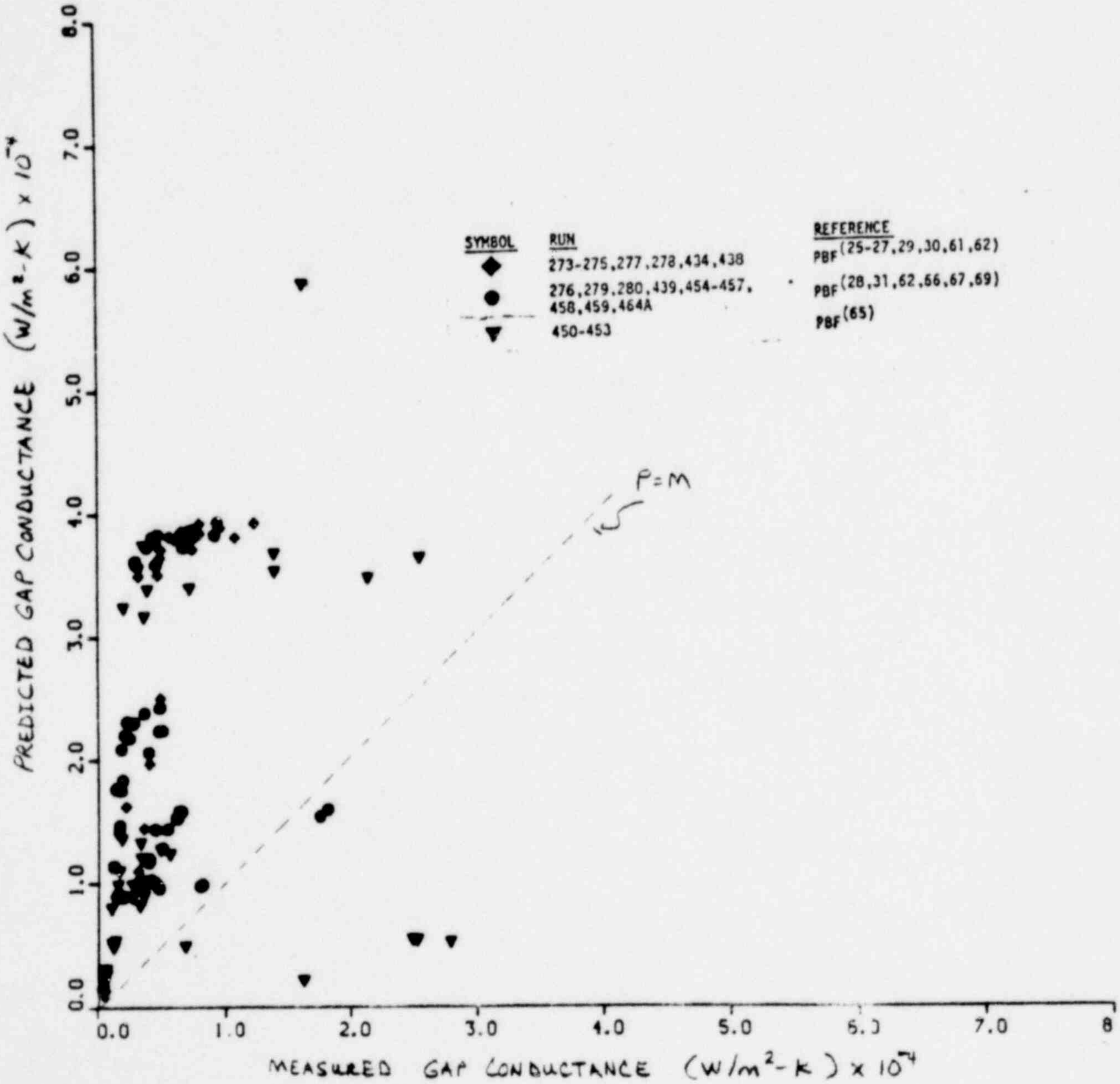

FIGURE 38 FRAP-S3 predicted versus experimentally inferred gap conductance - pressurized rods . . . .

23-385

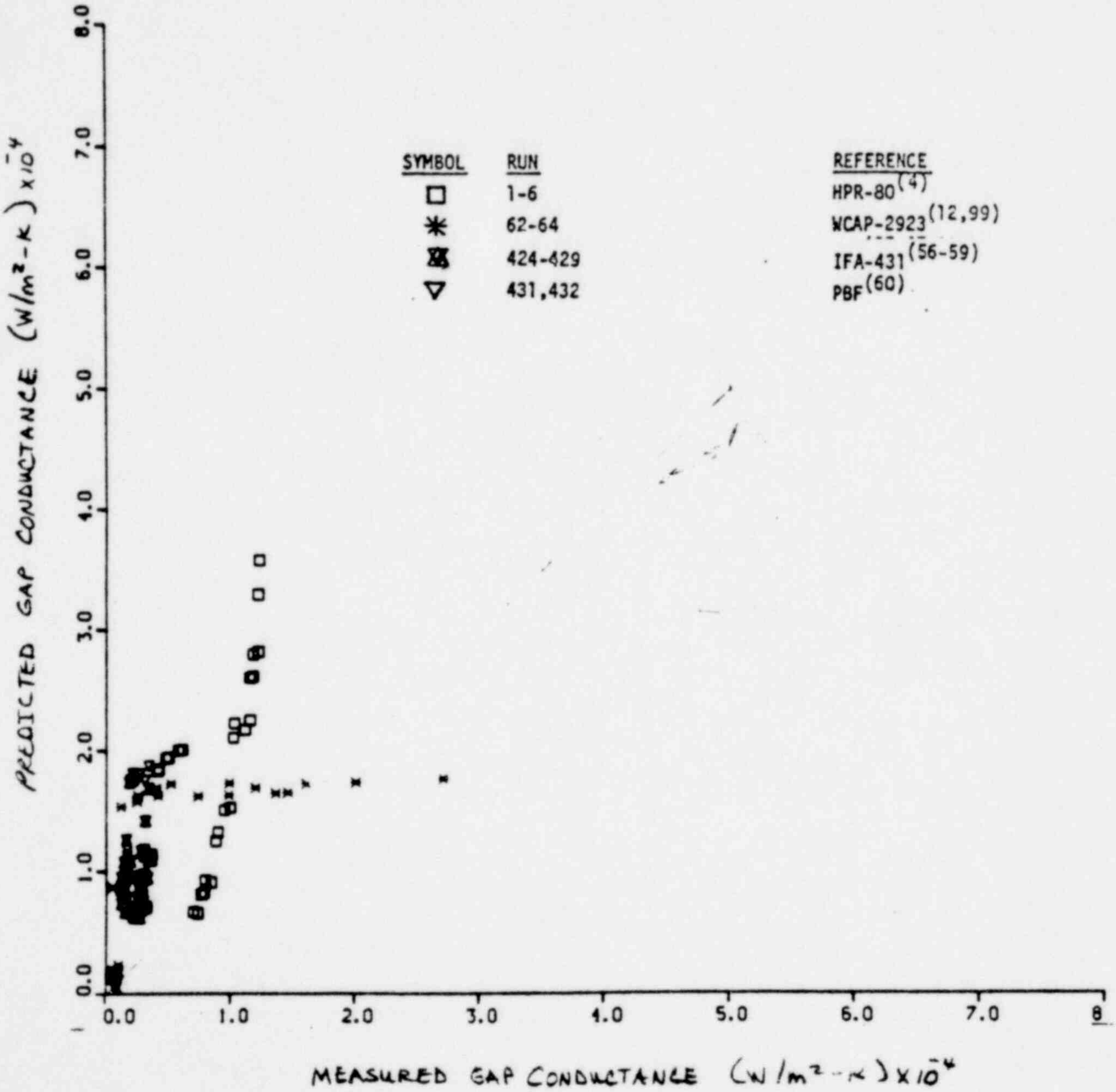

FIGURE 39 FRAP-S3 predicted versus experimentally inferred gap conductance - unpressurized rods . . . .

1569 209

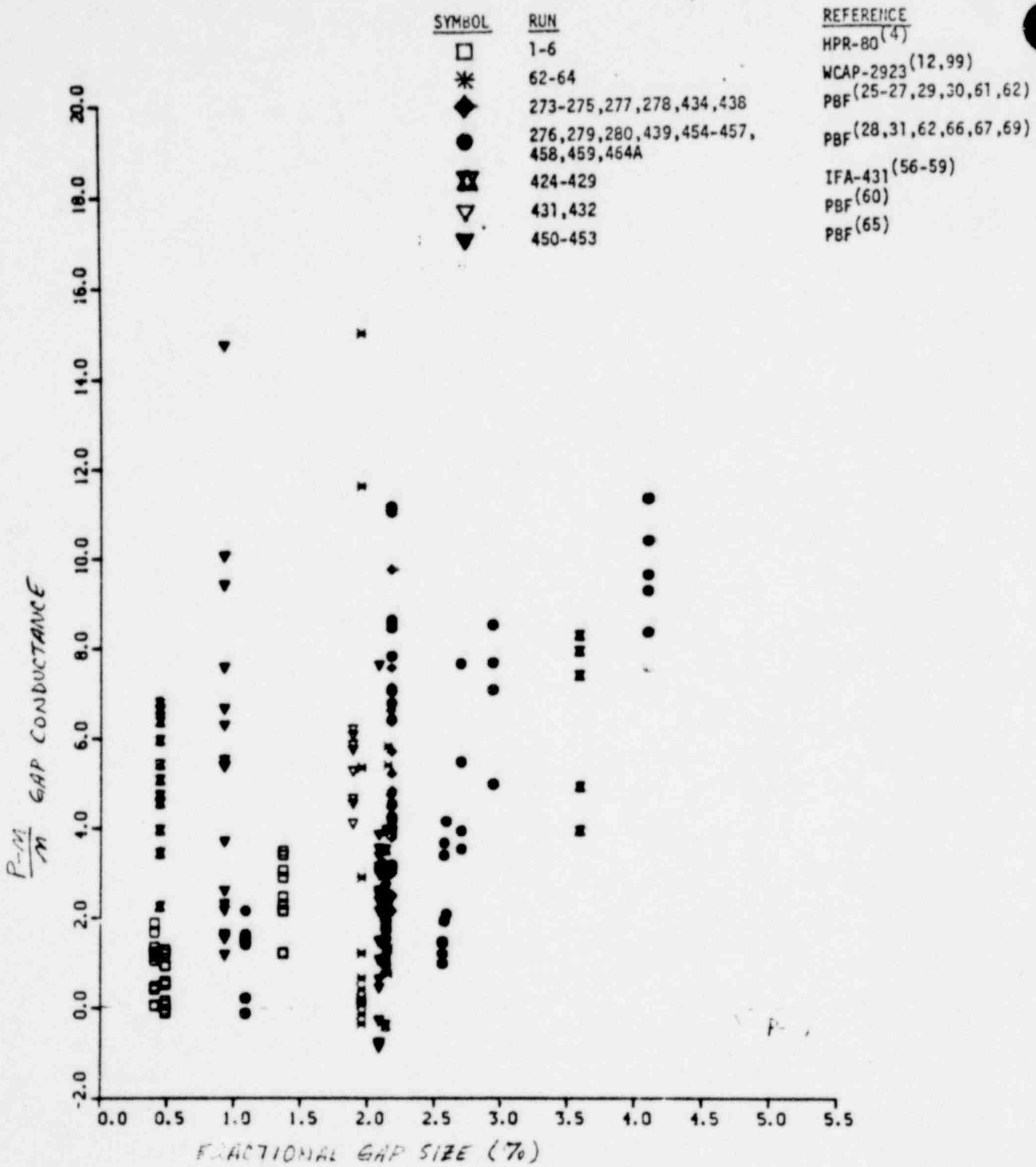

FIGURE 40 Effect of gap size on FRAP-S3 gap conductance error.

1569 210

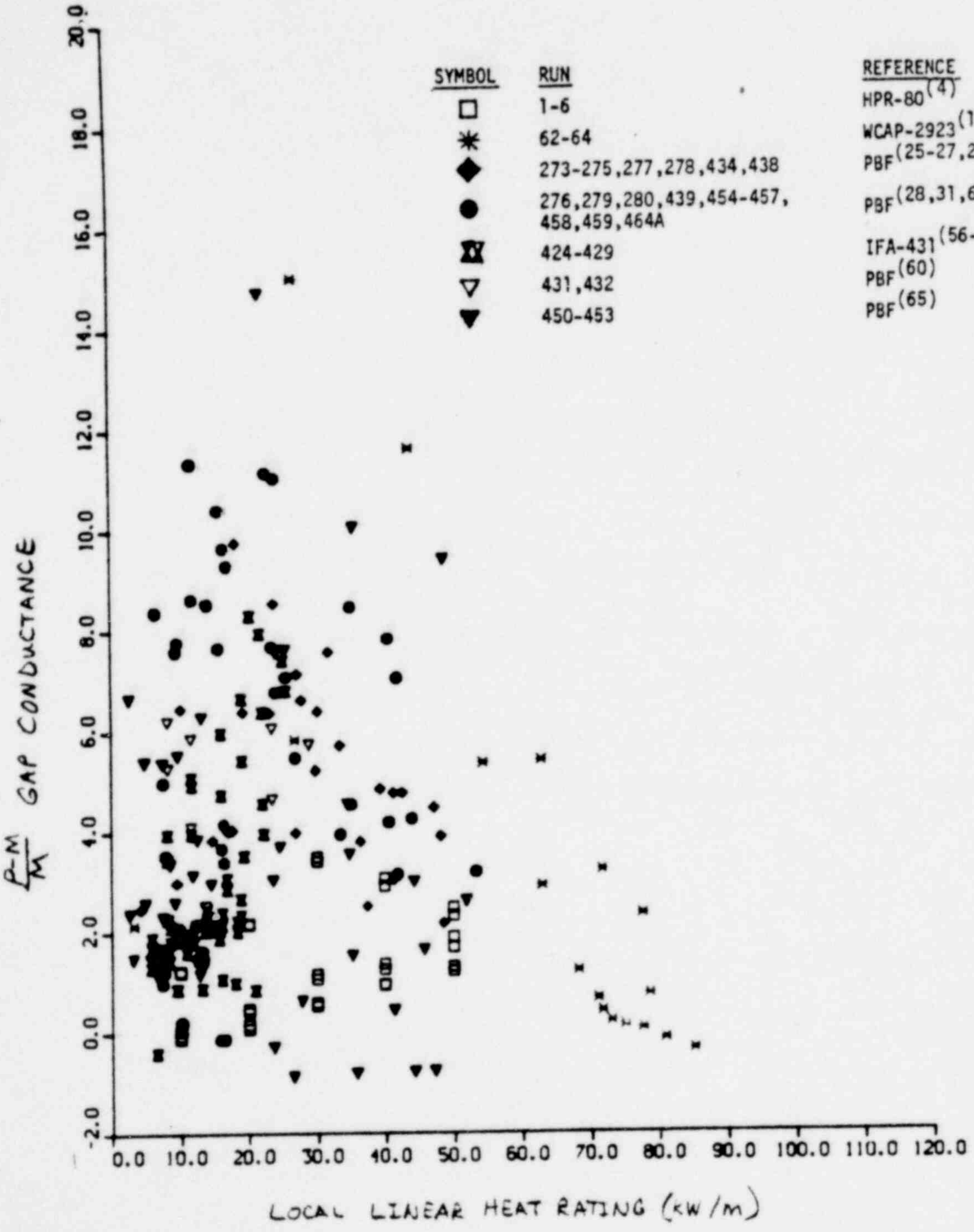

FIGURE 41 Effect of local heat rating on FRAP-S3 gap conductance error. . . . .

1569 211

data reduction techniques. Experimental thermal data could then reflect more realistic gap geometry conditions consistent with cladding deformation measurements.

3.2 Fission Gas Model

The relative amount and composition of rod internal gas and void volume has strong influence on operating pressure, effective gap size, and fuel thermal conditions. Data comparisons using previous code versions[3,107] had indicated that gas composition had too much influence on calculated gap heat transfer. Since FRAP-S3 incorporates pellet relocation and revised conductivity models, data comparisons for fission gas release and rod internal pressure could be analyzed within the framework of a more mechanistic fuel temperature moc.l. Backfill pressure, gas release, void volume and void temperature mechanisms control fission product inventory and cladding hydrostatic stress level for analysis of core depressurization consequences.

3.2.1 Gas Release Fraction. Fission gas release fraction will be discussed before rod internal pressure since interpre:ation of results is less dependent on being able to model rod internal void volume changes. The rods used for data comparison purposes represent a wide range of design, operating, and burnup conditions. Capability of the current, primarily temperature dependent model is presented in the following section. The evaluation of model results is followed by a data analysis section in which an attempt is made to separate relative influence of temperature and burnup in terms of current versus cumulative effects of matrix diffusion processes.

3.2.1.1 Current Model Results. Figure 42 compares measured and predicted gas release fraction for the data sample of about 180 unpressurized rods. Despite incorporation of different thermal models in FRAP-S3, the tendency to overpredict low to moderate release conditions is similar to that exhibited by FRAP-S2. Also, relatively high gas release conditions in excess of 10% are again better represented by the model. The fact that these trends exist for two different thermal models indicates that errors in calculated gas release reflect the lack of some mechanistic quality in the current model, rather than inability to calculate fuel temperature conditions. Considering all the data, the standard error between measured and calculated gas release fraction is 18.8%. At high burnup, such a value represents considerable error in establishing the initial disposition of fission product inventory for transients.

Figure 43 shows relative gas release model error as a function of fuel temperature. The fuel temperature axis represents the maximum rod average value calculated by FRAP-S3 for each irradiation. Previous verification results[3] demonstrated that model error was sensitive to calculated temperature conditions during peak duty operating periods. In this case, there is a general trend of decreasing model error with increasing fuel temperature. High gas release conditions, more dominated

1569 213

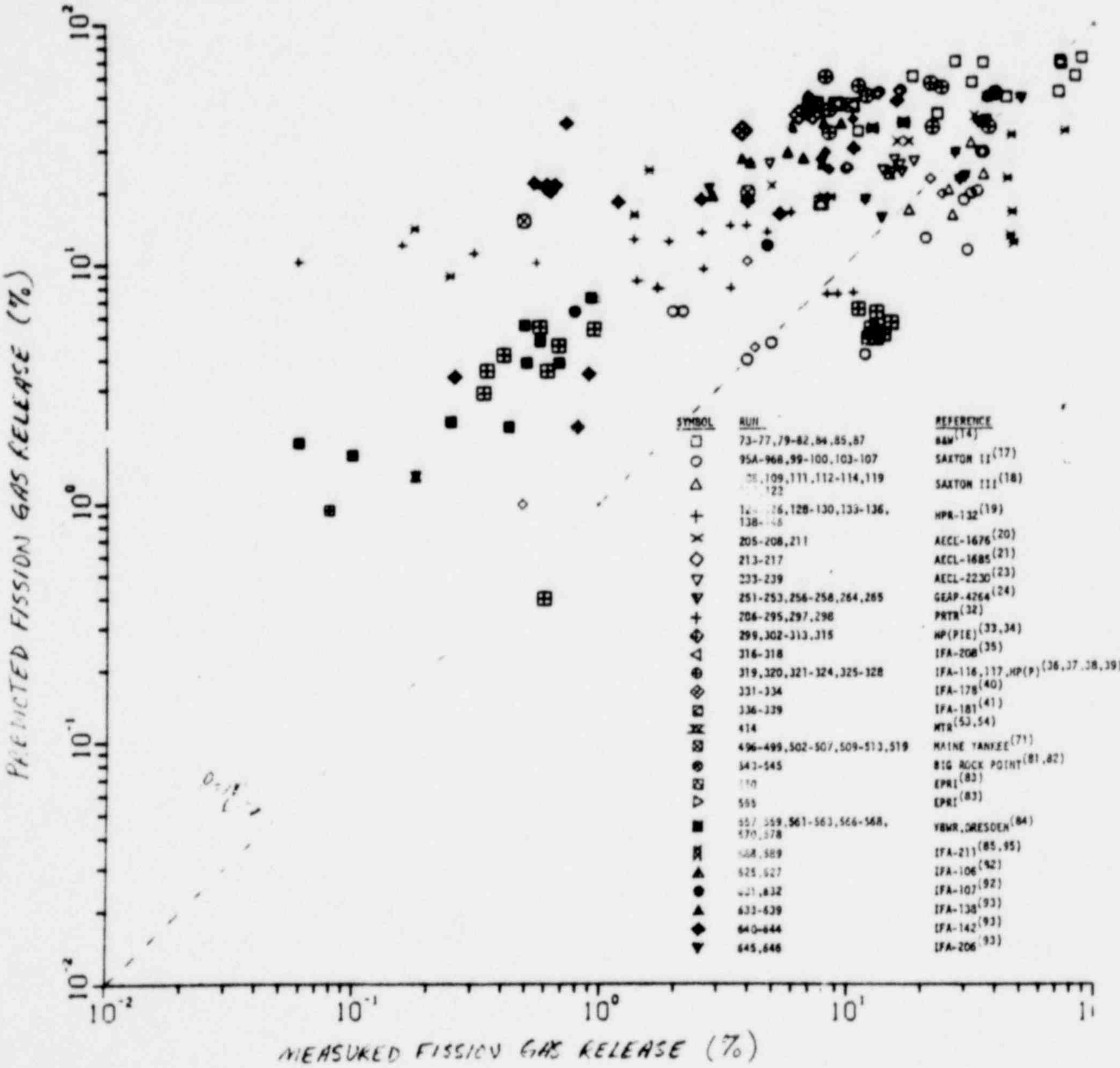

FIGURE 42 FRAP-S3 predicted versus measured fission gas release fraction . . . .

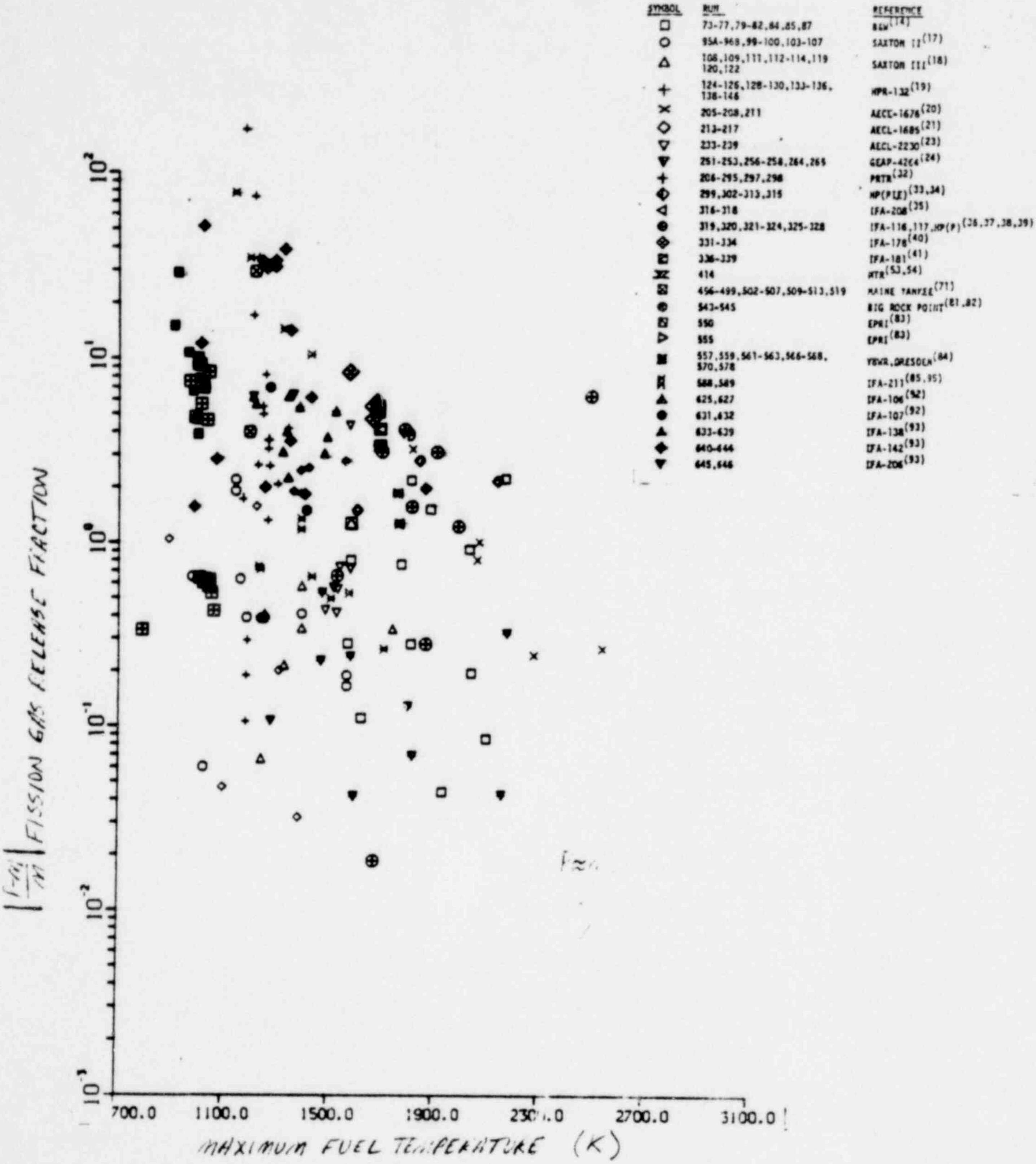

FIGURE 43 Effect of maximum fuel temperature on FRAP-S3 fission gas release error. . . . .

1569 215

by current as opposed to cumulative effects of fuel temperature, have always been better represented by the current, empirically based, instantaneous release model. It is likely that the kinetics of gas bubble mobility and disposition with respect to trapping and preferential venting sites play an as yet unaccounted for role in the calculated release mechanism.

3.2.1.2 Data Analysis. Results of the previous section suggested that mechanistic relationships exist between propensity for gas release and the effect of fuel temperature and burnup conditions on gas bubble mobility and location. The gas release data by itself were plotted versus temperature, burnup, and a diffusion dependent parameter as shown in Figures 44 through 47. Both maximum and life-averaged temperatures were used as the basis for investigating relative influence of thermal effects. The influence of temperature on diffusion coefficient is perhaps the strongest physical relationship between a mechanistic approach to calculating gas release and the temperature dependence of the current model. It should be recognized that the following discussion represents a scoping study only. Irradiation conditions were not analyzed in sufficient detail for results to constitute a quantitative model derivation. The influence of unaccounted for fabrication and local power history effects, together with the inherent statistical nature of gas release behavior contribute to significant scatter in both data and calculated results.

1569 216

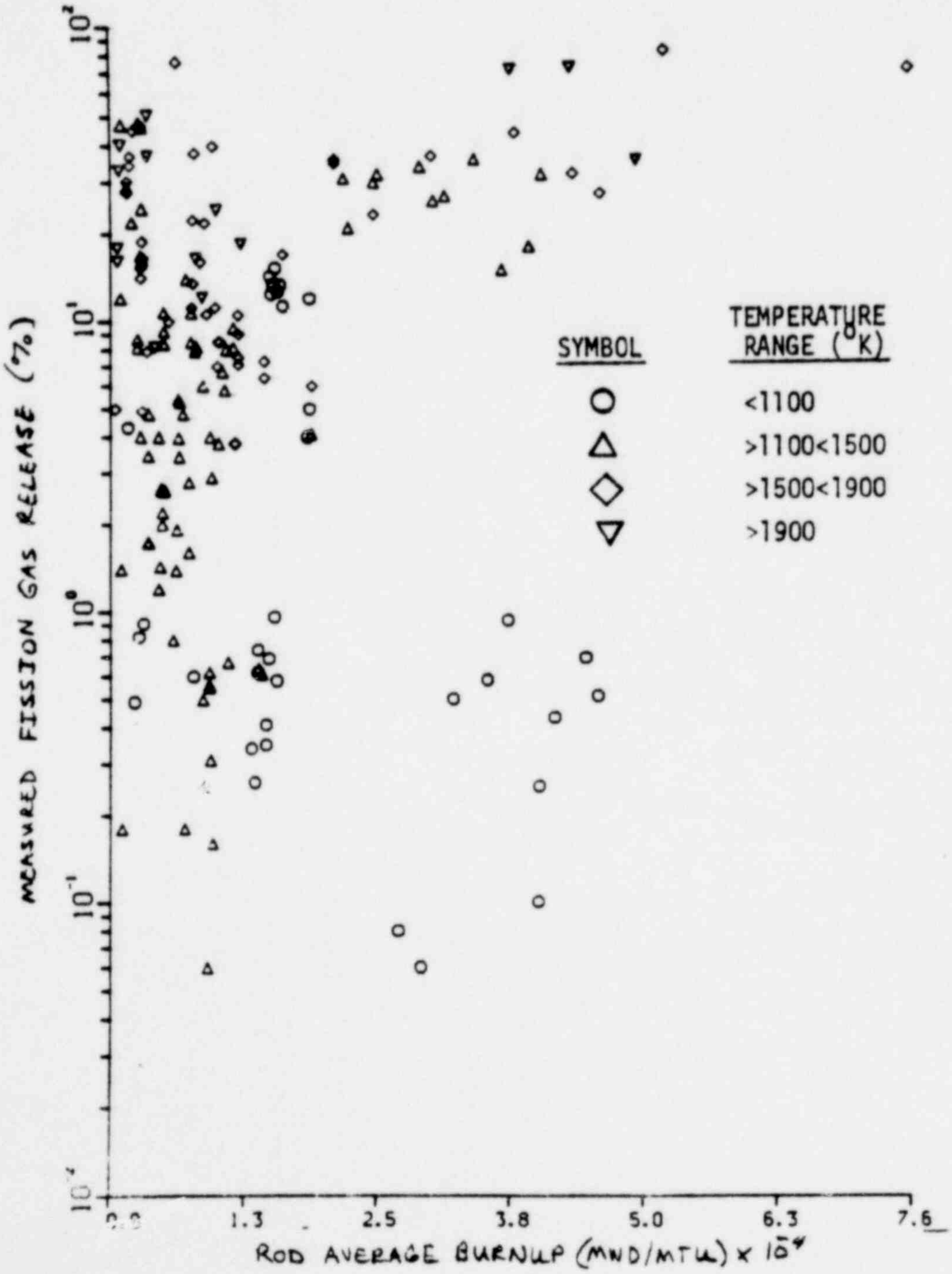

FIGURE 44 Measured fission gas release fraction versus burnup for different maximum fuel temperature ranges. . . . .

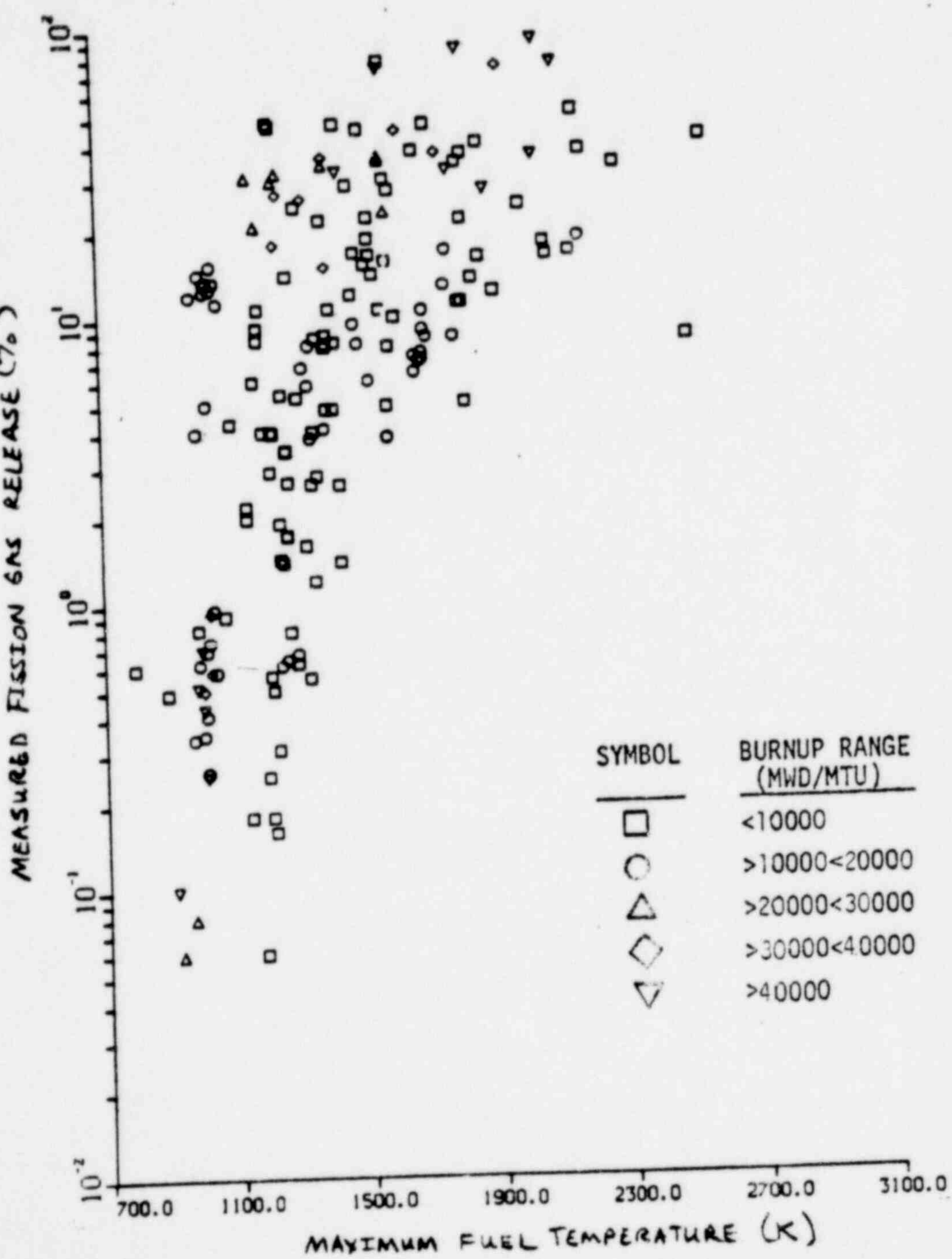

FIGURE 45 Measured fission gas release fraction versus maximum fuel temperature for different burnup ranges . . . . .

1569 218

23-390

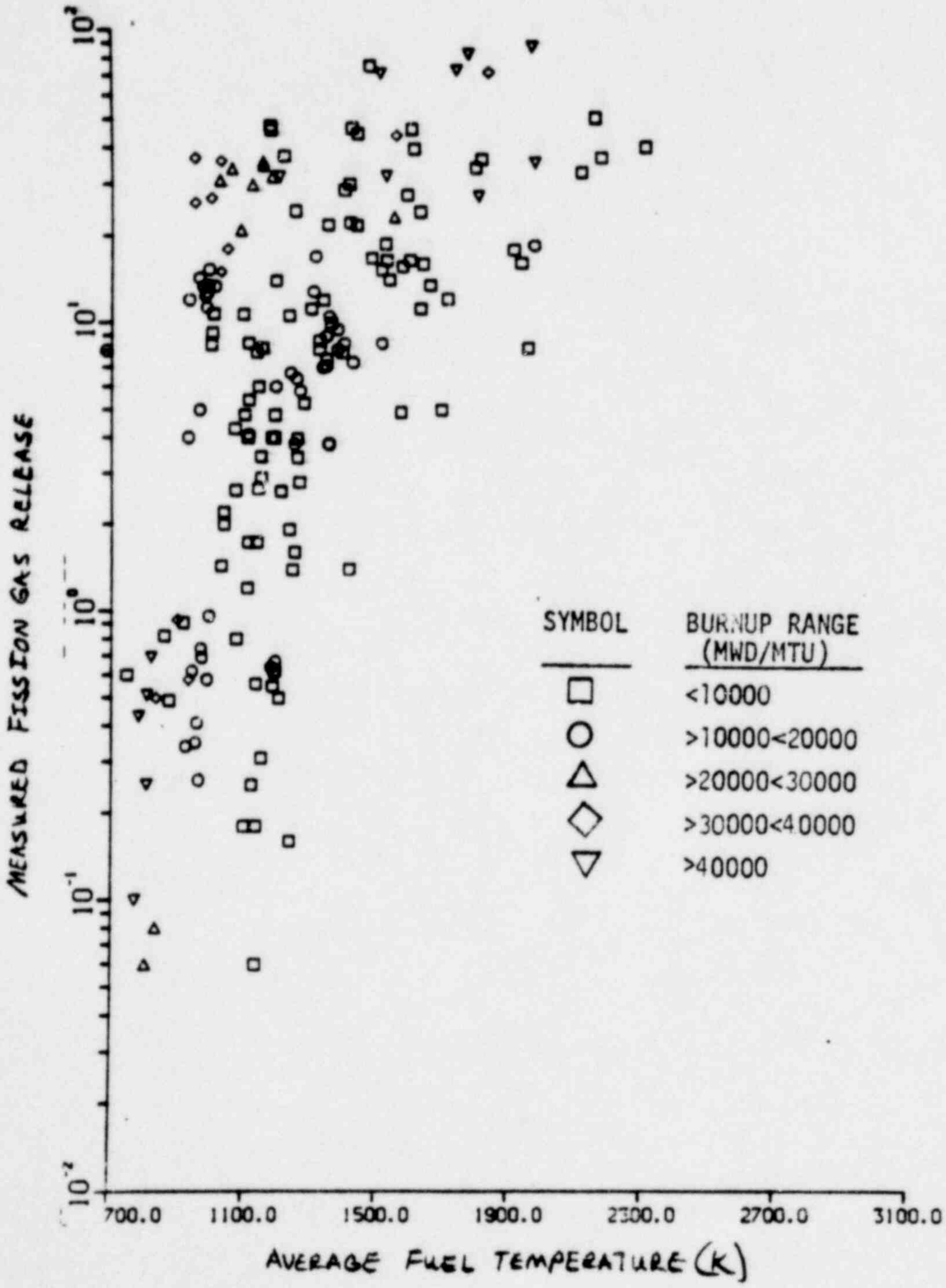

FIGURE 46 Measured fission gas release fraction versus average fuel temperature for different burnup ranges . . . . .

1569 219

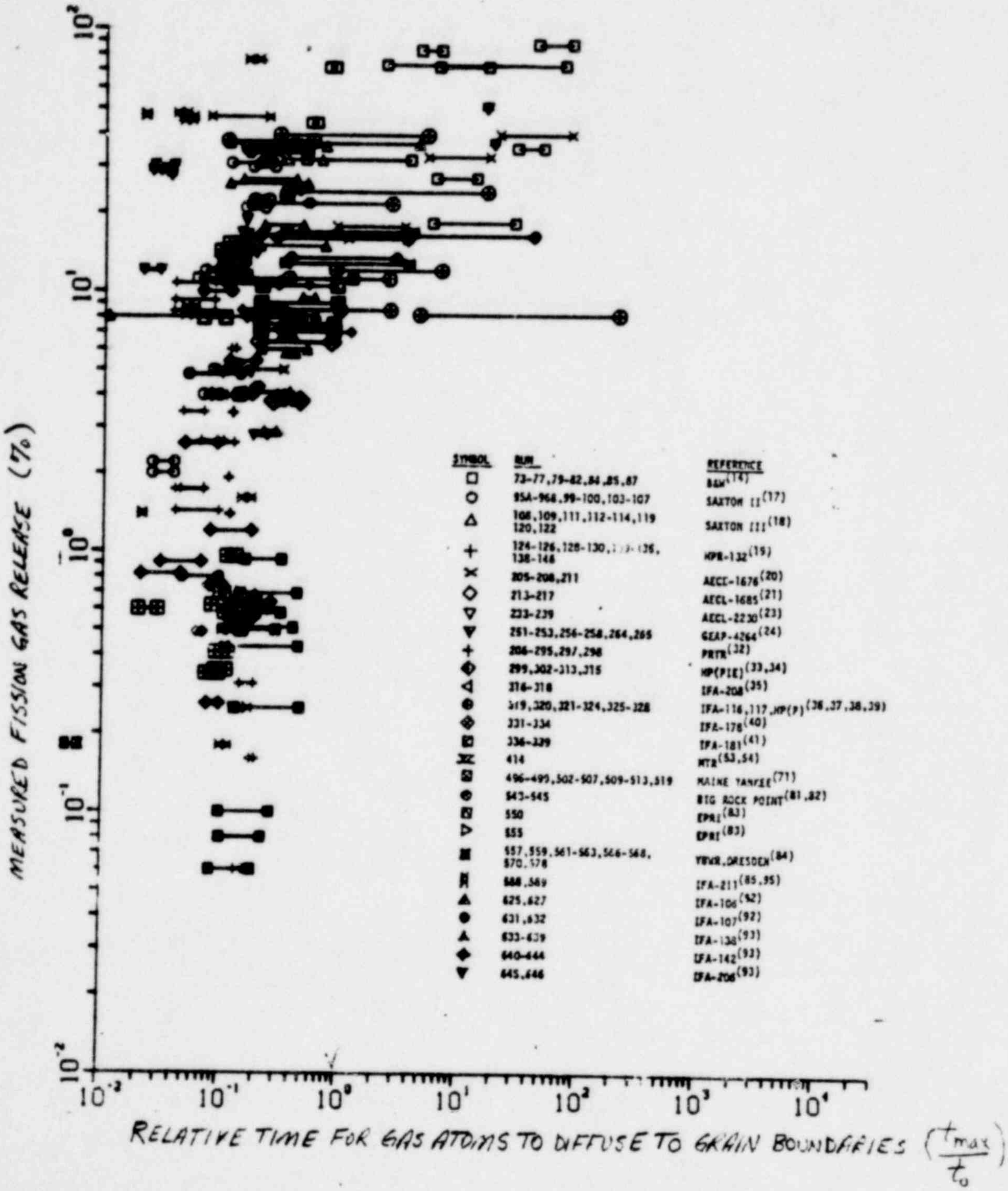

FIGURE 47 Measured fission gas release fraction versus diffusion dependent parameter t_{max}/t_o. . . . .

1569 220

23-391

The rod average end-of-life burnup was a measured value directly reproduced in the model by the input operating history. Since there was some confidence that FRAP-S3 could represent fuel temperature conditions within 20% of the actual values, the opportunity was available to analyze the first order effects of fuel temperature and burnup independently. The temperature effect really corresponds to gas bubble mobility and the relatively rapid influence of temperature on fuel structure. The burnup effect lumps together the influence of gas bubble location, gradual development of inter-connected porosity and buildup of retained fission product concentration.

Figure 44 identifies no clearcut influence of burnup on gas release unless fuel temperature conditions are considered based on FRAP-S3 predictions. A trend of increasing gas release with burnup is only observed for the moderate fuel temperature range between 1000 and 1500 C. At lower temperatures, burnups in excess of 50000 MWd/MTM would be required before the cumulative effect of very low gas mobility became evident. Burnup effects are also less apparent at high temperature. The influence of cumulative gas mobility is less dominant in these cases than the relatively instantaneous influence of rapid mobility (exponential with temperature), fuel cracking, and restructuring. These trends provide incentive for introducing some straight forward treatment of cumulative fission gas location effects on release probability.

Figure 45 summarizes measured gas release versus maximum calculated fuel temperatures for all of the data. Different symbols have been used to correspond with different burnup ranges. Consistent with Figure 44 results, the indicated trends suggest that temperature exerts a decreasing influence on fission product release kinetics as burnup increases. This

1569 221

observation corresponds at higher burnups to increasing influence of cumulative effects on gas bubble location and decreasing influence of instantaneous gas bubble mobility. Similar observations can be made based on Figure 46 using time averaged fuel temperature as the thermal effect index. Considering the indicated variation in gas release at any given maximum or average fuel temperature condition, the fact that temperature dependent models are associated with significant variation in accuracy is not surprising.

The interplay between instantaneous gas bubble mobility and its cumulative effect on bubble location with respect to trapping and release sites is shown more specifically in Figure 47. Measured gas release fractions have been plotted versus the dimensionless parameter $\frac{t_{max}}{t_o}$. The irradiation time is t_{max}. The minimum time required for the gas atom arrival rate at a grain boundary of equivalent radius, a, (via simple diffusion mechanics[102] to equal the gas atom production rate inside the grain is defined at t_o where t_o is proportional to a^2/D. Diffusion coefficients, D, were based on time averaged and maximum fuel temperatures calculated by FRAP-S3. Temperature dependence of D was initially based on an experimental correlation.[103] Reported values were then adjusted upward consistent with theoretical considerations[104,105] for small bubbles (10^{-3} - 10^{-4} mm) inside grains, i.e., for single or clustered gas atoms beyond the resolution of experimental techniques. Grain size (equivalent sphere radius, a) was assumed to vary between 5 and 15 μm. The trend of increasing gas release with respect to $\frac{t_{max}}{t_o}$ shows the combined effect of fuel temperature and burnup.

Release fractions greater than 10% are consistently observed when the value of t_{max}/t_o exceeds 1.0. It is expected that a description of t_o which took more explicit account of cumulative temperature history effects, (rather than using time averaged or maximum values), would reduce the scatter for t_{max}/t_o values below 1.0. For this low range of values, diffusion processes are not calculated to have had sufficient time to contribute significantly to the observed release. Instantaneous temperature effects or recoil/knockout mechanisms should dominate in this range. In any event, dependence of gas release on the mechanistic parameter, t_{max}/t_o seems as reproducible as the temperature dependence, previously seen in Figures 45 and 46, which now governs the model. It is likely that considering some parallel combination of instantaneous and cumulative gas mobility effects would improve model performance.

3.2.2 Rod Internal Pressure. Mixed results were obtained when operating pressure measurements were compared with FRAP-S3 predictions for various experiments. Ability of the code to track fission gas behavior is strongly dependent on the calculated fuel temperature distribution. Also, even if plenum temperature is well characterized by knowing external system conditions, comparisons are confounded by unknown differences between predicted and actual plenum void volume changes. Another factor affecting pressure results is that fuel stack volume changes resulting from mechanical deformation are not considered by the model. Gas absorption is not treated. Gas release is modeled by an empirical, primarily temperature dependent release mechanism.

Sample size for FRAP S3 analysis of rod internal pressure measurements has mainly been expanded relative to FRAP-S2 verification in terms of pressurized rod startup conditions. Relative agreement between early life data and calculated pressure is evaluated separately in order to benchmark the fuel heatup effect on void volume and gas temperature. Basic gas volume and temperature response at startup initially establishes some level of rod operating pressure. This level is often both calculated and observed to remain relatively stable (±20%) for moderate duty pressurized rod operation up to significant burnup. Interpretation of burnup comparisons, especially for unpressurized rods, reflects an additional strong dependence of the results on performance of the gas release model.

Figure 48 compares measured and predicted internal pressure for the 50 rod data sample considered. The indicated standard error for pressurized and unpressurized rods, regardless of burnup, is respectively 1.35 and .65 MPa. The data comparisons, though somewhat limited in representing high burnup conditions, span the range of BWR and PWR hot operating pressure levels. Experimental data in excess of 3.45 MPa generally correspond to startup operation for pressurized rods backfilled to either 2.41 or 3.79 MPa. The group of underpredictions at measured pressures between 7.58 and 11.72 MPa corresponds to startup measurements for two rods exhibiting significant transducer drift. Lower end measurements refer to unpressurized rods with maximum burnups between 3000 and 20000 MWd/MTM.

The relative model error is plotted versus rod average burnup in Figure 49. The fact that overpredictions correspond most often with

1569 224

23-393

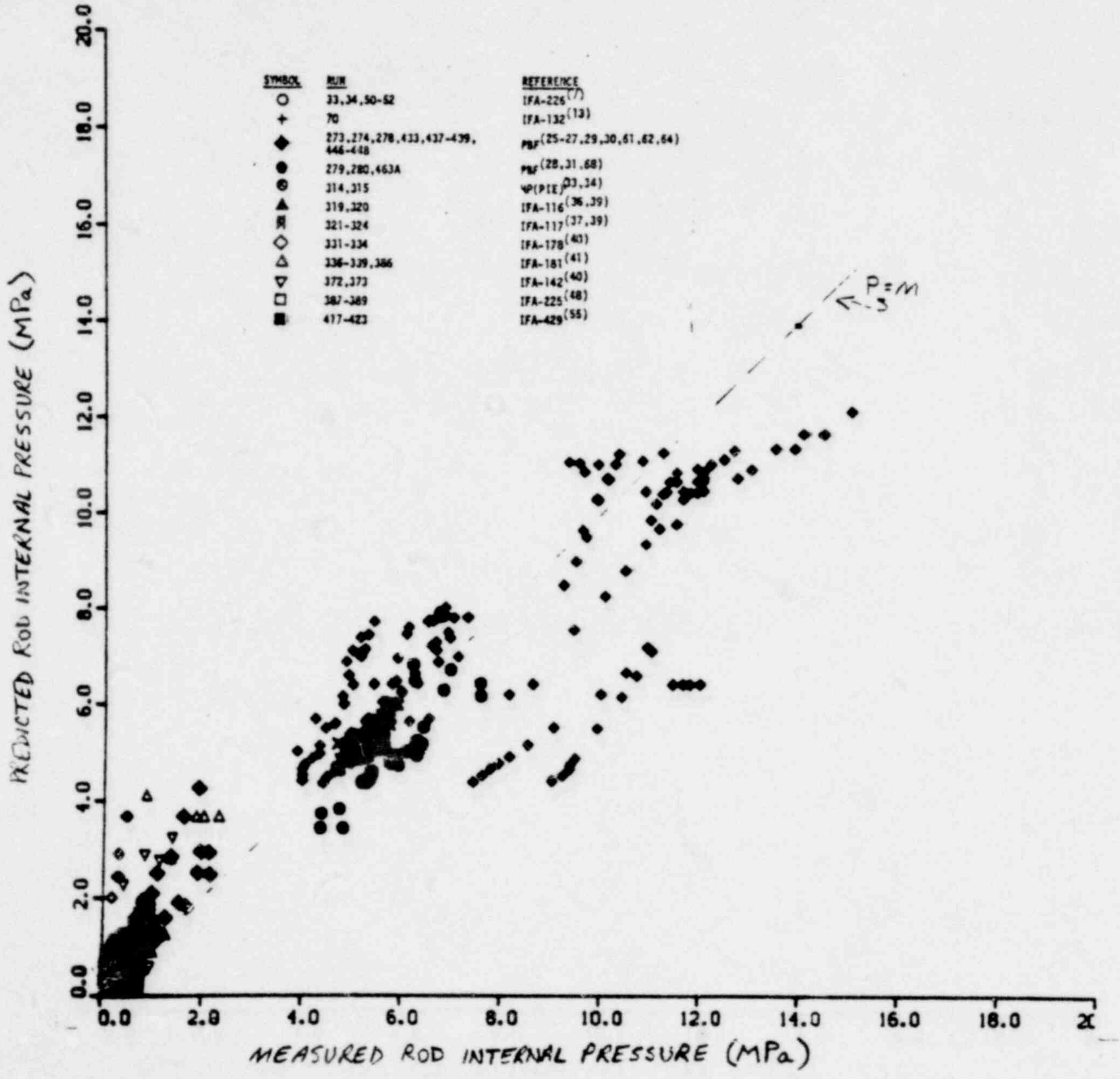

FIGURE 48 FRAP-S3 predicted versus measured rod internal pressure . . . .

1569 225

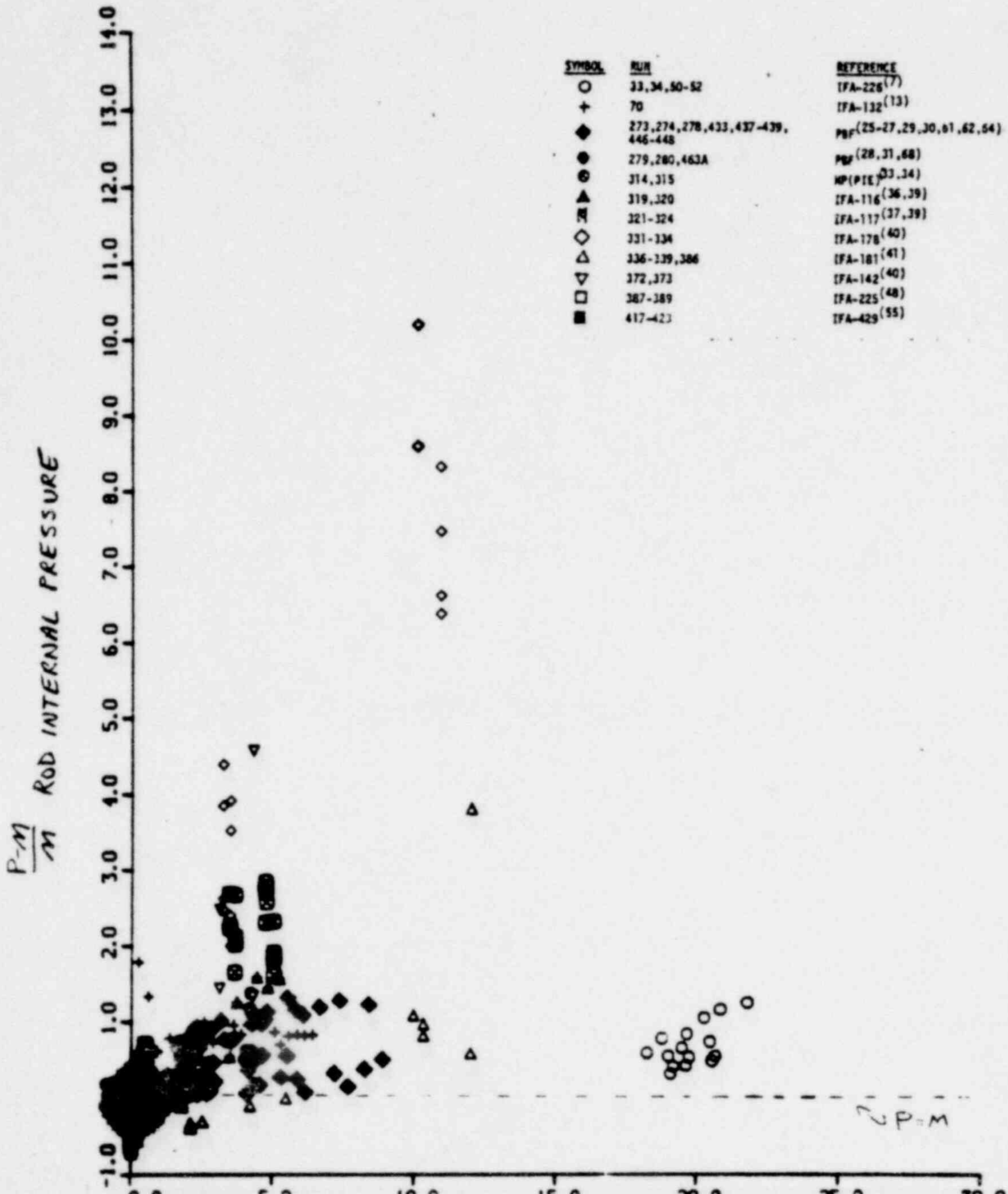

FIGURE 49 Effect of burnup on FRAP-S3 rod internal pressure error. . . . .

1569 225

1569 226

burnup data indicates that fission gas release is being overestimated. This trend is not unexpected given the previously mentioned tendency of the model to overpredict fuel temperature under burnup conditions. Startup data is better represented since the model need only account for initial gas content, thermal expansion and elastic strain effects on void volume and void temperature. The strong effect of gas release on pressure uncertainty is indicated by the fact that the standard error values for unpressurized rods under startup and burnup conditions are respectively .17 and .66 MPa.

Error for the startup data comparisons is shown in Figure 50 plotted against the as-built plenum void volume fraction. Results indicate that correctly modeling the active length void volume and temperature contribution to operating pressure has a somewhat increasing influence on the relative model error as the more easily characterized plenum contribution decreases. FRAP-S3 active length void volume is calculated to change based on effective gap and crack volume changes and ring thermal expansion axially into dishes if present. Since the power reactor plenum volume fraction ranges between 40 and 60%, more detailed representation of active length volume and temperature behavior may be warranted in subsequent code versions. This point is illustrated by Figure 51 which shows that relative model error at startup is somewhat dependent on calculated fuel temperature conditions. Accounting for the effect of pellet relocation in redistributing significant amounts of gap volume into the hot fuel region is one way to make the calculated heat-up effect on pressure conditions more realistic.

1569 227

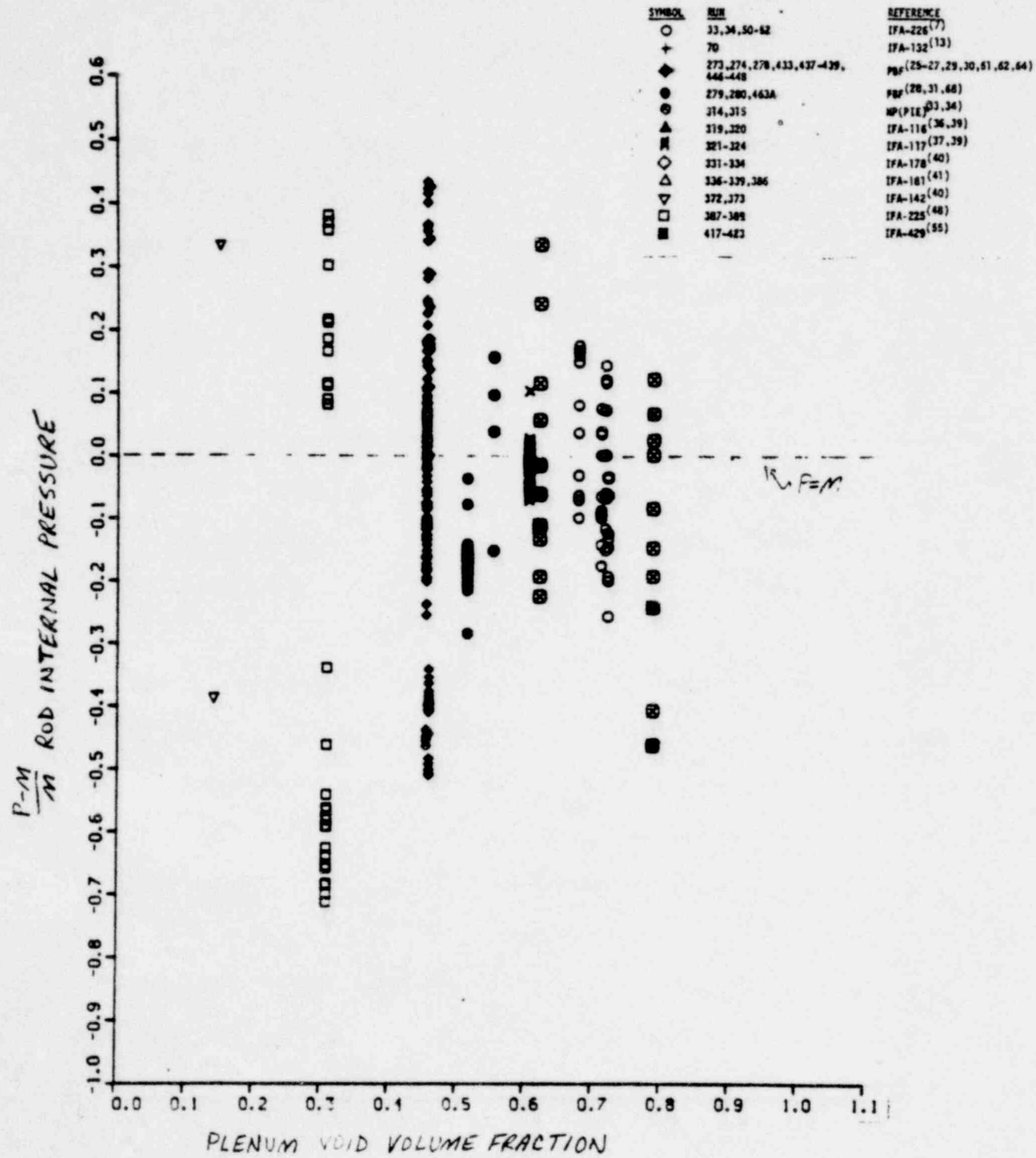

FIGURE 50 Effect of plenum volume fraction on FRAP-S3 rod internal pressure error - startup data . . . .

1569 228

23-395

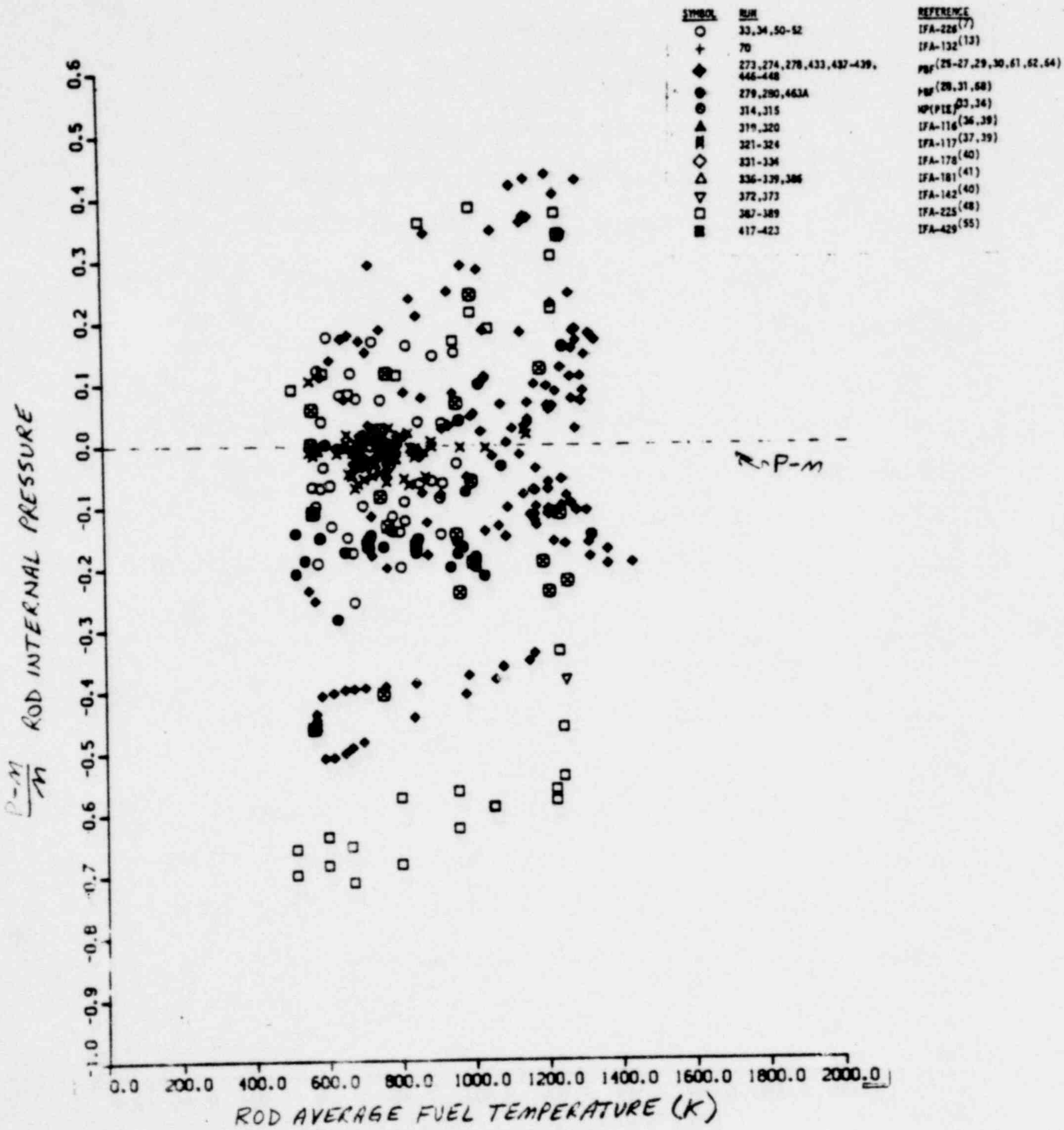

FIGURE 51 Effect of average fuel temperature on FRAP-S3 rod internal pressure error - startup data . .

1569 229

3.3 Rod Deformation Model

Various comparisons were performed to determine capability of FRAP-S3 to account for steady-state fuel and cladding deformation. Ability of the code to predict and distinguish between open, soft, and hard gap closure conditions has strong influence on both thermal and mechanical aspects of the model. Results of both Standard Design and data comparison runs indicate that proper representation of fuel temperature and thermal expansion can account for most of the difference between cold and hot void volume in full size rods with stable fuel. The net effect of densification and swelling on fuel geometry is normally not observed to exceed the combined influence of fuel thermal expansion and relocation. Irradiation induced growth, PCMI, and creep collapse represent the contributing cladding response mechanisms for determining rod length, gap, and thermal conditions at initiation of a transient. The PCMI effect is not expected to dominate core wide cladding dimensional changes for power reactor operating conditions.

In the following rod deformation section, gap closure results are shown first, followed by discussion of fuel thermal expansion and permanent length change. The section concludes with presentation of summary data comparison results for cladding permanent hoop and axial strain.

3.3.1 Gap Closure Conditions. Figure 52 shows measured versus predicted heat rating corresponding to onset of gap closure for about 80 instrumented test rods. The measurement ranges correspond to observed departure of cladding strain response from linear thermal expansion during startup power increases. Wide ranges of rod geometry,

23-396

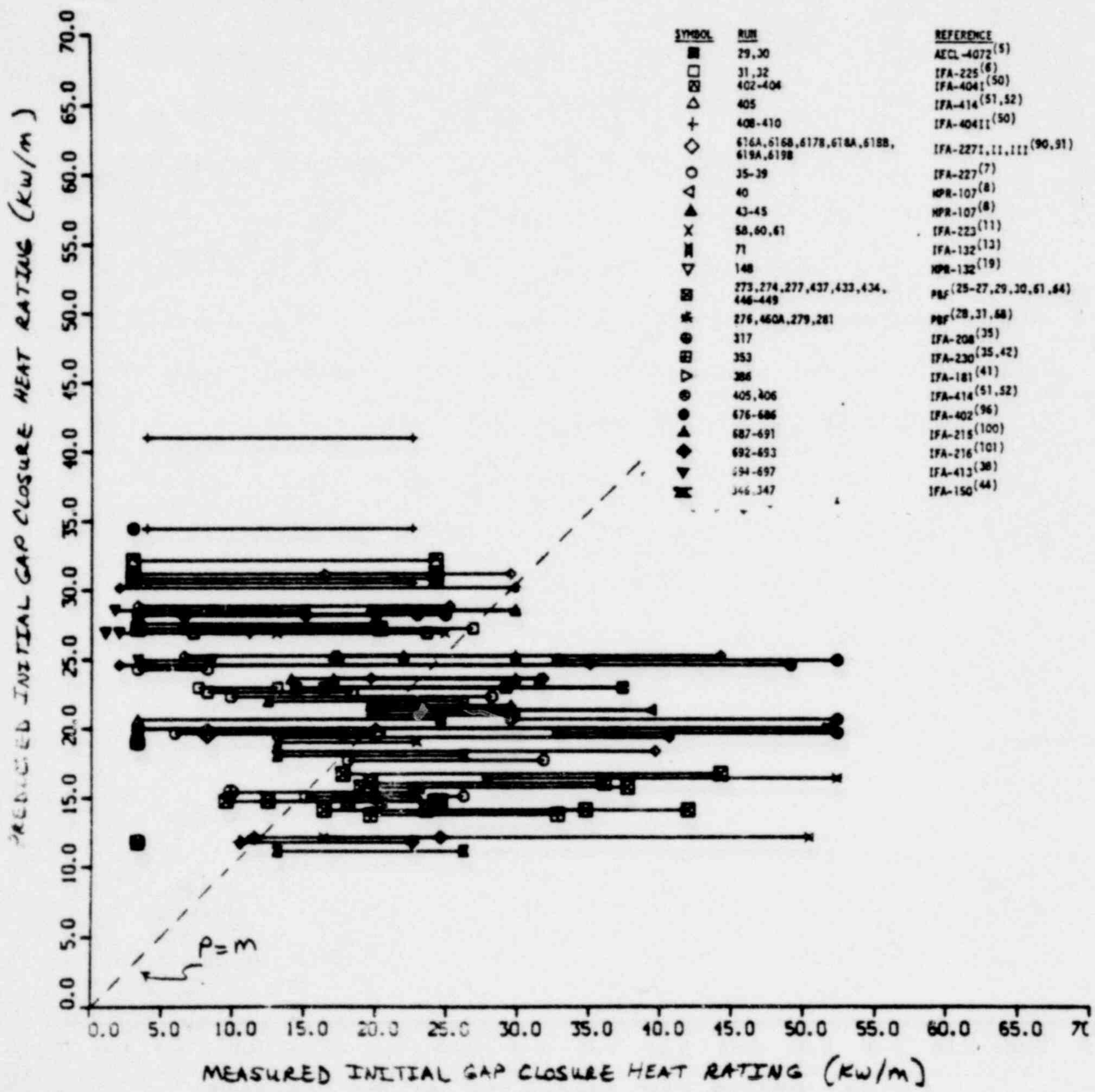

FIGURE 52 FRAP-S3 predicted versus measured gap closure heat rating . . . .

1569 231

design, and instrument configuration are represented in the sample. Much of the data represents rods other than those previously used[110] for diagnosis of the preliminary fuel relocation fix, later implemented in FRAP-S3.

Calculated gap closure is generally within the rather large data uncertainty bands of the measured values. The standard error between measured and calculated gap closure heat rating is 13.4 kW/m. The measured initial gap closure power levels mainly fall between 6.6 and 39.4 kW/m. The data suggests that typical power reactor fuel may often operate under soft pellet-cladding contact conditions. Calculated gap closure shows improvement relative to previous models which would generally not predict gap closure below 60 to 66 kW/m for rods with typical geometry. Fuel and cladding strain consequences due to hard gap closure are normally observed to increase gap closure heat rating for subsequent cycles. PCMI deformations however, are conservatively treated by the current rigid pellet model and represent special cases of less interest for establishing core-wide initial transient conditions.

Relative error in predicted gap closure heat rating is plotted versus gap size in Figure 53. More tendency to overestimate the gap closure heat rating is indicated for gap sizes less than 1%. In these cases, the currently applied modification of relocated pellet diameter by the original repack factor (.25%) may not be justified. The fact that no trend in relative model error was found with respect to fuel

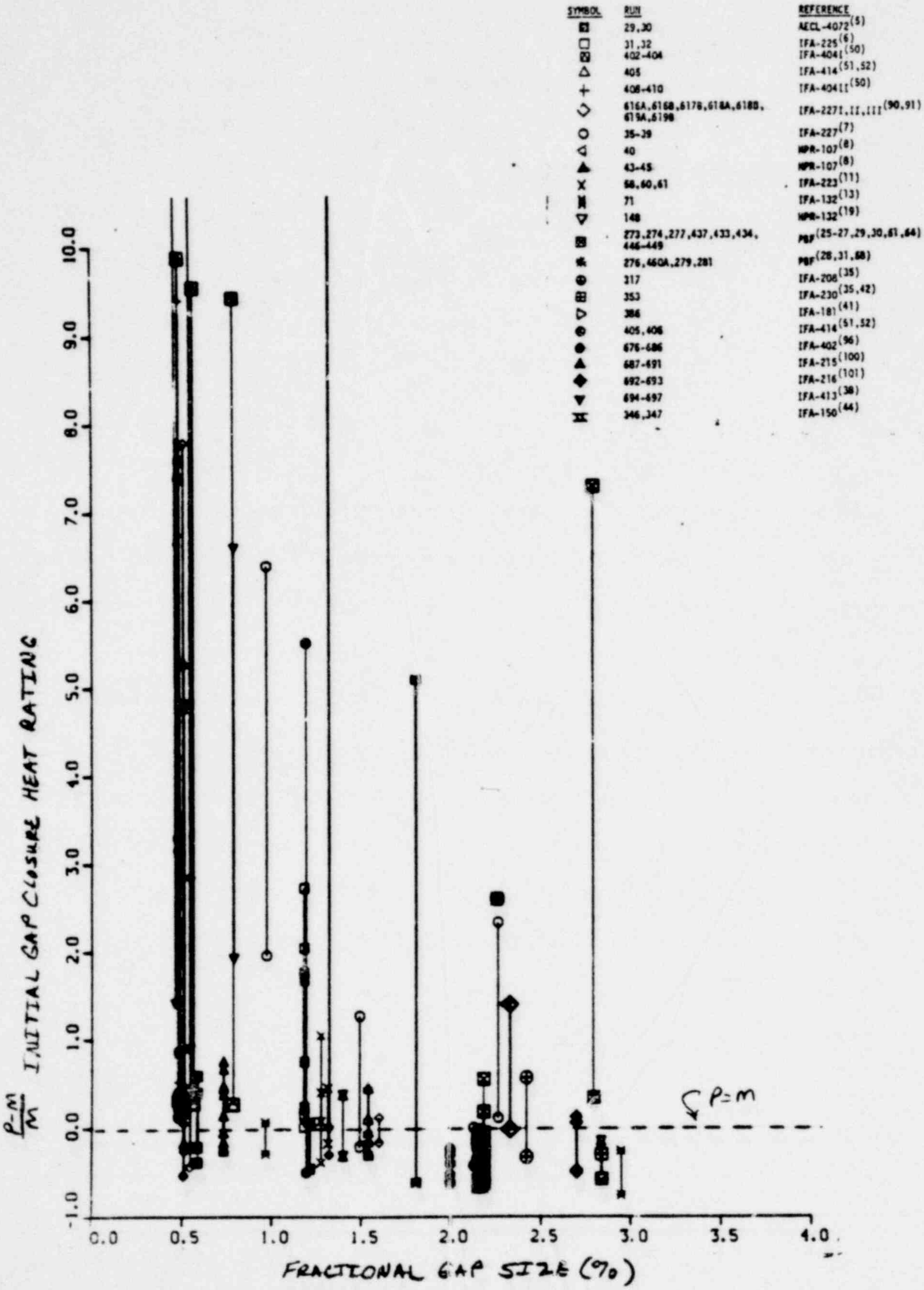

FIGURE 53 Effect of gap size on FRAP-S3 gap closure heat rating error . . . .

1569 233

density and temperature is not unexpected. These same bulk fuel parameters were previously found[110] to have no identifiable influence on the degree to which relocation occurred.

3.3.2 Fuel Deformation. Data comparisons involving permanent fuel stack deformation mechanisms are preceded by summary thermal expansion results.

3.3.2.1 Fuel Thermal Expansion. Figure 54 shows measured versus predicted fuel stack axial expansion (relative to the cladding hot standby length) during startup power ramps for about 20 rods representing both dished and flat pellet designs. For dished and flat end forms, the governing temperature for predicted axial expansion is set respectively at the pellet shoulder and centerline. Calculated results generally lie within the range of data reproducibility, prior to the buildup of PCMI induced restraint for measurements >.3%. Beyond this point, a tendency to overestimate fuel stack expansion is evident. Maximum expansions are both observed and calculated for flat pellet rods. The standard error in FRAP-S3 calculated fuel axial expansion represents .37% of the stack length.

Figures 55 and 56 show relative error in predicted fuel expansion respectively versus average stack temperature and as-built gap size. The results indicate that unaccounted for gap closure effects are a larger source of model error than fuel temperature conditions. Figure 55 shows that both favorable and unfavorable data comparisons results can

23-398

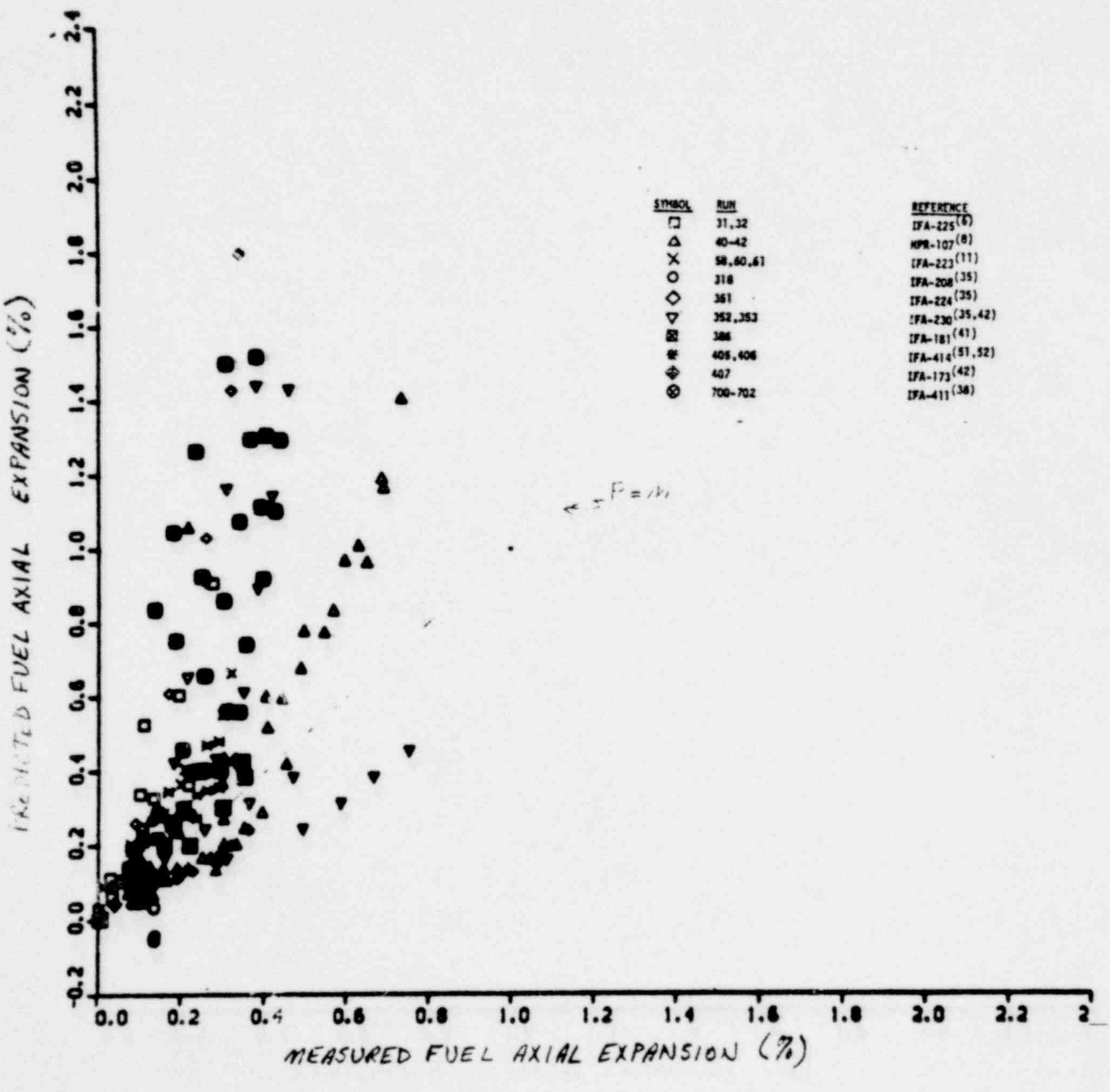

FIGURE 54 FRAP-S3 predicted versus measured fuel axial expansion during heatup. . . . .

1569 235

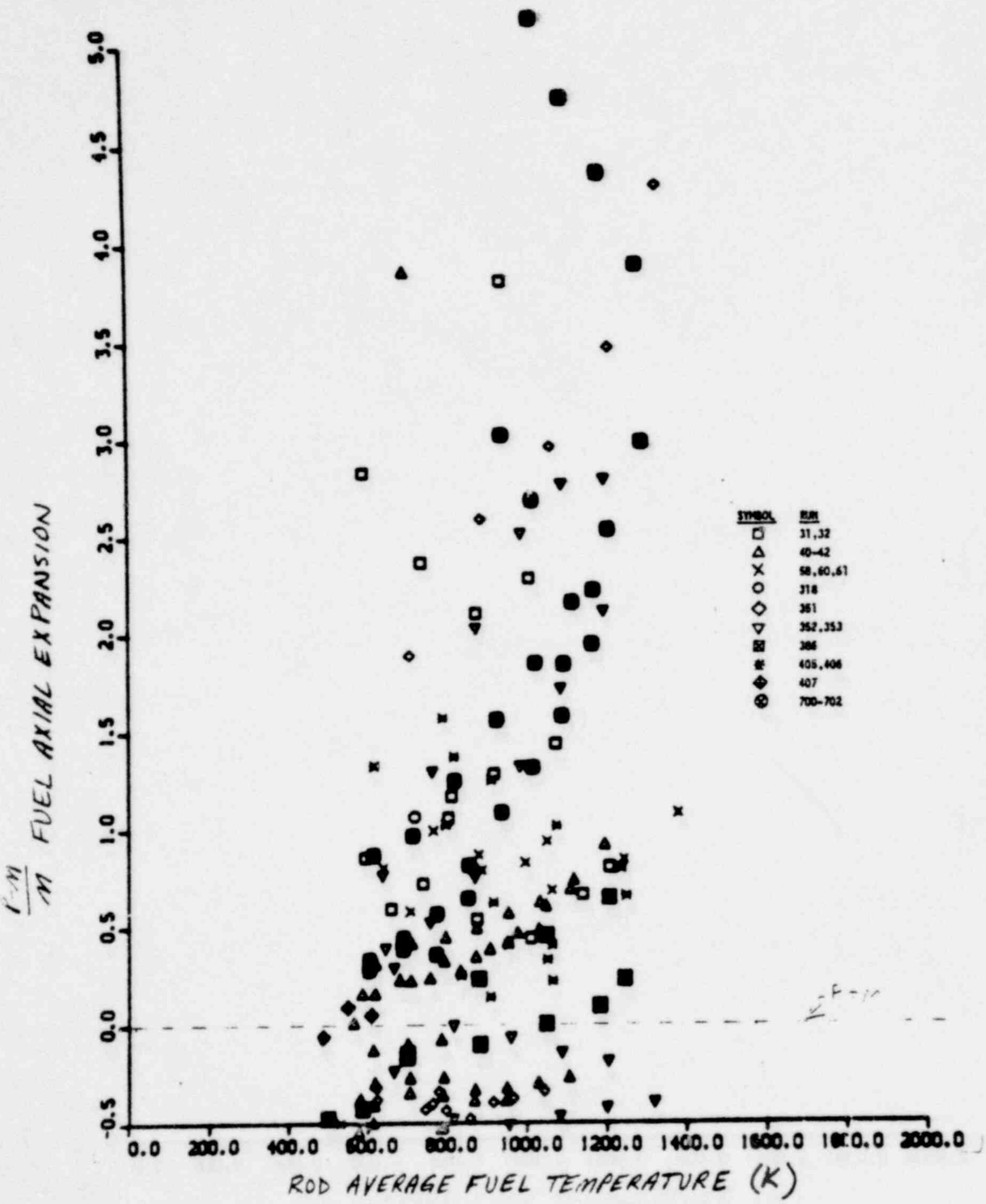

FIGURE 55 Effect of average fuel temperature on FRAP-S3 fuel axial expansion error during heatup. . . . .

1569 235

1569 236

23-290

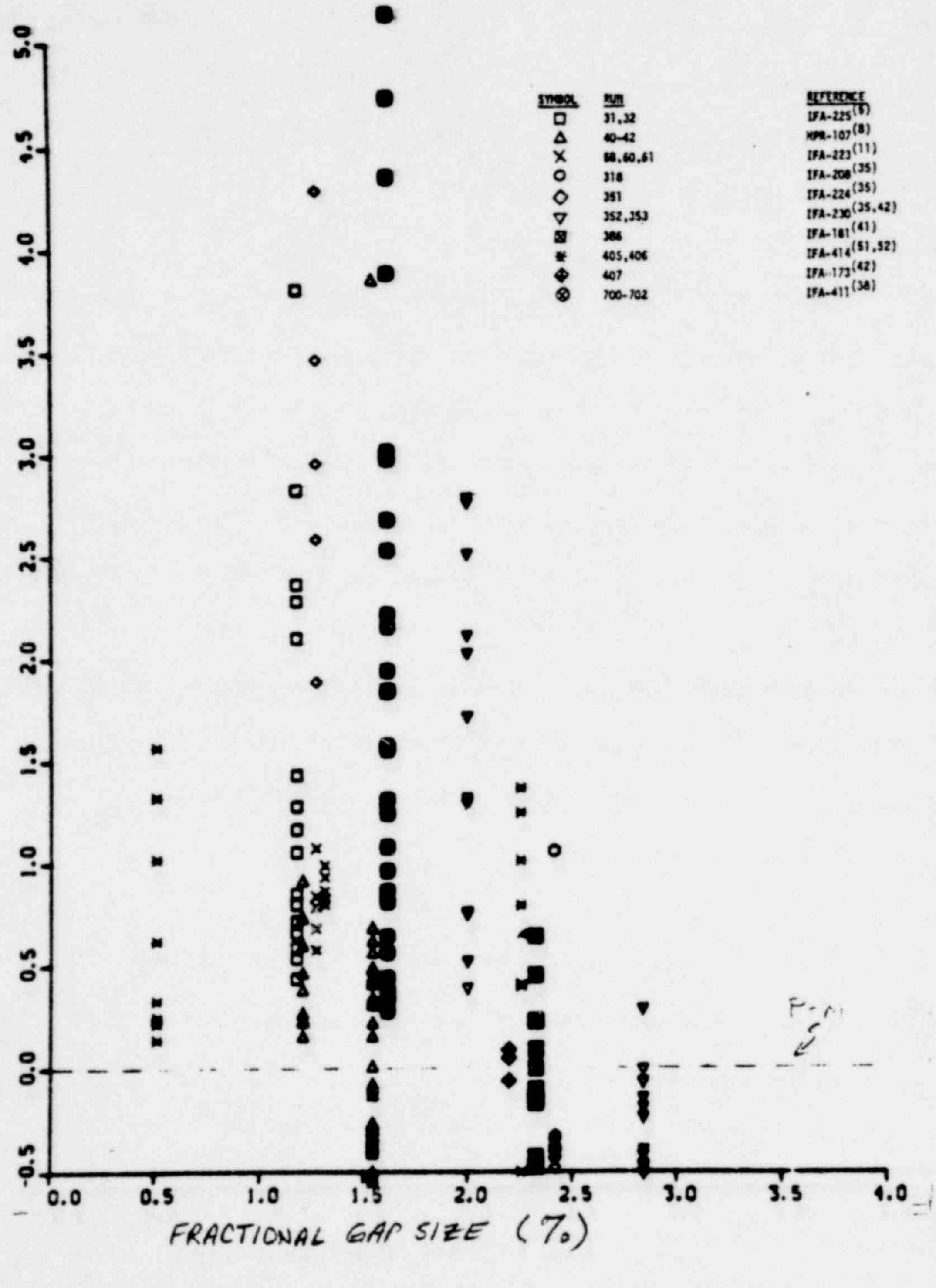

FIGURE 58 Effect of gap size on FRAP-S3 fuel axial expansion error during heatup. . . . .

1569 237

be obtained for any of the indicated fuel temperature ranges. Figure 56 indicates that overpredictions mainly correspond to those small gap sizes which promote occurrence of PCMI. Better agreement between measured and calculated fuel stack expansion is seen for gap sizes greater than 2%, ie, for design conditions which tend to moderate mechanical effects of PCMI on the data.

3.3.2.2 Fuel Stack Permanent Deformation. The main burnup effects contributing to permanent stack volume changes are some combination of swelling, densification and creep/hot pressing. The latter two mechanisms moderate the dimensional effects of swelling until their influence decreases due to saturation of stable porosity and stress accommodation in the fuel. FRAP-S1 had a swelling model but did not include fuel mechanical deformation or densification models. FRAP-S2 considered both fuel swelling and densification but had no pellet mechanical deformation model. The FRAP-S3 fuel deformation model is essentially unchanged with the exception of indirect relocation feedbacks on temperature distribution and swelling.

Figure 57 compares measured and predicted permanent fuel stack length changes for a data sample of some 100 rods. About half of the data reflect design and operating conditions expressly intended to investigate the magnitude of fuel densification and thermal stability effects on axial gap formation. In these cases, operating conditions or rod design were chosen so as to minimize influence of PCMI on experiment results. Relative to FRAP-S2 verification in this area, the burnup range reflected in the data sample has been significantly extended based

1569 238

23-400

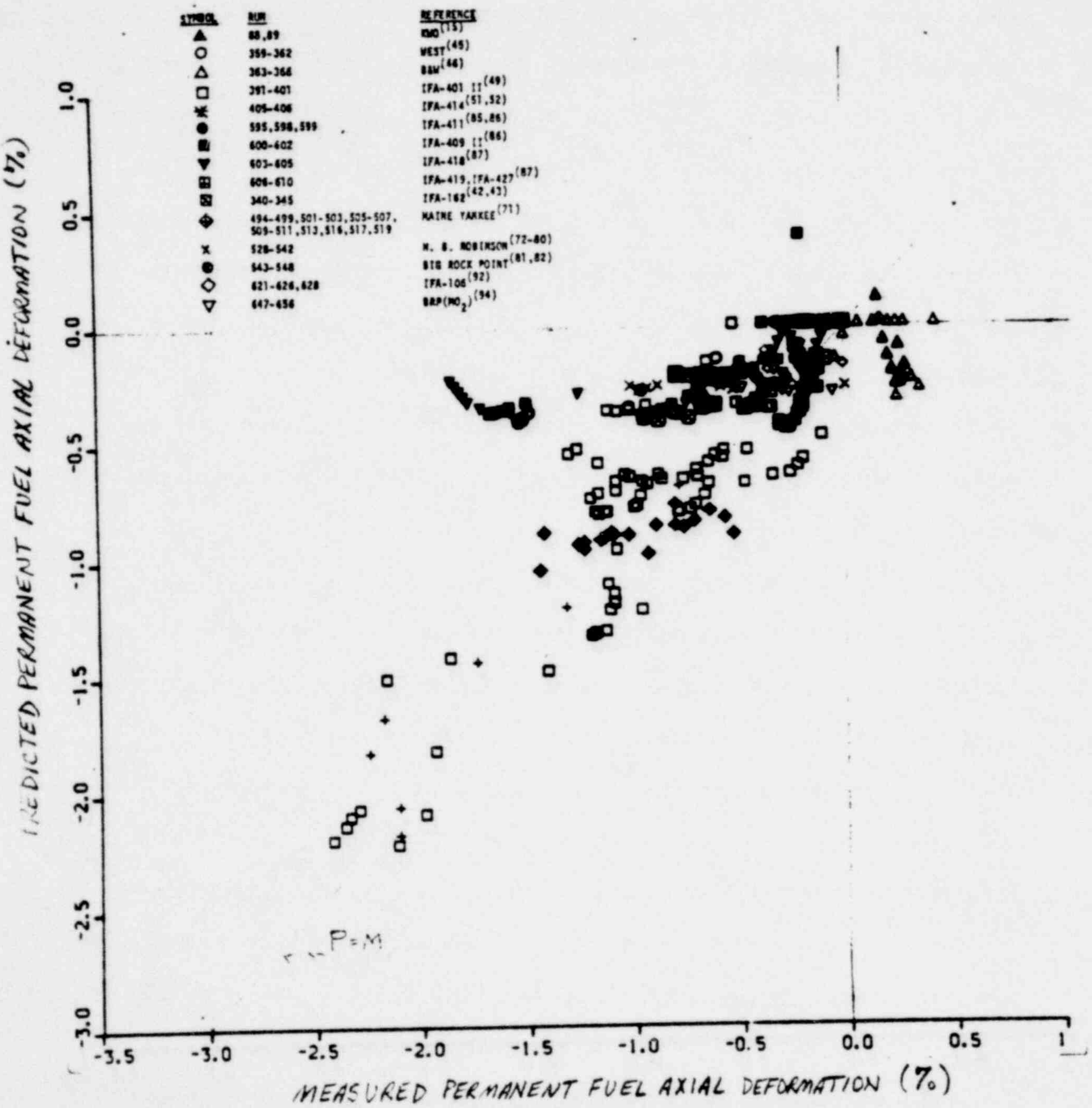

FIGURE 57 FRAP-S3 predicted versus measured permanent fuel axial deformation. . . . .

1569 239

on additional consideration of power reactor PIE results. Nonetheless, relatively few rods exhibit enough fuel swelling to give positive net length changes when combined with the mainly negative length effect of fuel compression, densification, and thermal instability. The net direction of predicted stack deformation is in most cases consistent with this observation. The amount of permanent axial stack deformation is generally underestimated due at least in part to not modeling fuel compression effects. The largest negative deformations correspond to irradiations of relatively unstable fuel types, the results of which are represented in the densification model's data base. Overall results indicate that adequate model capability exists for characterizing initial plenum volume conditions for transient analysis. The standard error in representing burnup effects on fuel and plenum axial dimensions corresponds to .44% of the stack length.

The effect of fuel density on relative model error shown in Figure 58 indicates that no systemmatic problems are introduced by the relatively strong effect of this parameter in the empirical densification model. Occurrence of underpredictions seems to be independent of fuel density conditions. The burnup effect on model error shown in Figure 59 should reflect some sensitivity to buildup of fuel swelling contributions in the net calculated length change, as well as decreasing influence of the unmodeled PCMI effect. Limited results at burnups in excess of 20000 MWd/MTM suggest either that 1) extended burnup fuel swelling rates (.3 to .9 vol % per 10^{20} fiss/CC) may be somewhat underestimated or 2) the accommodating influence of fuel porosity is overestimated. Since the relatively rapid

23-401

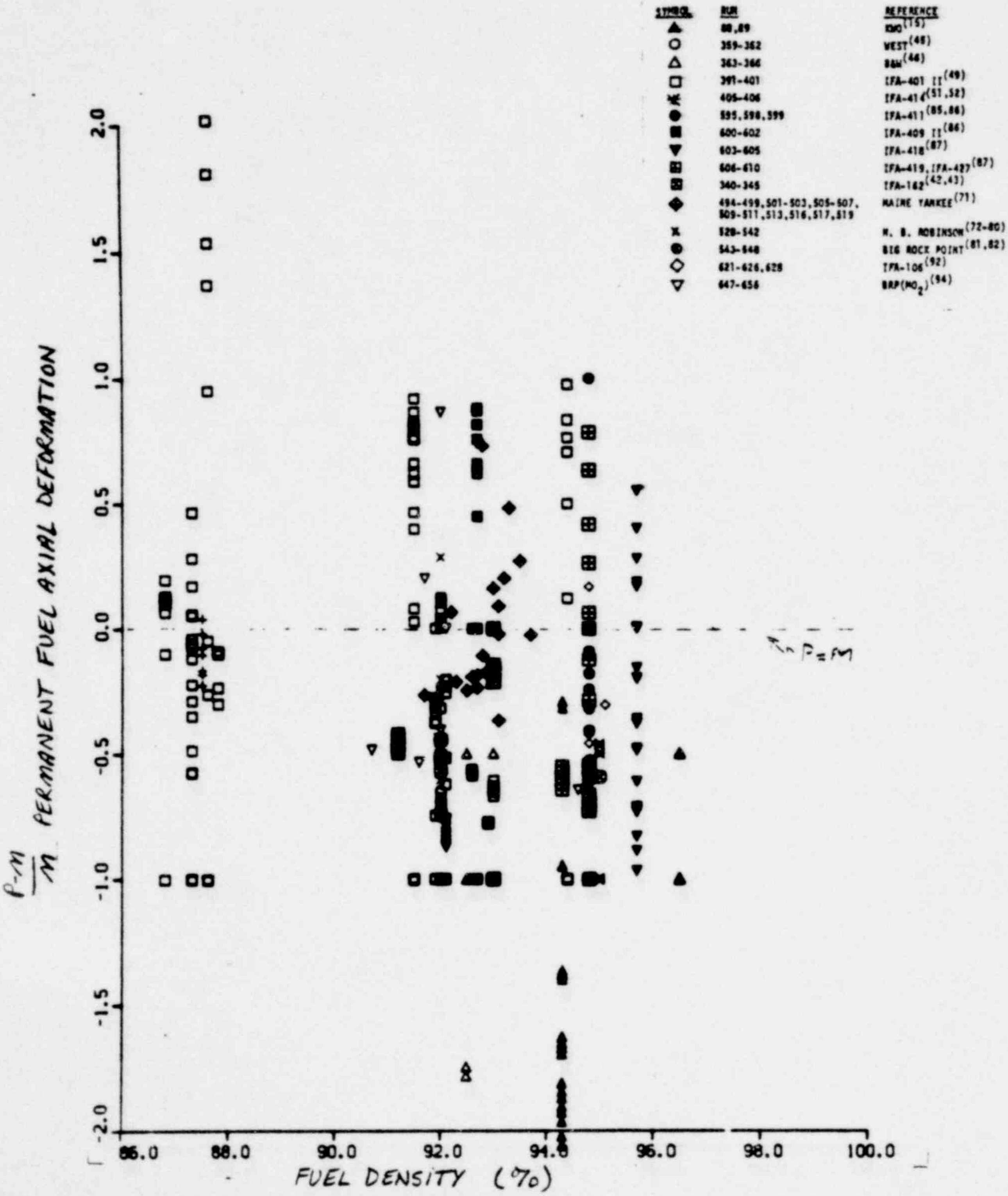

FIGURE 58 Effect of density on FRAP-S3 permanent fuel axial deformation error. . . . .

1569 241

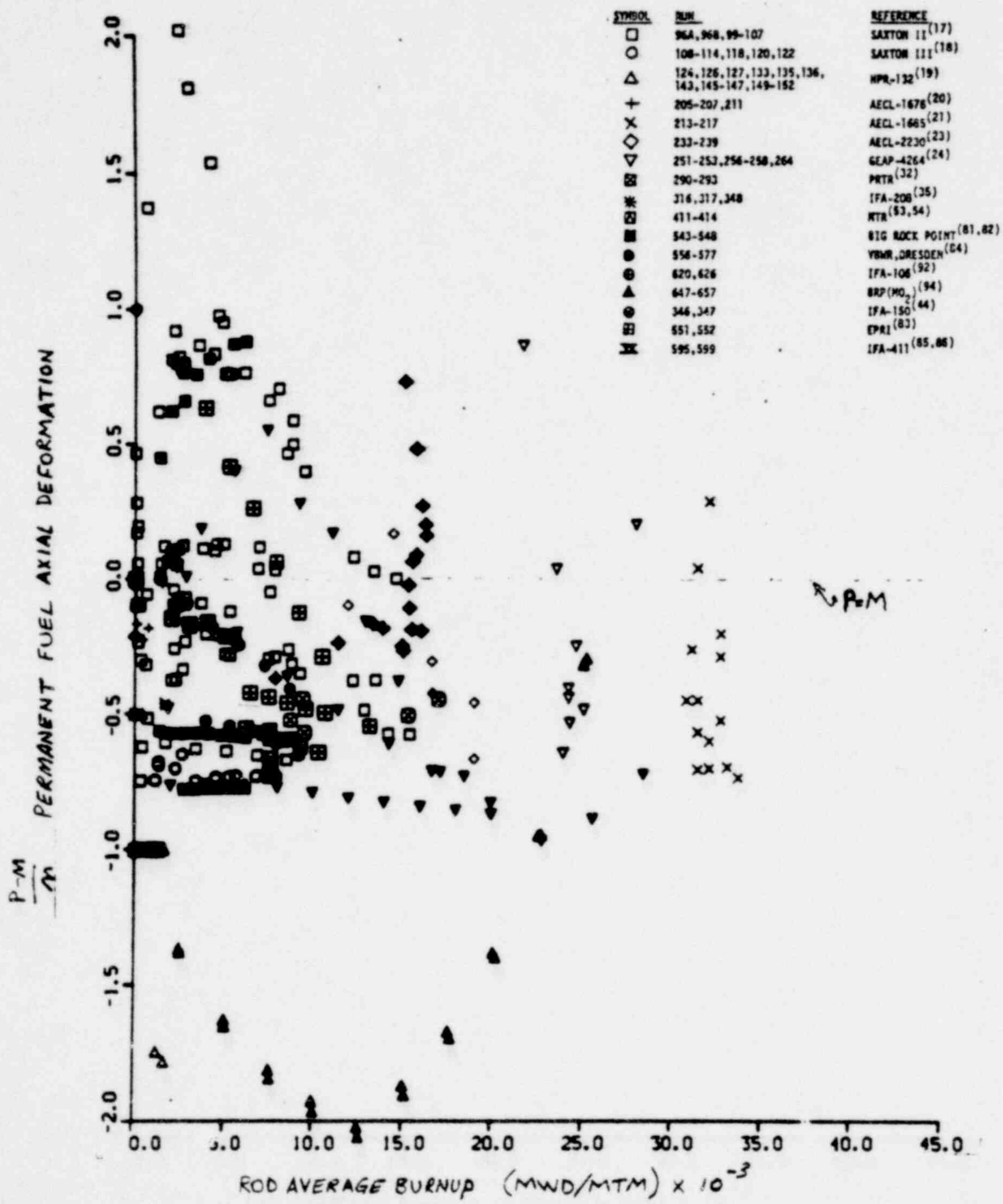

FIGURE 59 Effect of burnup on FRAP-S3 permanent fuel axial deformation error. . . . .

influence of negative deformation occurs mainly below 10,000 MWd/MTM, it is not surprising that the lower burnup comparisons indicate more than usual variation in the model error parameter.

3.3.3 Cladding Deformation. It has not been well established how prior cladding deformation by itself (i.e., apart from its influence on effective gap size) affects high temperature transient performance. Some rod bowing was seen in early fuel designs under normal operation where inadequate assembly axial clearance was provided. Uneven cladding temperature distributions could conceivably result during transients from the presence of small sub-channel eccentricities. For test rods, maximum total and permanent cladding axial elongation beyond thermal expansion is typically less than .5% and .2% respectively. Permanent deformations of even high burnup full size rods are consistent with these values. Crack closure, slip, densification, compressive stack shortening and filling of dishes all contribute to decreasing the effect of gap closure on cladding strain. In the more limiting hoop direction, concentrated PCMI effects in rods ramped to new peak heat ratings under normal flow and ramp rate conditions, have been blamed for occasional failures. These mechanically induced failures show varying degrees of influence from contributing environmental (SCC) effects. The majority of power reactor rods may operate without building up sustained tensile stresses from hard gap closure. In this main case of interest, permanent decreases in diameter due to creep collapse are normally observed to occur.

1569 243

Both the state of the model and its application to full size rods thus requires a verification emphasis on design and operating conditions for which creep collapse dominates other cladding strain mechanisms. It is mainly desirable for FRAP-S3 cladding deformation models to be able to characterize the resulting effective gap size from the standpoint of initial stored energy, off-normal mechanical interaction, and gas flow. Cladding deformation input to the transient code accounting for prior strain hardening or accumulation of mechanical damage may also be needed in subsequent code versions. The efficiency with which high temperature annealing can consolidate irradiated cladding mechanical properties under accident conditions is not well known.

Figure 60 compares measured and predicted permanent cladding hoop strain for a data sample of 170 rods. Respectively the data and calculated values reflect average and uniform diameter changes, localized only with respect to axial power distribution. Negative cladding strain is both observed and predicted in most cases. A combination of effects could explain the observed tendency to overpredict creep collapse, even though gas release and internal pressure are likely to have been overpredicted as well for most runs. Default input describing the often undocumented fast flux level, or the influence of fast flux itself on calculated creep rate may be too high. A contributing effect is the fact that in the absence of structural (hard) gap closure, the current model considers the cladding to be completely free-standing. Instrumented rod data suggests that relocated pellets provide at least some cladding support during soft gap closure. Operating mechanisms leading to positive cladding plastic strain are less well characterized by the model than

23-403

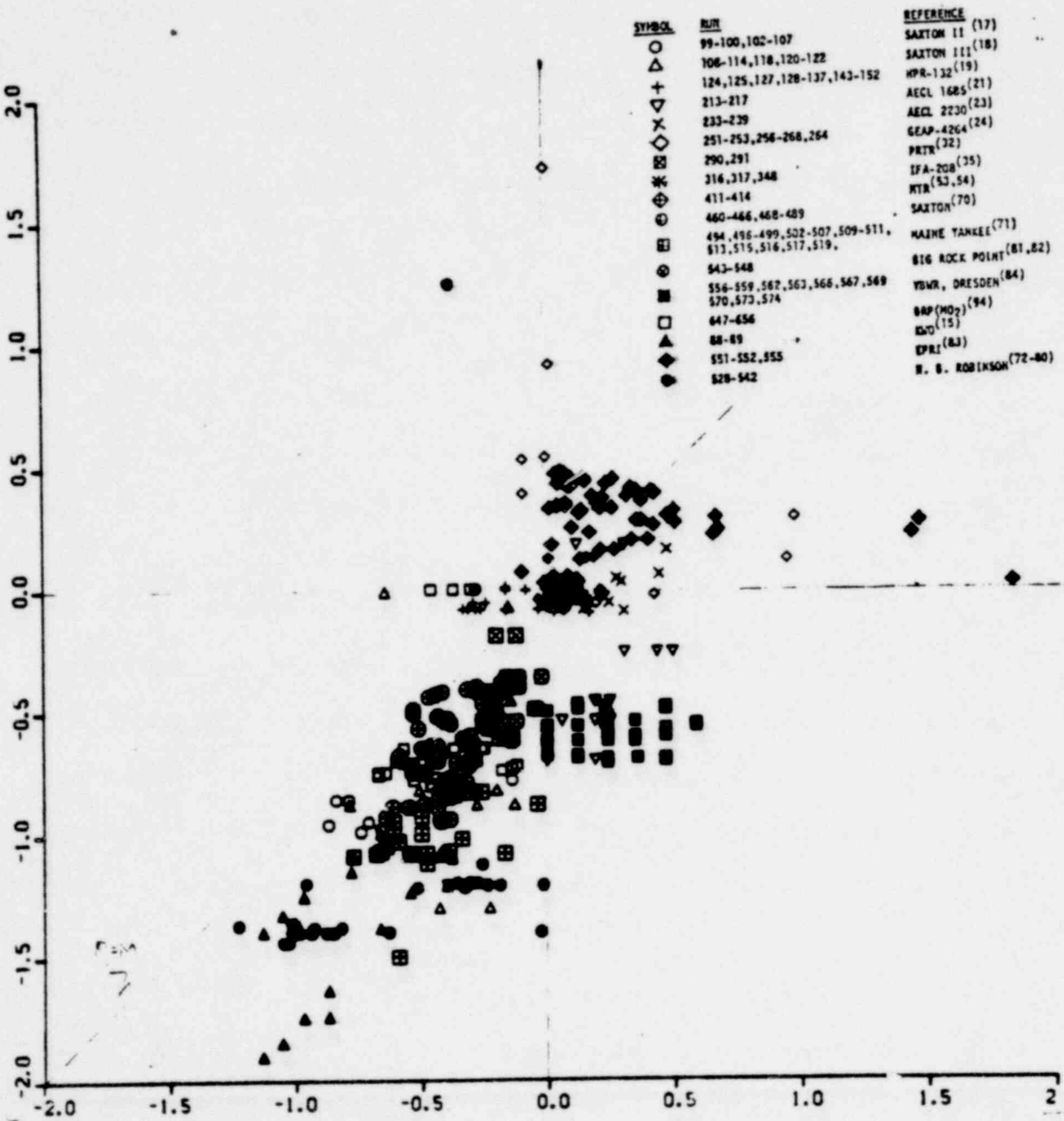

FIGURE 60 FRAP-S3 predicted versus measured permanent cladding hoop strain. . . . .

1569 245

creep collapse conditions. Some underpredictions occur, again since the effect of relocation on gap closure and soft thermal interaction is not mechanically coupled to cladding deformation. Overpredicting positive strain corresponds to cases where, without pellet mechanical deformation, the strain consequences of calculated structural gap closure are over-estimated. Nevertheless, results indicate that standard error in the FRAP-S3 calculated permanent cladding deformation value is within .6% of the cladding diameter.

The threshold effects of calculated gap closure on cladding hoop strain results are shown by plotting relative model error versus gap size in Figure 61. Overpredicting creep collapse dominates model errors for gap sizes greater than about 2%. Structural gap closure would not be predicted for these cases at heat ratings below 15 to 20 kW/ft. Underestimating positive strain generally occurs for smaller gap sizes. Structural gap closure is still generally not predicted in these cases, but the data are more prone to reflect positive strain consequences of soft PCMI. Overpredictions occurring for the smallest gap sizes correspond to cases in which calculated effects of structural gap closure dominate the comparison.

The cladding permanent axial strain results shown in Figure 62 are also dominated by correspondence between predicted and actual gap closure conditions. Predictions include the effects of irradiation induced, stress-free growth. Unlike the case of hoop strain, the axial comparisons are relatively insensitive to the calculated rod/system pressure difference. Underpredictions reflect the fact that mechanical

1569 246

23-404

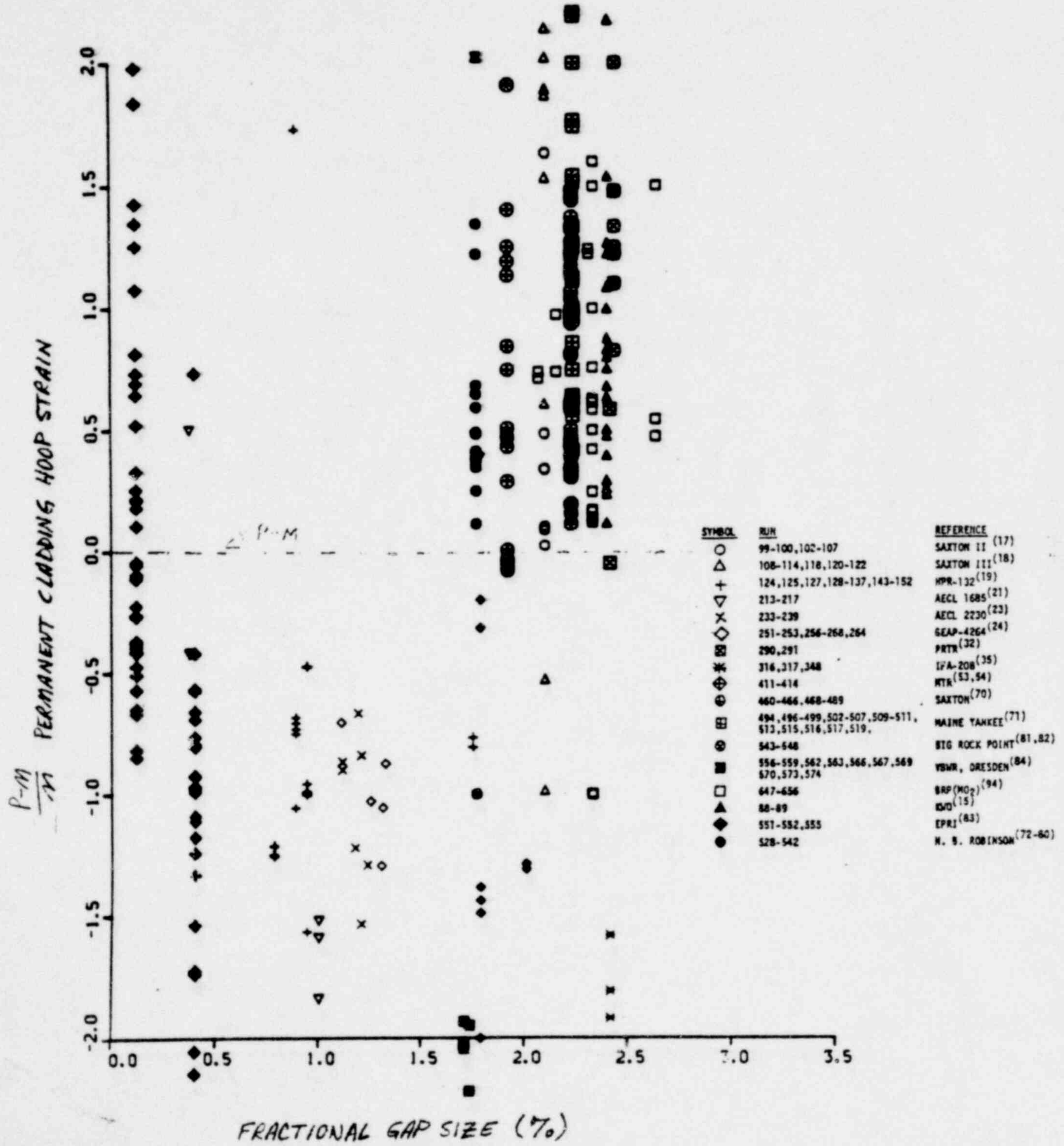

FIGURE 61 Effect of gap size on FRAP-S3 permanent cladding hoop strain error . . . .

1569 247

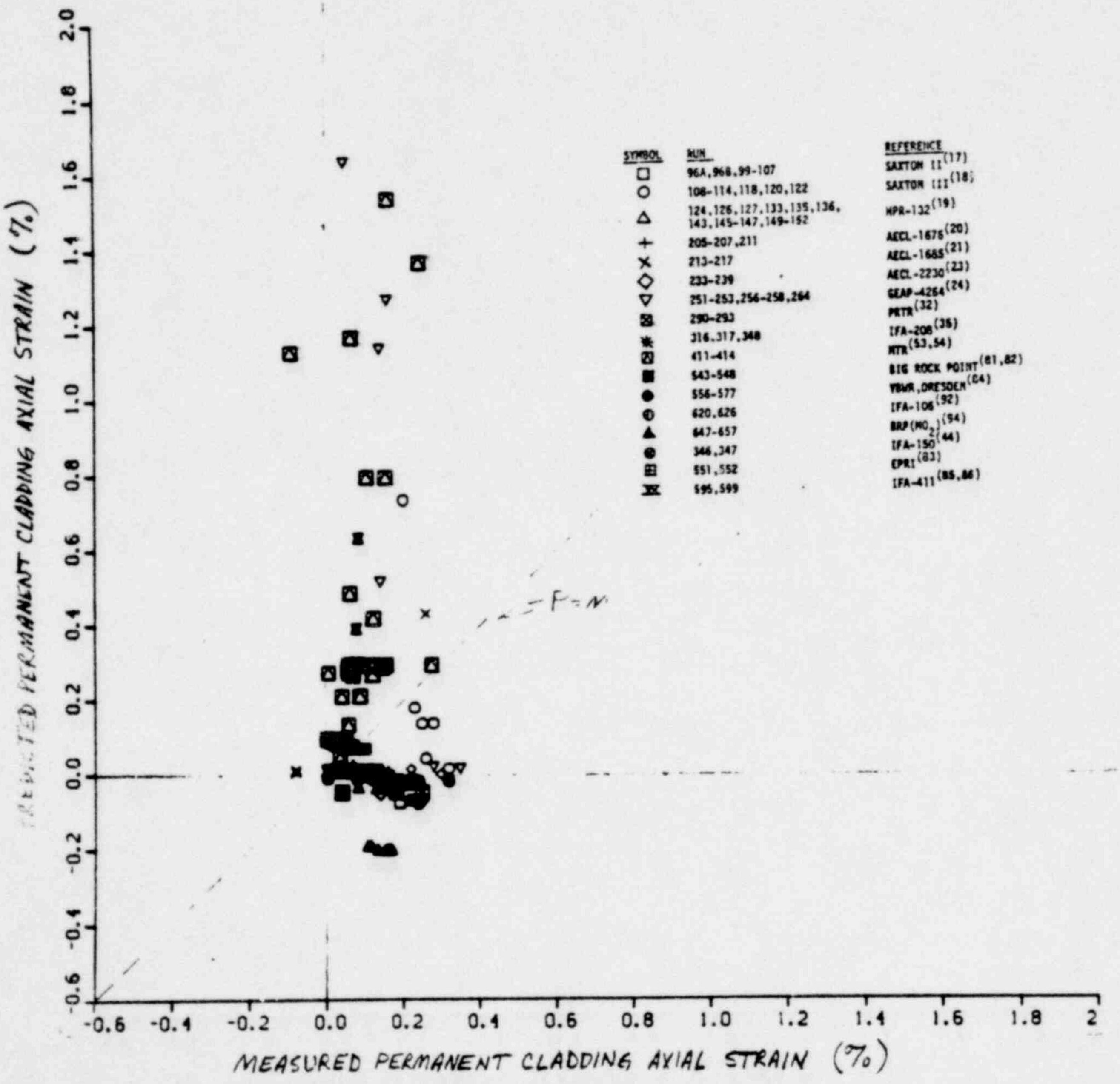

FIGURE 62 FRAP-S3 predicted versus measured permanent cladding axial strain . . . .

gap closure is not calculated to occur, while the data are always affected to some extent by axial stresses during soft gap closure. Overpredictions result from small gap or high temperature conditions under which structural gap closure is calculated. Since the fuel is not calculated to deform in these cases, cladding strain consequences of gap closure are again overestimated. Since permanent cladding deformation is typically a small effect, FRAP-S3 is able to characterize this parameter with a standard error equivalent to .4% of the rod active length.

3.4 Cladding Surface and Impurity Effects

Two types of data comparisons were performed in order to evaluate the ability of revised FRAP-S3 models to predict buildup of cladding surface corrosion and hydrogen concentration. There is currently no coupling for hydrogen concentration in the transient model. Determining the effects of initial material conditions on high temperature cladding reaction rates and deformation properties are among the objectives of current experimental programs.

3.4.1 Corrosion. The metal water reaction rates predicted by FRAP-T4 are sensitive to initial oxide thickness when the reaction becomes more rapid in steam at high LOCA cladding temperatures. Many of the rods affected by accidents will have accumulated varying amounts of corrosion over long-term operation prior to the transient. It is relevant then to evaluate model capability in this area. Only rod surface corrosion is considered.

1569 249

The FRAP-S3 corrosion mechanism is now dependent on coolant conditions in addition to cladding surface temperature. The effect on corrosion rates due to differences in system temperature and oxygen availability are such that previous user supplied lab corrosion rate acceleration factors for BWR and PWR conditions were respectively 10 and 3[3]. FRAP-S3 now incorporates internal logic by which to calculate in-pile corrosion rates directly.

Figure 63 shows measured versus predicted cladding surface corrosion for several experiments representing both BWR and PWR system conditions. Bar figures on the predictions account for variation due to pre-irradiation surface treatment effects which typically result in as-built corrosion layer thicknesses between 0 and .1 mils. Significant scatter exists in the apparent model agreement with the data due in part to grid-induced flow patterns and programmed changes in system chemistry not considered by the model. In any event, oxide layer thicknesses greater than about .3 mils are usually underpredicted. The standard error in characterizing the end-of-life corrosion layer is 6 μm.

Figures 64 and 65 indicate that relative model error is not clearly related to either time at temperature or system inlet temperature. Since PIE measurements are often made at locations exhibiting some departure from an expected effect, it is likely that some of the available data are not indicative of the uniform corrosion mechanisms considered by the model. Fractional accuracy of the corrosion model should generally be no worse than the ±50% reflected in the current results.

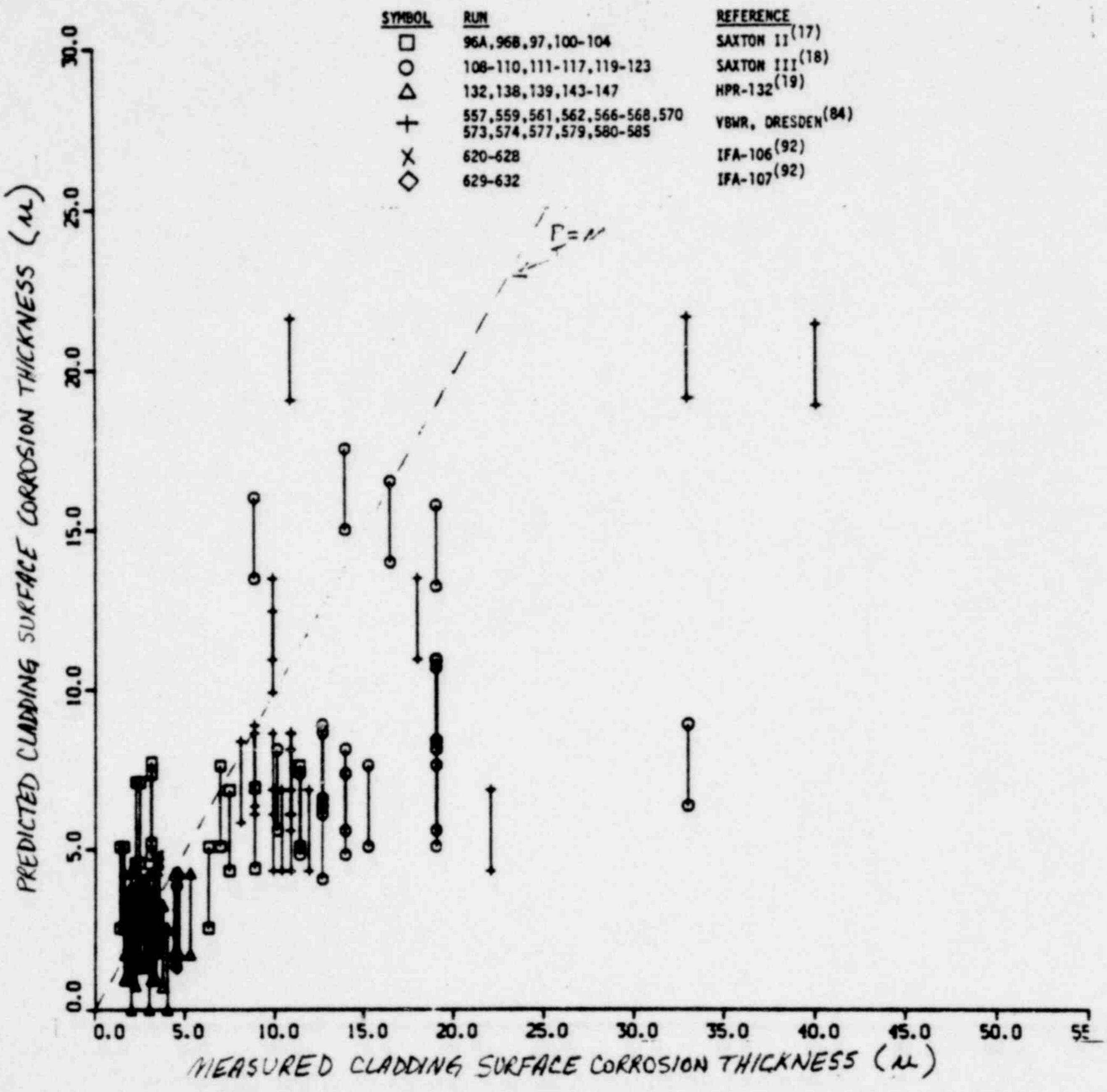

FIGURE 63 FRAP-S3 predicted versus measured rod surface corrosion buildup. . . . .

1569 251

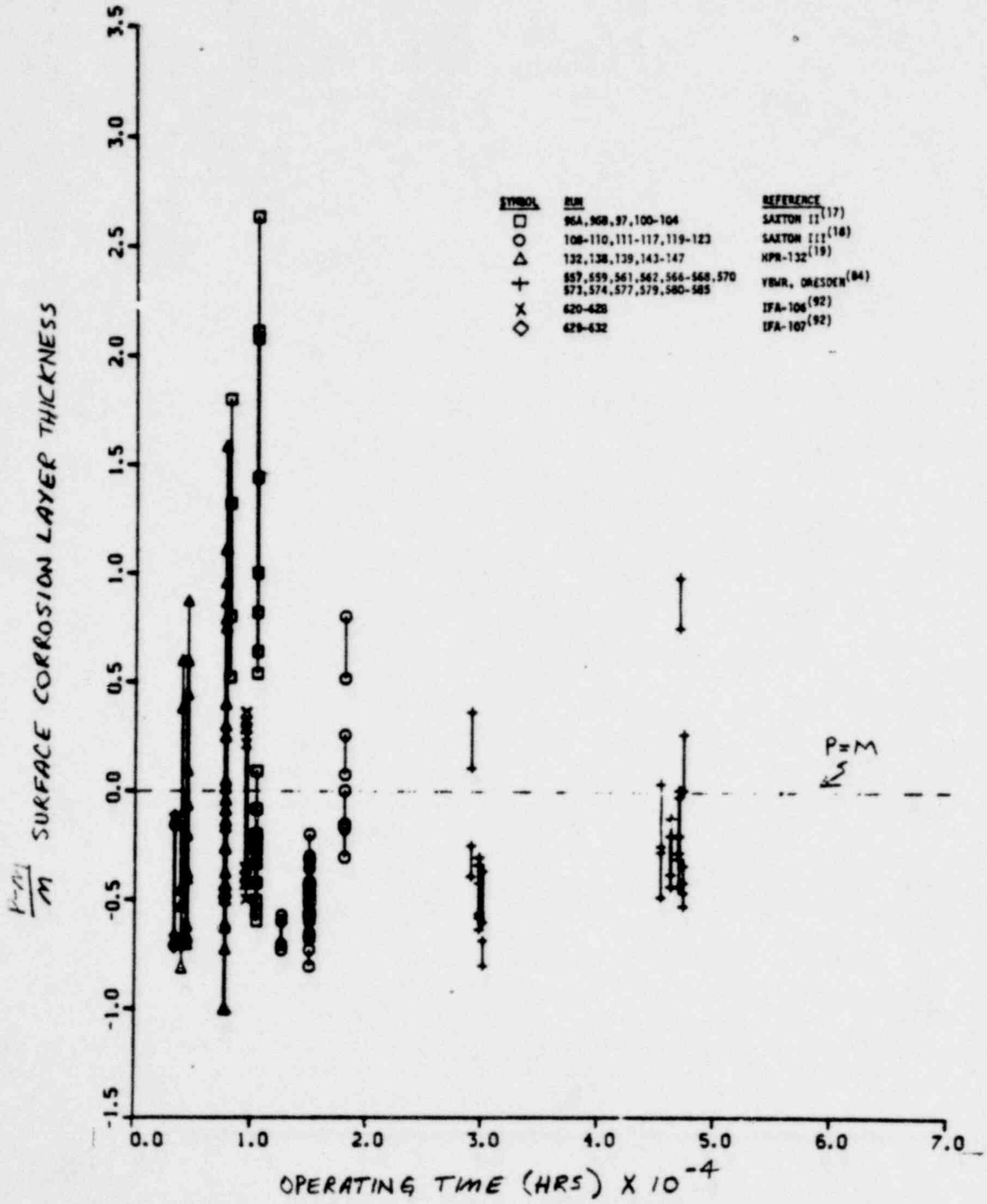

FIGURE 64 Effect of operating time on FRAP-S3 error in rod surface corrosion buildup. . . . .

23-407

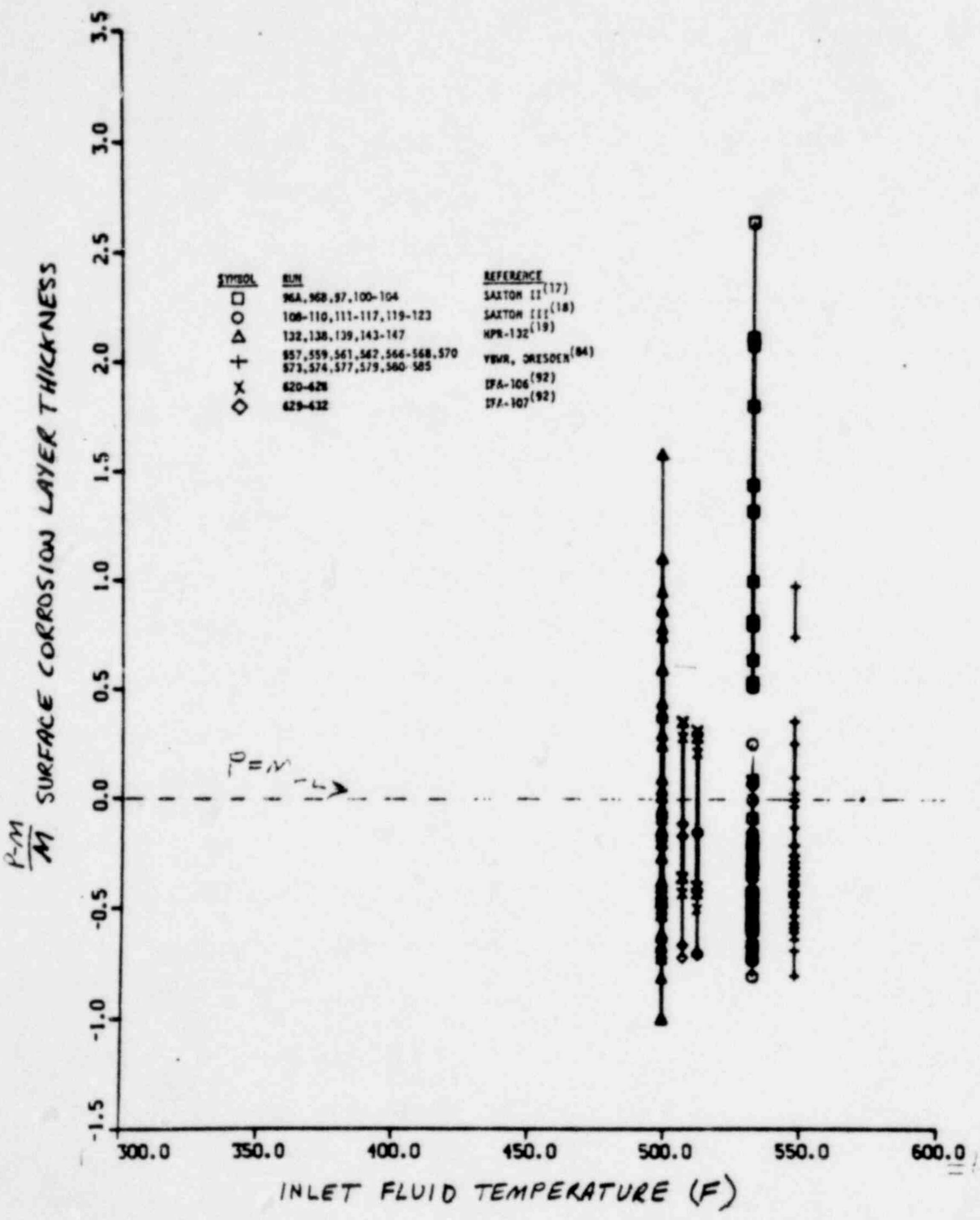

FIGURE 65 Effect of system inlet temperature on FRAP-S3 error in rod surface corrosion buildup. . . . .

1569 253

3.4.2 Hydrogen Pickup. Pickup of hydrogen by the cladding normally occurs as a result of both the oxidation process and early outgassing of small amounts of sorbed moisture from the fuel. Orientation of zirconium hydride platelets seems to have more influence on cladding mechanical properties than overall hydrogen concentration below about 200 PPM. Rods operated under normal conditions with internal hydrogen contamination problems show areas of high concentration (>600 PPM) and low ductility near failure locations. Normally, internal sources of hydrogen do not raise the as-fabricated hydrogen content to limiting levels. For accident calculations however, the impact of as much as 300 PPM hydrogen content in high burnup cladding may reduce maximum ballooning strain. Current understanding of the disposition and effect of accumulated chemical impurities on zircaloy behavior is inconclusive due to strong sensitivity of mechanical properties to temperature alone.

Figure 66 shows measured versus predicted cladding hydrogen concentration for many of the same rods used for corrosion data comparisons. In this case, bar symbols are intended to allow for up to 30 PPM hydrogen content in the as-built condition. As pointed out in the discussion of standard design analysis results, FRAP-S3 predicts that initial fuel moisture content has a stronger influence on the amount of hydrogen uptake than does corrosion. For this reason, underpredicting the amount of cladding surface corrosion does not always imply an underprediction of hydrogen uptake. Using the mean fabrication correction, the standard error between measured and FRAP-S3 predicted end-of-life hydrogen concentration is 39 ppm.

23-408

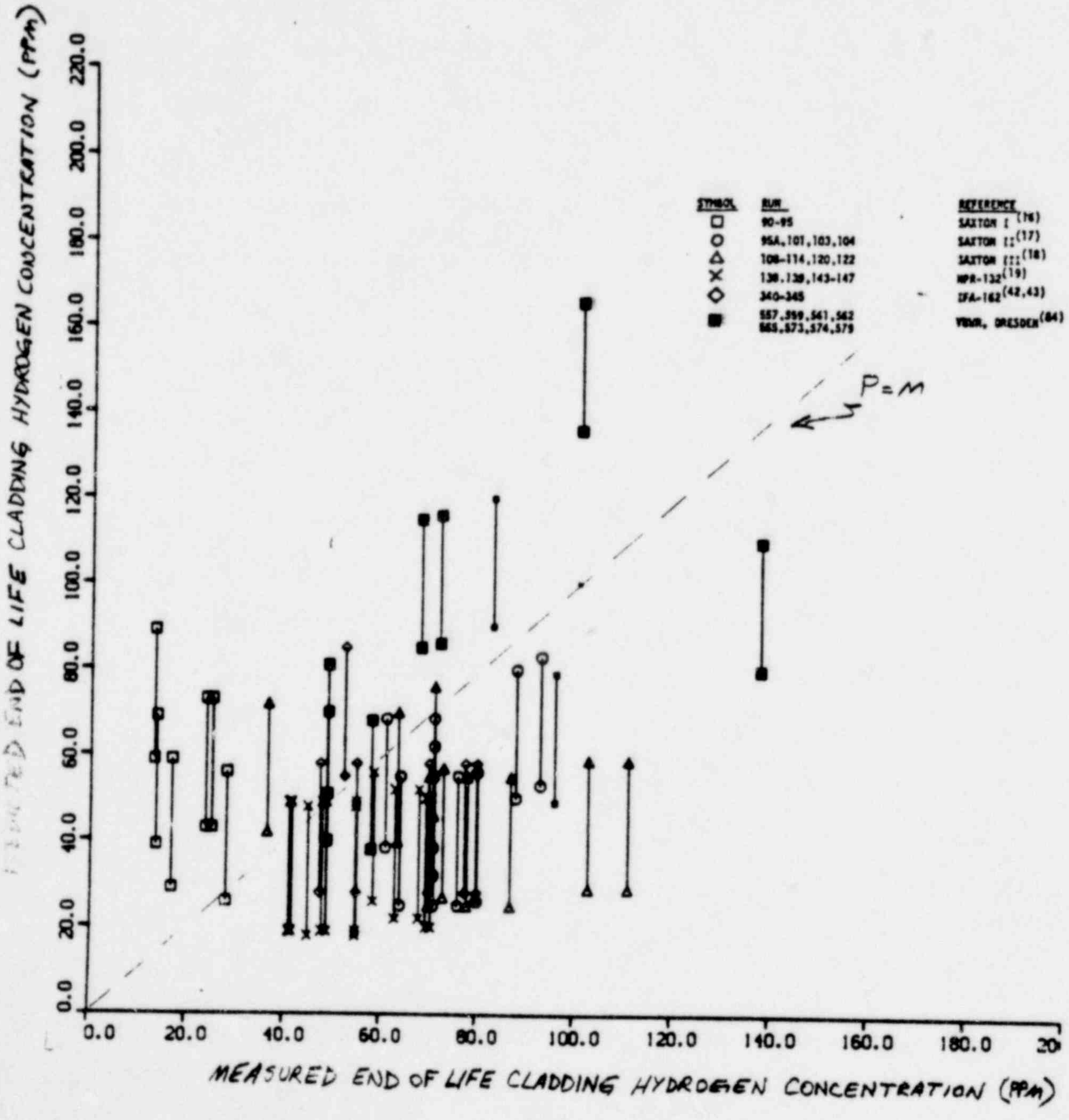

FIGURE 66 FRAP-S3 predicted versus measured cladding hydrogen concentration. . . . .

1569 255

Figure 67 shows the relative model error parameter plotted versus operating time at temperature. More tendency to overpredict the buildup of cladding hydrogen concentration corresponds to relatively short irradiation periods. This fact may be an argument for delaying the currently calculated instantaneous absorption of fuel moisture until such time as the ID surface layer is calculated to no longer be intact.

Another related parameter effect by which to interpret accuracy of predicted cladding hydrogen levels should be initial fuel moisture content. Fractional model error is plotted versus this parameter in Figure 68. Lack of fabrication details requires use of a default input value of 5 ppm for many cases. Nonetheless, adequate model capability is indicated for both low and moderate fuel moisture concentrations up to 15 PPM. Consistent overpredictions occur however when higher moisture concentrations have been reported and used in the code input. The highest overpredictions reflect a combination of relatively high rod internal moisture content and relatively low irradiation time. This coincidence is not unexpected since the hydrogen pickup model would make an increasing amount of surplus impurity instantaneously available to the cladding ID.

c3-409

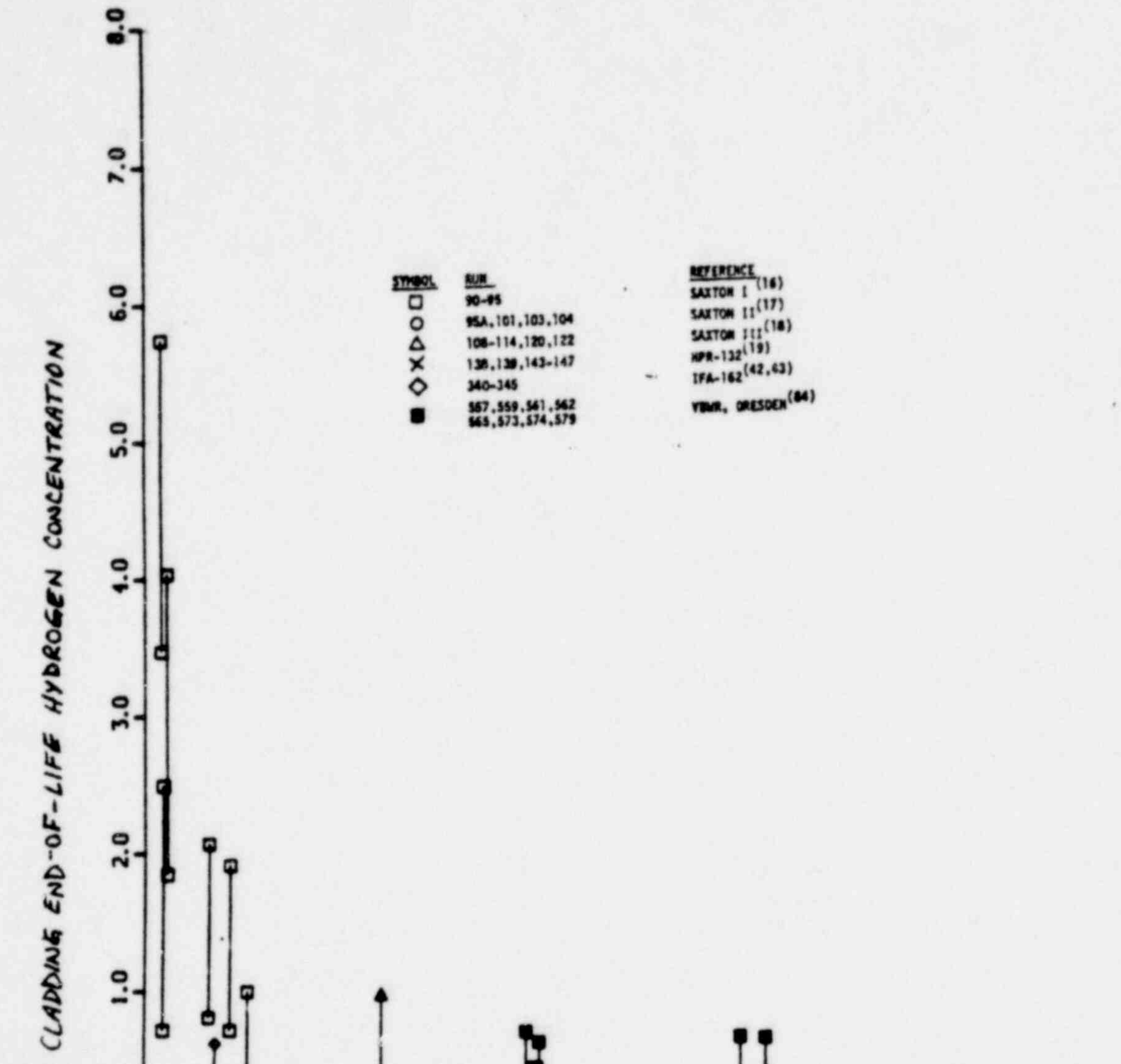

FIGURE 67 Effect of operating time on FRAP-S3 cladding hydrogen concentration error. . . . .

1569 257

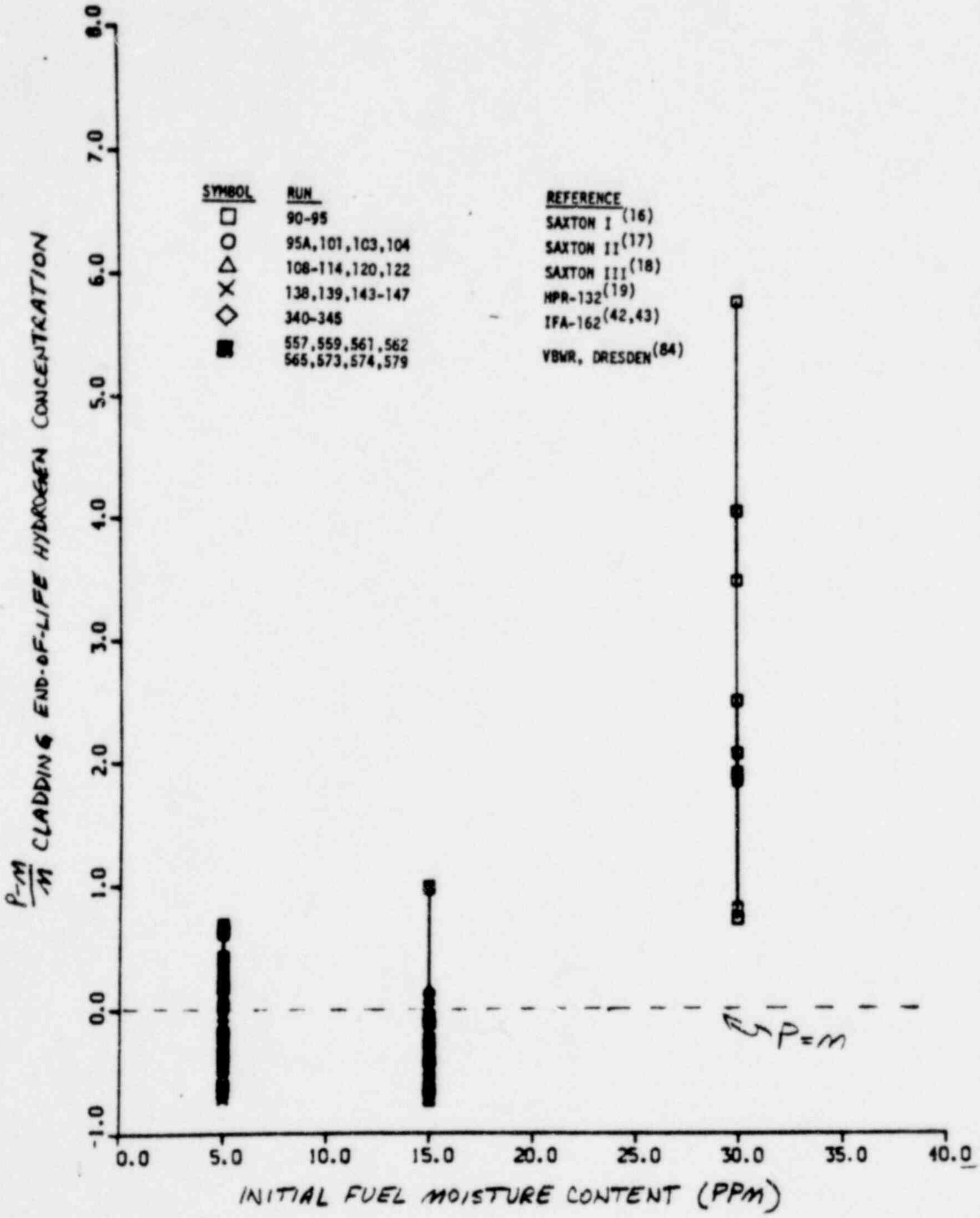

FIGURE 68 Effect of initial fuel moisture concentration on FRAP-S3 cladding hydrogen concentration error. . . . .

1569 258

23-410

IV. REFERENCES

1. J. A. Dearien, et al, FRAP-S: A Computer Code for Steady-State Analysis of Oxide Fuel Rods, Vol. 1 - FRAP-S3 Analytical Models and Input Manual, TFBP-TR-164 (January 1977).

2. P. E. MacDonald, L. B. Thompson, ed., MATPRO - Version 09, A Handbook of Materials Properties for Use in the Analysis of Light Water Reactor Fuel Rod Behavior, TREE-NUREG-1005 (December 1976).

3. D. R. Coleman, E. T. Laats, FRAP-S2: A Computer Code for Steady-State Analysis of Oxide Fuel Rods, Vol. 2 - Model Verification Report TREE-NUREG-1107, (July 1977).

4. G. Kjaerheim and E. Rolstad, In-Pile Determination of UO_2 Thermal Conductivity, Density Effects and Gap Conductance, HPR-80 (1966).

5. M. J. F. Notley, et al, Measurements of the Circumferential Strains of the Sheathing of UO_2 Fuel Elements During Reactor Operation, AECL-4072 (1972).

6. M. J. Brakas, "Cladding Strain Measurments Using Strain Gauges," Paper F-7 presented at the Enlarged Halden Programme Group Meeting, Sanderstolen, March 18-23, 1973.

* Halden Project Use Only

1569 259

7. E. T. Laats et al, USNRC-OECD Halden Project Fuel Behavior Test Program - Experiment Data Report for Test Assemblies IFA-226 and IFA-239, ANCR-1270 (December 1975).

8. G. Kjaerheim and E. Rolstad, In-Core Study of Fuel/Clad Interaction and Fuel Centre Temperature, HPR-107 (1969).

*9. G. Fayl and K. Hansen, In-Reactor Determination of the Thermal Conductivity of UO_2-Pellets up to 2200 C, RISO Report No. 269 (July 1972).

*10. G. Fayl and K. Hansen, Observations of Increase in Fuel Centre Temperature with Burn-Up in UO_2/Zr-2 Fuel Rods, RISO Report No. 415 (May 21, 1974).

*11. Y. Iwano, et al, "Irradiation Behavior of Fuel Assembly IFA-223," Enlarged Halden Programme Group Meeting, Sanderstolen, Norway, March 18-23, 1973.

12. M. G. Balfour, J. A. Christensen, and H. M. Ferrari, Final Report on In-Pile Measurement of UO_2 Thermal Conductivity, WCAP-2923 (March 1, 1966).

13. G. Testa, et al, "In-Pile Fuel Studies for Design Purposes," Nuclear Applications and Technology, Volume 7., (December 1969).

* Halden Project Use Only

1569 260

14. C. J. Baroch and M. A. Rigdon, "Irradiation Behavior of UO_2 at Burn-Ups from 10 t0 80 GWD/tonne U," Paper No. 58., presented at conference, BNES, 1973, CONF-731004.

15. D. Knodler and H. Stehle, "PWR Fuel Reliability and Quality Assurance KWU Experience," Paper No. 87., presented at conference, BNES, 1973, CONF-731004.

16. E. A. Bassler, et al, Saxton Core I Performance Summary, WCAP-3269-43 (1965).

17. W. R. Smalley, Saxton Core II Fuel Performance Evaluation, WCAP-3385-56 (September 1971).

18. W. R. Smalley, Evaluation of Saxton Core III Fuel Materials Performance, WCAP-3385-57 (1974).

19. D. G. Bridge, et al, UKAEA Fuel Test Assemblies Irradiated in HBWR 1964-1966, HPR-132 (1970).

20. M. J. F. Notley, et al, Zircaloy Sheathed UO_2 Fuel Elements Irradiated at Values of $\int kd\theta$ Between 40 and 83 W/cm, AECL-1676 (1962).

21. R. D. MacDonald and A. S. Bain, Irradiation of Zircaloy-2 Clad UO_2 to Study Sheath Deformation, AECL-1685 (1962).

1569 261

22. I. Devold, A Study of the Temperature Distribution in UO_2 Reactor Fuel Elements, AE-318 (1968).

23. M. J. F. Notley and J. R. MacEwan, The Effect of UO_2 Density on Fission Product Gas Release and Sheath Expansion, AECL-2230 (1965).

24. M. F. Lyons, et al, UO_2 Fuel Rod Operation with Gross Central Melting, GEAP-4264 (1963).

25. Z. R. Martinson, et al, Power-Coolant-Mismatch Test Series, 8-1 Reduced Shroud Test, Test Results Report, TFBP-TR-109 (October 1975).

26. J. R. Larson, et al, Power-Cooling-Mismatch Test Series, CHF Scoping Test, Test Results Report, TFPB-TR-114 (March 1976).

27. R. W. Garner, et al, Gap Conductance Thermal Oscillator Feasibility Test 1-1 Test Results Report, TFBP-TR-108 (September 1975).

28. W. J. Quapp, et al, Irradiation Effects Test Series, Scoping Test 1 Test Results Report, TFBP-TR-110 (January 1976).

29. Z. R. Martinson, et al, Power-Cooling-Mismatch Test Series, Test PCM 8-1 RF Test Results Report, TFBP-TR-119 (June 1976).

30. G. W. Cawood et al, Power-Cooling Mismatch Test Series, Test PCM-2A Test Results Report, ANCR-NUREG-1347 (September 1976).

31. W. J. Quapp, et al, Irradiation Effects Test Series Scoping Test 2 Test Results Report, TFBP-TR-137 (September 1976).

32. M. D. Freshly, "Mixed-Oxide Fuel Irradiations in the Plutonium Recycle Test Reactor," Nuclear Technology, Vol. 15, (August 1972), pp. 138, 141, 169, 172-3.

*33. K. Joon, "Verification of Four Models for Fission Gas Release," Enlarged Halden Programme Group Meeting, Geilo, Norway, March 16-21, 1975.

34. M. Hurme, Observation of Fuel Pin Internal Pressure, OECD Halden Reactor Project, HPR-110 (June 1969).

35. K. Taketani and M. Ichikawa, "Fuel Irradiation Experiments by JAERI for Light Water Reactors," Contribution to Crest Specialist Meeting, Sacley, France, October 21-24, 1973.

36. OECD Halden Reactor Project Quarterly Progress Report, January - March 1968, HPR-099 (May 1968).

* Halden Project Use Only

1569 263

37. J. B. Ainscough, An Assessment of the IFA-116 and 117 Irradiations from Data Obtained from the In-Reactor Instrumentation, HPR-129 (April 1971).

*38. OECD Halden Reactor Project Quarterly Progress Report, October - December 1973, HPR-167 (February 1974).

*39. H. Christensen, et al, Iodine Release from Defect Fuel Elements in the HBWR, HPR-169 (March 1974).

40. OECD Halden Reactor Project Quarterly Progress Report, July - September 1970, HPR-128 (November 1970).

41. OECD Halden Reactor Project Quarterly Progress Report, April - June 1971, HPR-140 (August 1971).

*42. OECD Halden Reactor Project Quarterly Progress Report, January - March 1972, HPR-150 (May 1972).

43. F. List, et al, "Fuel Column Shortening In Irradiation UO_2-Zr Fuel Pins," Paper # 75, presented at conference, BNES-73 (1975).

44. M. Ichikawa, et al, "Uranium Oxide Fuel Pin Elongation Behavior Under Irradiation," Journal of Nuclear Science and Technology, Vol. 8. No. 9, (September 1971), pp. 5254.

* Halden Project Use Only

45. H. M. Ferrari, et al, "Fuel Densification Experience in Westinghouse Pressurized Water Reactors," Paper # 54, presented at conference, BNES (1973), CONF-731004.

46. M. A. Rigdon, et al, "Babcock and Wilcox's Irradiation Program on Fuel Densification," Paper # 59, presented at conference, BNES (1973), CONF-731004.

47. OECD Halden Reactor Project Quarterly Progress Report, October - December 1970, HPR-130 (February 1971).

*48. OECD Halden Reactor Project Quarterly Progress Report, April - June 1972, HPR-152 (August 1972).

49. A. Hanevik, et al, "In-Reactor Measurements of Fuel Stack Shortening," Paper 89, BNES Conference, (1973), CONF-731004.

*50. E. Kolstad, "The 3-Rod Diameter Rig Experiment IFA-404 I (HP) and IFA-404 II (HP)," Enlarged Halden Programme Group Meeting Geilo, Norway, March 16-21, 1975.

*51. E. Kolstad and E. Rolstad, "The High Pressure Rig Experiment IFA-414 (N) In-Pile Results Obtained with First Test Rod," Enlarged Halden Programme Group Meeting, Geilo, Norway, March 16-21, 1975.

* Halden Project Use Only

1569 265

*52. E. Kolstad, et al, "The High Pressure PWR Rig IFA-414 (N), A Short Description of the Design and the Performance Characteristics," Enlarged Halden Programme Group Meeting, Geilo, Norway, March 16-21, 1975.

53. R. M. Berman, et al, Irradiation Behavior of Zircaloy-Clad Fuel Rods Containing Dished End UO_2 Pellets, WAPD-TM-629 (July 1967).

54. J. T. Engle and H. B. Meieran, Performance of Fuel Rods Having 97 Percent Theoretical Density UO_2 Pellets Sheathed in Zircaloy-4 and Irradiated at Low Thermal Ratings, WAPD-TM-631 (July 1968).

55. W. F. Domenico and J. A. Ramsthaler, IFA-429 Data Report No. 1, TREE-NUREG-1009 (December 1976).

56. C. R. Hann, et al, "Experimental Verification of Nuclear Fuel Rod Stored Energy Calculations," Enlarged Halden Programme Group Meeting, Sanderstolen, Norway, March 8-12, 1976.

*57. OECD Halden Reactor Project Quarterly Progress Report, April - June 1975, HPR-187 (September 1975).

* Halden Project Use Only

58. C. R. Hann, et al, "A Comparison of Pretest Predictions With Preliminary Data From NRC/PNL Halden Assembly IFA-431," Fourth Water Reactor Safety Research Information Meeting, Gaithersburg, Maryland, September 28, 1976.

59. C. R. Hann, et al, "Application of Experimental Data to the Reduction of Stored Energy Uncertainty," Fourth Water Reactor Safety Research Information Meeting, Gaithersburg, Maryland, September 30, 1976.

60. R. W. Garner, et al, Gap Conductance Test Series Test GC 1-3 Test Results Report and Summary of Piggyback Tests, TFBP-TR-186 (March 1977).

61. W. F. Domenico, et al, Power-Cooling-Mismatch Test Series Test PCM-3 Test Results Report, TFBP-TR-181 (March 1977).

62. Z. R. Martinson and R. K. McCardell, Power-Cooling-Mismatch Test Series Test PCM-2 Test Results Report, TREE-NUREG-1038 (February 1977).

*63. B. Brzoska and P. Dewes, "Measurement and Analysis of Central Fuel Temperatures," Enlarged Halden Program Group Meeting, Sanderstolen, March 8-12, 1976.

64. Z. R. Martinson, et al, Power-Cooling-Mismatch Test Series Test PCM-4 Quick Look Report, TFBP-TR-143 (November, 1976).

* Halden Project Use Only

1569 267

65. R. W. Garner and D. T Sparks, Gap Conductance Test Series Test GC 2-1 Quick Look Report, TFBP-TR-150 (December 1976).

66. R. W. Garner and D. T. Sparks, Gap Conductance Test Series Test GC IE-2 Quick Look Report, TFBP-TR-132 (October, 1976).

67. R. W. Garner and D. T. Sparks, Gap Conductance Test Series Test GC IE-3 Quick Look Report, TFBP-TR-146 (November, 1976).

68. D. T. Sparks and D. R. Chick, Gap Conductance Test Series Test GC IE-5 Quick Look Report, TFBP-TR-173 (February 1977).

69. W. J. Quapp, et al, Irradiation Effects Test Series Test IE-1 Test Quick Look Report, TREE-NUREG-1046 (March 1977).

70. G. W. Gibson, et al, Characteristics of UO_2-Zircaloy Fuel Rod Materials from Saxton Reactor for Use in Power Burst Facility, ANCR-NUREG-1321 (September 1976).

71. N. Fuhrman, et al, Evaluation of Fuel Rod Performance in Maine Yankee Core I, Task C, EPRI-NP-218 (November 1976).

72. Light-Water-Reactor Safety Research Program: Quarterly Progress Report, January - March 1976, ANL-76-49 (March 1976).

73. Light-Water-Reactor Safety Research Program: Quarterly Progress Report, April - June 1975, ANL-75-58 (June 1975).

74. Light-Water-Reactor Safety Research Program: Quarterly Progress Report, July - September 1975, ANL-75-52 (September 1975).

75. Light-Water-Reactor Safety Research Program: Quarterly Progress Report, October - December 1975, ANL-76-15 (December 1975).

76. Light-Water-Reactor Safety Research Program: Quarterly Progress Report, April - June 1976, ANL-76-87 (June 1976).

77. Light-Water-Reactor Safety Research Program: Quarterly Progress Report, July - September 1976, ANL-76-121 (September 1976).

78. Evaluating Strength and Ductility of Irradiated Zircaloy, Quarterly Progress Report for April - June 1975, BMI-1935 (June 1975).

79. Evaluating Strength and Ductility of Irradiated Zircaloy, Quarterly Progress Report for July - September 1975, BMI-1938 (September 1975).

80. Evaluating Strength and Ductility of Irradiated Zircaloy, Quarterly Progress Report for October - December 1975, BMI-1942 (December 1975).

81. Plutonium Utilization in Boiling Reactors, Phase II, Semi-Annual Report, July - December 1971, NEDO-10747 (December 1971).

82. S. Y. Ogawa and D. L. Zimmerman, Plutonium Utilization in Boiling Reactors, Phase II, Post Irradiation Examination of Four Fuel Rods After One Cycle of Operation in Big Rock Point Reactor, NEDO-10387 (July 1971).

83. H. R. Freeburn, et al, Light Water Reactor Fuel Rod Modeling Code Evaluation, EPRI-NP-369 (March 1977).

84. F. H. Megerth, et al, Zircaloy-Clad UO_2 Fuel Rod Evaluation Program, GEAP-10371 (June 1971).

*85. E. Kolstad, et al, "In Reactor Determination of Gap Conductance In UO_2 Pellet Fuel Rods Irradiated up to 12000 Mwd/t UO_2," Enlarged Halden Program Group Meeting, Sanderstolen, Norway, March 8-12 1976.

*86. H. Devold and T. C. Rowland, "A Review of Experimental Data from Some Densification Tests Performed in the Halden Reactor," Enlarged Halden Program Group Meeting, Sanderstolen, Norway, March 8-12 1976.

*87. G. H. Chalder, et al, "Measurement and Analysis of Fuel Densification and Rod Internal Gas Pressure in IFA-418 and IFA-419 Experiments," Enlarged Halden Program Group Meeting, Sanderstolen, Norway, March 8-12 1976.

* Halden Project Use Only

1569 270

*88. G. Fayl, et al, "In-Reactor Temperature Measurements," Enlarged Halden Program Group Meeting, Sanderstolen, Norway, March 18-23 1973, Paper No. 32.

*89. G. Fayl, et al, "Effect of Released Fission Gases on UO_2 - Temperatures," Enlarged Halden Program Group Meeting, Geilo, Norway, March 16-21 1975.

*90. V. Hazel, "The IFA-227^{II} (HP) to 227^{IV} (HP) Diameter Measurements in HBWR," Enlarged Halden Program Group Meeting, Geilo, Norway, March 16-21 1975.

*91. E. Rolstad, "IFA-227^{I} (HP) Diameter Rig Experiments," Enlarged Halden Program Group Meeting, Sanderstolen, Norway, March 18-23 1973.

92. R. Ueda, et al, Irradiation Testing of IFA-106 and IFA-107, JAERI-MEMO-4344 (February 1971).

*93. Personal Communication with K. Joon, OECD Halden Reactor Project, October 21, 1976.

94. D. M. Bishop and W. E. Baily, Nondestructive Examination of Plutonium Recycle Fuel Rods Irradiated to 30,000 Mwd/t, NEDO-12552 (December 1974).

* Halden Project Use Only

1569 271

*95. H. G. Walger, et al, A Parametric Study of the Influence of Important Fuel Design Parameters on the Elongation and Bamboo-Ridge Formation of Zr-2 Clad UO_2 Fuel Rods, HPR-141 (August 1971).

*96. P. Hofgaard, "Preliminary Results of the Project Interaction Experiment IN-1 (IFA -402 (HP))," HPR 173 (December 1973).

*97. H. Devold and N. T. Fordestrommen, "The Influence of Burnable Poison on Fuel Center Temperature and Rod Power as a Function of Burnup," Enlarged Halden Porogram Group Meeting, Sanderstolen, Norway, March 8-12, 1976.

*98. N. T. Fordestrommen, "Factors Influencing Fuel Temperature During Irradiation," Enlarged Halden Program Group Meeting, Sanderstolen, Norway, March 8-12, 1976.

99. J. A. Christensen, "Fuel-Cladding Gap Conductance from Large Diameter UO_2 Specimens," Enlarged Halden Program Meeting, Geilo, Norway, March 16-21, 1975.

*100. V. Albergamo, "In-File Measurement of Cladding Length Changes in IFA-215 (HP)", HPR-173 (December 1973).

*101. E. Kolstad, "Fuel Rod Length Measurements Up to 8200 MWd/t Oxide Burnup - IFA-216 (HP)", HPR-173 (December 1973).

* Halden Project Use Only

1569 272

102. S. D. Beck, "The Diffusion of Radioactive Fission Products From Porous Fuel Elements," BMI-1433, April 1960.

103. R. Godesar, et al, COMETHE II - A Computer Code for Predicting the Mechanical and Thermal Behavior of a Fuel Pin, Nuclear Applications and Technology, Vol 9, August 1970.

104. R. B. Poeppel, "An Advanced Gas Release and Swelling Subroutine," Proc. Conf. on Fast Reactor Fuel Element Technology, Am. Nucl. Soc., Hinsdale, Illinois, pp 311-326, 1971.

105. J. W. Dias and R. B. Poeppel, "Transient Swelling Studies with the GRASS Code", ANL-7992, March 1973.

106. J. A. Dearien, et al, "FRAP-T3 - A Computer Code for the Transient Analysis of Oxide Fuel Rods - Vol I - Analytical Models and Input Manual," TREE-NUREG-1163, to be published.

107. D. R. Coleman, "FRAP-S1: A Comouter Code for Steady State Analysis of Oxide Fuel Rods - Vol 3 - Model Verification Report, SSRD-6-76, September 1975.

108. T. G. Odekirk, "Detailed Test Plan Report for PBF Test Series PCM-20," ANCR-1095, April 1974.

109. D. R. Coleman, E. T. Laats, "FRAP-T2: A Computer Code for Transient Analysis of Oxide Fuel Rods - Vol II - Model Verification Report," TREE-NUREG-1040, March 1977.

1569 273

110. D. R. Coleman, E. T. Laats, "FRAP-T3: A Computer Code for Transient Analysis of Oxide Fuel Rods - Vol II - Model Verification Report," TREE-NUREG-1163, to be published.

111. J. D. Kerrigan, D. R. Coleman, "Standard Design Analysis: FRAP-S Procedures and Results" TFBP TR Report to be published.

24-419

1569 275

7812190305